GCA Technical Report No. 66-11-N

MEASUREMENT OF UPPER ATMOSPHERIC IONIZATION AND WINDS WITH A COMBINED PAYLOAD

L.G. Smith J.F. Bedinger G.T. Best

INTERIM REPORT

Contract No. NASw-1083

June 1966

GCA CORPORATION
GCA TECHNOLOGY DIVISION
Bedford, Massachusetts

Prepared for

NATIONAL AERONAUTICS AND SPACE ADMINISTRATION
HEADQUARTERS
WASHINGTON 25, D. C.

TABLE OF CONTENTS

LIST OF ILLUSTRATIONS

LIST OF ILLUSTRATIONS (continued)

LIST OF ILLUSTRATIONS (continued)

MEASUREMENT OF UPPER ATMOSPHERIC IONIZATION AND WIND WITH A COMBINED PAYLOAD

By L. G. Smith, J. F. Bedinger, and G. T. Best
GCA Corporation, GCA Technology Division
Bedford, Massachusetts

INTRODUCTION

The principal scientific objective of this contract is the study of the relation between the structure of the electron density profile and wind in the E region. Such observations had previously been obtained at Wallops Island using separate rockets, suitably instrumented, one to obtain the electron density profile and the other to lay down the vapor trail used in obtaining the wind data. The Wallops Island experiments gave information which is believed typical of mid-latitudes. The new program is based on observations in the auroral zone, for which Fort Churchill provides a convenient launch site.

The first phase of the contract consisted of development of a payload which combines the canister of the vapor trail technique with Langmuir probe instrumentation for electron density observations; electron density being measured on the ascending part of the rocket trajectory and the vapor trail released during the descending portion. Some electron density information is sacrificed by this approach but the convenience and economy of the single launch outweigh these. A description of the "combined" payload is given in this report. The development of a canister for release of TMA (trimethyl aluminum) was the major portion of the effort in this phase.

Thirteen combined probe and vapor trail payloads were constructed, including both TMA and alkali vapor canister sections. Two were built specifically for delivery to the Indian Government. One additional payload is available for use on a subsequent phase of this program. The remaining ten combined payloads have been launched on Nike Apache rocket vehicles. Three, including one alkali vapor and two TMA sections, were successfully launched at Wallops Island, Virginia, as operational tests of the new design. The remaining seven payloads were launched at Fort Churchill on three different field trips. It had been intended to obtain at least one sequence of three launches during a single night, starting at evening twilight and ending at morning twilight. However, unfavorable weathre and a number of vehicle malfunctions resulted in only one successful

launch in each of the three trips to Fort Churchill. Further details of the launches are included under the discussion of rocket flights.

The results of the observations of electron density and wind obtained during the program are given for three rocket launches from Wallops Island (actually test-flights of the system) and three launches from Fort Churchill. The observations from Wallops Island produced excellent measurements of mid-latitude sporadic-E and wind profiles. The results of these and related measurements were reported at the Sporadic-E Seminar at Estes Park, Colorado, June 1965 and have been published in Radio Science.
These and other publications and presentations resulting from this contract are listed in Table 1.

The most striking visual characteristic of a sunlit TMA vapor trail in the upper atmosphere is the blue-green color. Spectrophotometric observations have shown that this color is due to the fluorescence spectrum of aluminum oxide (AlO). The relative population of the vibrational and rotational energy levels as evidenced in the spectrum may be used to obtain ambient temperature. Observations of the spectrum of sunlit trails were obtained at Wallops Island and Fort Churchill with a spectrophotometer furnished by W. G. Fastie of the Johns Hopkins University. This investigation and the temperature obtained are discussed under Measurements of Upper Atmosphere Temperatures in this report.

A similar instrument was used to observe the Comet Ikeya-Seki from a NASA aircraft near Hawaii. These results are also presented in this report.

Some conclusions concerning the experimental methods and data and some recommendations for future work are then presented.

Appendix A contains rocket launch and performance data.

The major disappointment of the program was the high proportion of vehicle failures in the launches from Fort Churchill. An analysis of these is given in Appendix B. Initially, it was believed that the payload may be a major contributor to the vehicle failure, but the analysis shows that this cannot be the case. It is now believed that the primary cause of failure is a weakness at the head-cap of the second-stage rocket (Apache).

TABLE 1

REPORTS AND ARTICLES ON CONTRACT NO. NASw-1083

Journal Articles

Bedinger, J. F. and Knaflich, H. B., "Observed Characteristics of Ionospheric Winds," Radio Science 1, pp. 156-168 (1966).

Smith, L. G., "Rocket Observations of Sporadic-E and Related Features of the E Region," Radio Science 1, pp. 178-186 (1966).

Smith, L. G., "Summary and Conclusions from the Estes Park Sporadic-E - Rocket Measurements," Radio Science 1, pp. 244-245 (1966).

GCA Technical Reports

Corman, A. and Guarino, N. J., "Canister for Producing TMA Trails in the Upper Atmosphere," GCA Technical Report No. 65-2-N (February 1965).

Coté, O., "Turbulent Diffusion of Sodium Vapor Trails in the Upper Atmosphere," GCA Technical Report No. 65-5-N (March 1965).

Smith, L. G., "Rocket Observations of Sporadic-E and Related Features of the E Region," GCA Technical Report No. 65-22-N (August 1965), published in Radio Science 1, (1966)(see above).

Bedinger, J. F. and Knaflich, H. B., "Observed Characteristics of Ionospheric Winds," GCA Technical Report No. 65-26-N (August 1965), published in Radio Science 1, (1966)(see above).

Bedinger, J. F., "Compendium of Wind Data from the Vapor Trail Technique," GCA Technical Report No. 66-7-N (March 1966).

Presentations at Scientific Meetings

Bedinger, J. F. and Knaflich, H. B., "Small Scale Structure Observed in Vapor Trails Around 100 km," paper presented at the Second Conference on Direct Aeronomic Measurements in the Lower Ionosphere, University of Illinois, 27-30 September 1965.

Smith, L. G., "Rocket Observation of Sporadic-E and Related Features of the E Region," paper presented at the URSI Fall Meeting, Dartmouth College, 4-6 October 1965.

TABLE 1 (Cont.)

Bedinger, J. F. and Smith, L. G., "Measured Wind Shears and Electron Densities," to be presented at the COSPAR Symposium on Interaction Between the Neutral Part and the Ionized Part of the Atmosphere on 17 May 1966 in Vienna.

PAYLOAD DEVELOPMENT

Various approaches to the problem of measuring the electron density profile with a rocket borne Langmuir probe and the wind profile with a vapor trail ejected from the same rocket were considered. The most desirable situation occurs when both profiles are obtained simultaneously at the same position in space; however, the nature of the two measuring techniques require that some compromises be made. The probe measurements are made very rapidly in time and space as the rocket vehicle moves along the trajectory, but the wind measurements require at least one minute to obtain the trail displacement required for accurate wind determination. Also, the operation of the probe and telemetry is affected by alkali vapor if both are operating at the same time and place. Several methods of separating either or both of the sections from the rocket vehicle were found not satisfactory due to the large impulses required, or to instability, or to unpredictable altitude and/or attitude of the separated instruments. The method chosen uses the normal rocket trajectory to produce the required separation by operating the Langmuir probe on the ascent and releasing the vapor on the descent. This method required minimum design changes of the individual systems, and thus the proven reliability of these payloads was retained.

The individual probe and vapor payloads were combined as shown in Figure 1. Each section was modified to shorten and lighten the overall combination, and the probe was then attached to the forward end of the canister section. A photograph of a combined probe-vapor payload is shown in Figure 2. The three sections, probe [1]*, alkali vapor [2], and TMA [3], have been completely described elsewhere so that only the basic operation and major modifications will be included here.

Langmuir Probe Section

The nose tip of the rocket is insulated from the rest of the vehicle and is programmed with a sweep voltage alternating with a fixed voltage. The sweep (-2.7 to +2.7 volts, duration 0.5 sec) is the conventional Langmuir mode and is used to obtain electron temperatures and electron density by the measurement of the probe current as a function of voltage. The fixed voltage mode (+2.7 volts, duration 1.5 sec) is used to obtain fine structure of the electron density profile and is particularly suited to the observation of Sporadic-E layers.

---

*Numbers in [] represent reference numbers.

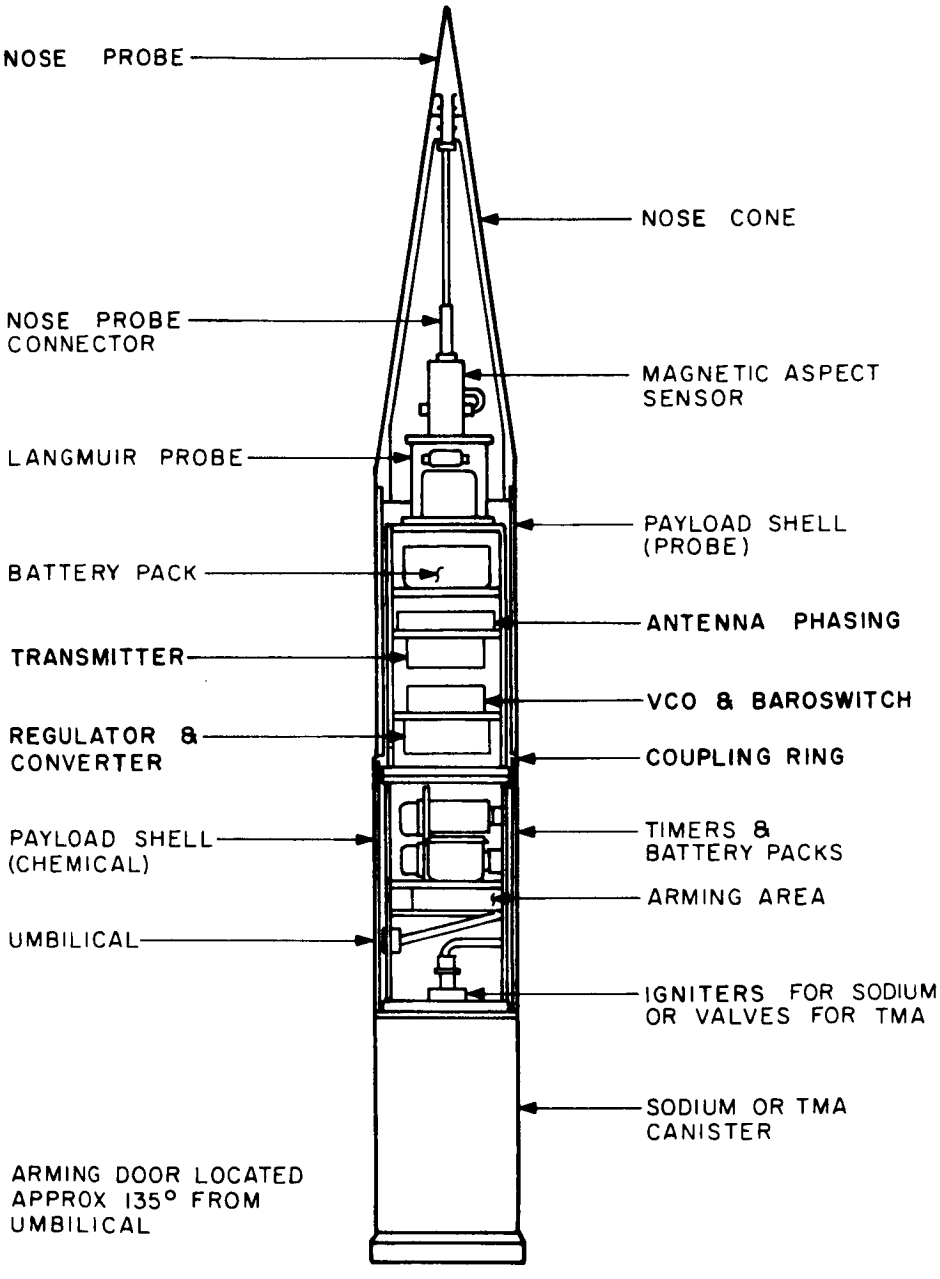

Figure 1. Layout of the combined payload.

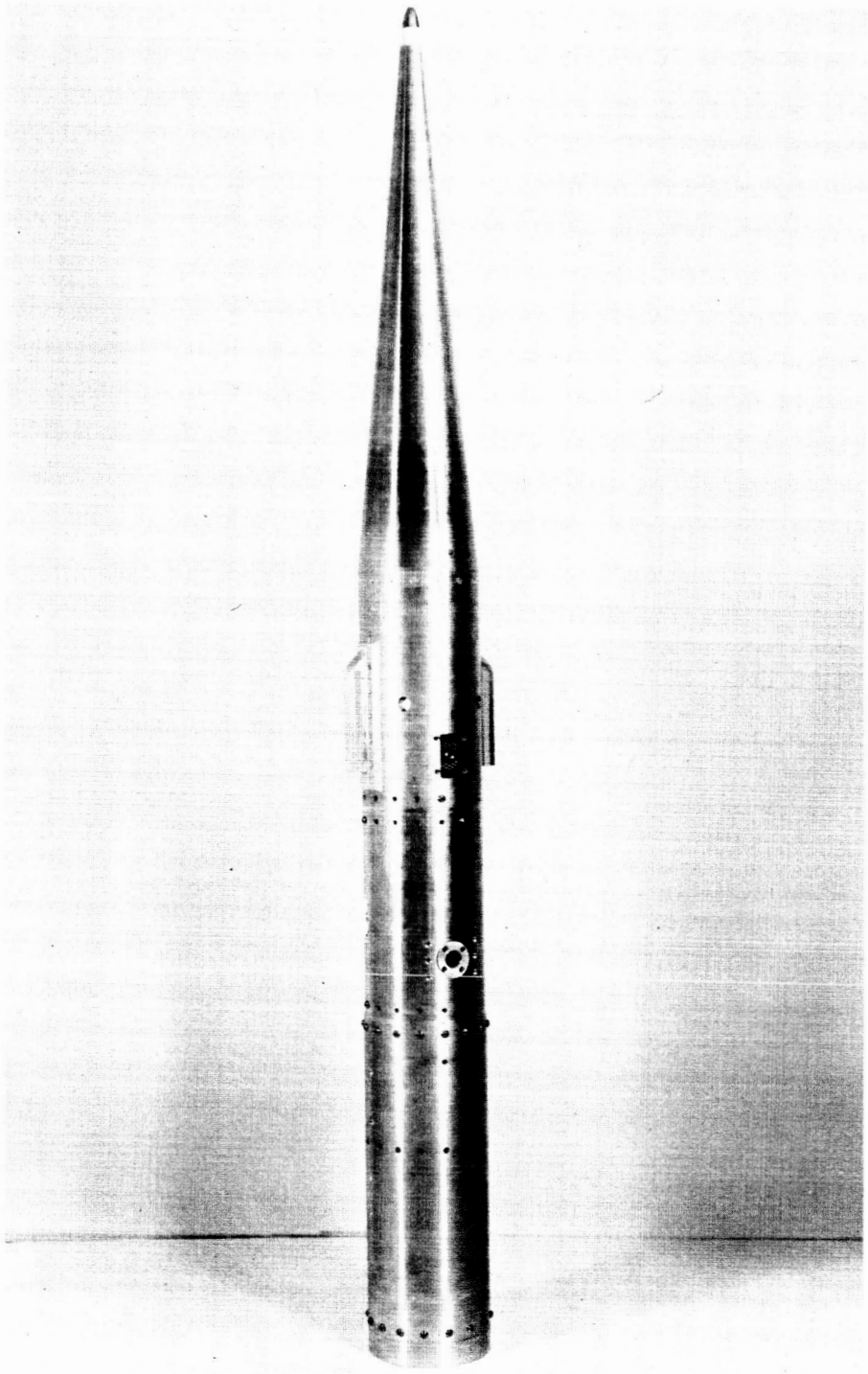

Figure 2. Combined probe-TMA payload.

The probe is calibrated periodically during the flight. The instrument is disconnected from the nose tip electrode and connected to a known resistor. This occurs for the duration of one sweep at intervals of 32 seconds (i.e., every sixteenth sweep).

The section also contains an aspect magnetometer transverse to the spin axis, which is primarily used to monitor the vehicle motion, and a baroswitch (nominally 75,000 ft.) which is used to determine rocket trajectory by a time-of-flight method [4]. The magnetometer and baroswitch signals are telemetered on one channel of the FM/FM System and the probe data on a second channel. The power supply for the probe section of the payload is independent of that for the vapor section, and each section is monitored and controlled through a separate umbilical cable. This is primarily a safety feature since the vapor section is considered to be hazardous.

Alkali-Vapor Section

The basic operation of the alkali-vapor section required no changes for the adaptation into the combined payload. A few modifications to shorten and lighten the instrument rack were made, but the completely isolated dual ignition system which initiates the vaporizer action was retained. This system uses two mechanical timers, two battery packs, and two igniters. The timers had previously been started at take-off by a built-in inertia switch. The longer time to vapor ejection on the down trail required the use of an explosive switch start for the timers. Provisions were made to start the timers about 30 seconds after launch with a baroswitch. The only other major change in the alkali-vapor section was the relocation of arming plugs. These plugs were originally located on the forward end of the instrumentation racks, and the vaporizer was armed by the removal of the nose cone. In the combined payload, the probe section is mounted to the forward end of the vapor rack, so the arming plugs were moved to the side of the rack and are accessible through a removable door in the skin.

TMA Section

The method of dispensing TMA is an entirely new design. However, the initiation circuits and safety monitors are intentionally the same as those for the alkali metal vaporizer. In fact, both dispensers are attached to the same type of instrumentation rack. Briefly, the TMA dispenser functions as follows. The TMA is contained in a specially designed flexible teflon bladder which is carefully mounted in an internally fitted aluminum canister. The assembly is filled with TMA at the manufacturer's plant and shipped to the launch site in the flight container. This procedure is particularly convenient since handling of TMA is tedious and requires special equipment and the shipping regulations

are stringent. Both the teflon bladder and the aluminum canister have an exit or entrance port through a valve system. When the valves to the bladder and canister are both opened and dry nitrogen under pressure is forced into the canister, the bladder is compressed and the TMA is forced out. During flight, the valves are operated by electrically initiated controlled explosives and the rate of ejection is controlled by the size of the exit port. The bladder assembly is shown in Figure 3.

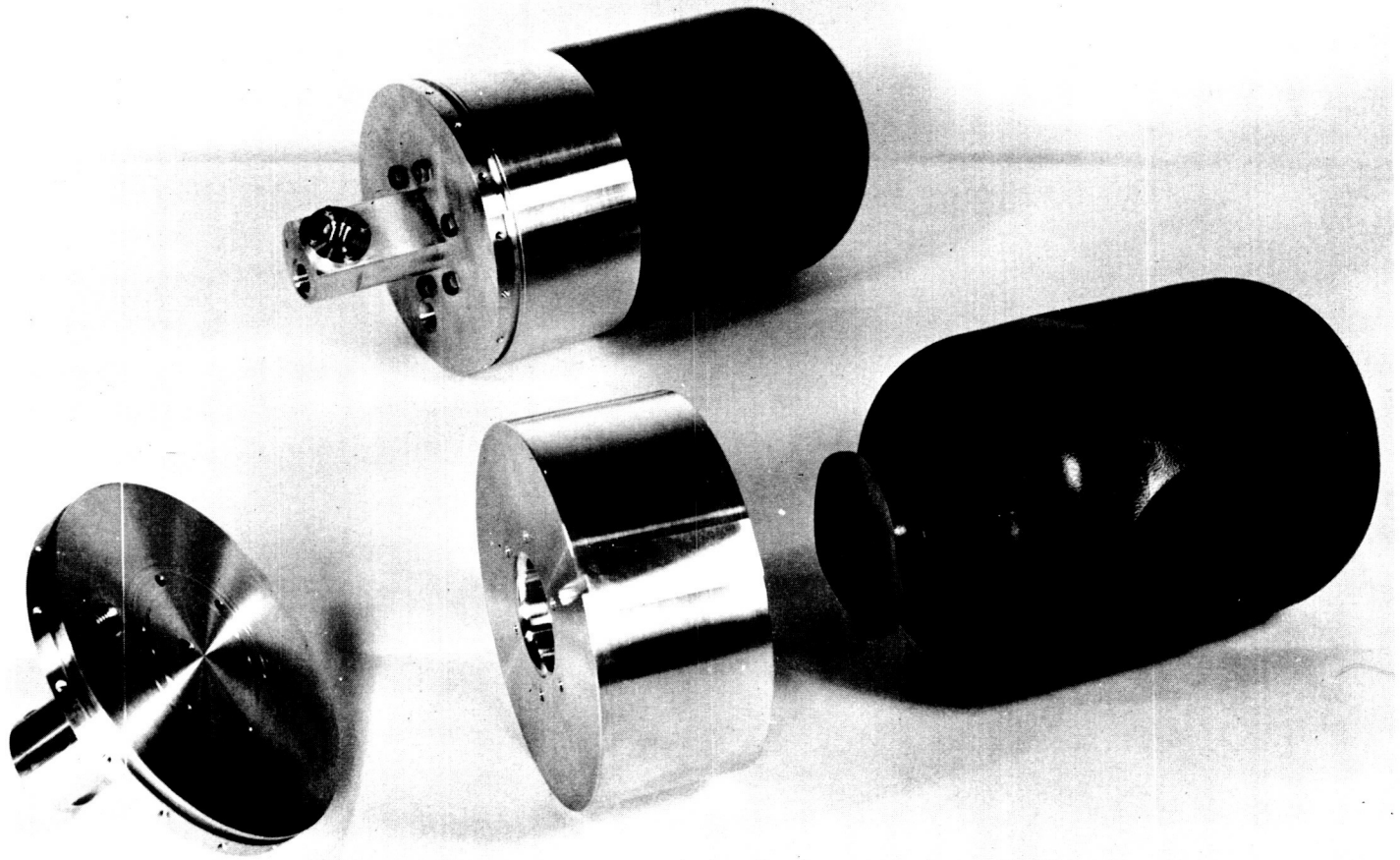

Figure 3. TMA teflon bladder and mounting.

ROCKET FLIGHTS

Table 2 presents a chronological synopsis of the ten firings of Nike Apache rockets that took place under Contract No. NASw-1083. The following is a summation of the activities during five field trips in which the firings took place. Further data on the rocket launches is given in Appendix A.

OCTOBER, 1964 - WALLOPS ISLAND

These first firings (14.194 and 14.195) constitute test flights for the prototypes of the two types of combined payloads: probe-TMA and probe-alkali vapor. These payloads had been subjected to environmental tests at GSFC. The flights were completely successful.

OCTOBER-NOVEMBER, 1964 - FORT CHURCHILL

This series was to include four firings of the combined payloads with test vehicles 14.196, 14.197, 14.198, and 14.199. The objective was to perform a four-shot series in one night that would provide additional information on the time dependence of the winds and electron density profiles. During a 19-day period, weather conditions were such that only one rocket was fired (14.197). Although this test was successful, a reversal in the forecast weather conditions prevented the continuation of the series. Unsatisfactory weather was the sole factor in the delay and termination of this series.

FEBRUARY, 1965 - FORT CHURCHILL

The objectives of this series were similar to those planned for the preceding series at Fort Churchill. Four vehicles were to be launched from evening through to the morning twilight. A week of unsuitable weather was experienced before all the rockets were launched during the night of 27-28 February. The first test (14.196) was successful with good payload performance. The three following tests were failures and no scientific data was obtained. A detailed analysis and discussion of the rocket failures is presented in Appendix B. It was demonstrated that the spin rate of these vehicles that failed was appreciably different from those which were routinely successful.

JUNE, 1965 - WALLOPS ISLAND

At the suggestion of the Sounding Rocket Branch, GSFC, the quadra-loop antennas (used on 14.194/.200) were replaced by dipole antennas on subsequent flights. The reason for this is that the aerodynamic lift

on the payload is reduced and the possibility of divergence failure becomes less likely. The analysis of Appendix B shows that quadraloop antennas contributed very little to the lift so that the effect of the change of antenna type is quite small.

Nike Apache 14.201 was scheduled as another test flight of the combined payload and was included in a series of four vapor trail rockets launched under Contract NAS5-3970. The flight was completely satisfactory and maximum altitude of 167 km was attained.

OCTOBER, 1965 - FORT CHURCHILL

With the success of the test flight at Wallops, the three remaining combined TMA-probe type payloads were scheduled for a series at Fort Churchill. After considerable delay caused by unfavorable weather, two of the rockets were launched on the night of 5 October 1965. The first at evening twilight was successful and excellent data was obtained. The second, launched two hours and thirty-nine minutes later, broke up during the burning of the second stage and no scientific data was obtained. The cause of failure could not be immediately determined and the series was terminated without launching the third rocket of the series.

It is interesting to note that all three rockets fired at Wallops Island were complete successes. Of the seven fired at Fort Churchill, three were successes and four were failures. Prior to each of the series at Fort Churchill, a test firing of the exact payload configuration had been successfully fired at Wallops.

All of the available information concerning the vehicle failures has been reported to the NASA section responsible for sounding rocket programs. The other major difficulty encountered during the Fort Churchill firings was the long periods of unfavorable weather and the uncertainty of forecasts. Some recommendations concerning weather difficulties are given in the concluding section of this report.

TABLE 2

SUMMARY OF ROCKET LAUNCHES USING COMBINED PROBE-VAPOR PAYLOAD

Nike Apache	Date	Time	Launch	Vapor	Apogee	Test Results
14.195	7 Oct.'64	1804 EST	W.I.*	TMA	172 km	Electron Density 76-172 km; Winds 90-157 km
14.194	8 Oct.'64	0523 EST	W.I.	Na-Li	160 km	Electron Density 78-160 km; Winds 84-160 km.
14.197	1 Nov.'64	0000 CST	F.C.**	Na-Li	165 km	Electron Density 70-165 km; Winds 94-125 km
14.196	27 Feb.'65	1821 CST	F.C.	Na-Li	155 km	Electron Density 67-155 km; Winds 90-150 km
14.198	27 Feb.'65	2130 CST	F.C.	TMA	--	None - Vehicle Failure
14.199	28 Feb.'65	0000 CST	F.C.	TMA	--	None - Vehicle Failure
14.200	28 Feb.'65	0611 CST	F.C.	TMA	--	None - Vehicle Failure
14.201	22 June'65	2300 EST	W.I.	TMA	167 km	Electron Density 70-167 km; Winds 94-123 km
14.202	5 Oct. '65	1821 CST	F.C.	TMA	181 km	Electron Density 65-181 km; Winds 92-155 km
14.203	5 Oct. '65	2100 CST	F.C.	TMA	--	None - Vehicle Failure

*W.I. - Wallops Island, Va.

**F.C. - Fort Churchill, Man.

OBSERVATIONS OF ELECTRON DENSITY AND WINDS

Wallops Island Observations

Three payloads were launched at Wallops Island, and good data were obtained from each. Excellent examples of various forms of mid-latitude sporadic E were observed. The electron density profiles are shown in Figures 4, 5, and 6. The magnetic North-South and East-West components of velocity from the corresponding wind profiles are shown in Figures 7, 8, and 9. The location of observed regions of enhanced electron density are indicated by the arrows. It is seen that generally these regions are not located at the zero point of an East-West shear as was originally predicted by the simple wind shear theory of sporadic E [5]. More recently, it has been shown that horizontal electric polarization fields and vertical wind motions can cause the ionized layers to be displaced from the position indicated by the simple theory [6]. Also due to the contour of the earth's magnetic field, similar effects may occur in North-South wind shears above 120 km [7]. At present, neither of these effects have been accurately evaluated; thus, there continues to be uncertainties in the interpretation of simultaneous observations of winds and electron density profiles.

Although the observations have shown no direct relation between the ionized layers and wind shear, it has been pointed out that the position of the layers are usually closely associated with another feature of the wind profiles [8]. This relation is best demonstrated by a wind hodograph. A hodograph is obtained when the wind is represented by vectors on a polar plot and the tips of these vectors are joined consecutively in height by a continuous arc. Often in the region 90 to 120 km, this arc contains sharp corners or reversals in direction which occur in a very small height interval and are usually associated with only a very small change in velocity. These sharp directional changes in the hodograph have been shown to coincide with the ionized layers. From a total of seven nearly simultaneous profiles, Bedinger and Knaflich [8] demonstrated that 14 of 17 observed ionized layers could be associated with such corners. Hodographs of the three observations obtained at Wallops Island during the period of this contract are shown in Figures 10, 11, and 12. The peaks of the ionized layers are marked by arrows, and the dashed lines around the arrows represent the general region of the electron enhancement.

Fort Churchill Observations

The probe data from the three launchings at Fort Churchill are given in Figures 13, 14, and 15. Figures 16, 17, 18, 19, 20, and 21 contain the corresponding wind data. The high electron densities and absence of structure in the profiles during the 1 November 1964 and 22 February 1965 observations are thought to be due to the presence of active aurora at the time of the firings. A generally lower density and some structure was present in the E-region at the time of the 5 October 1965 observations.

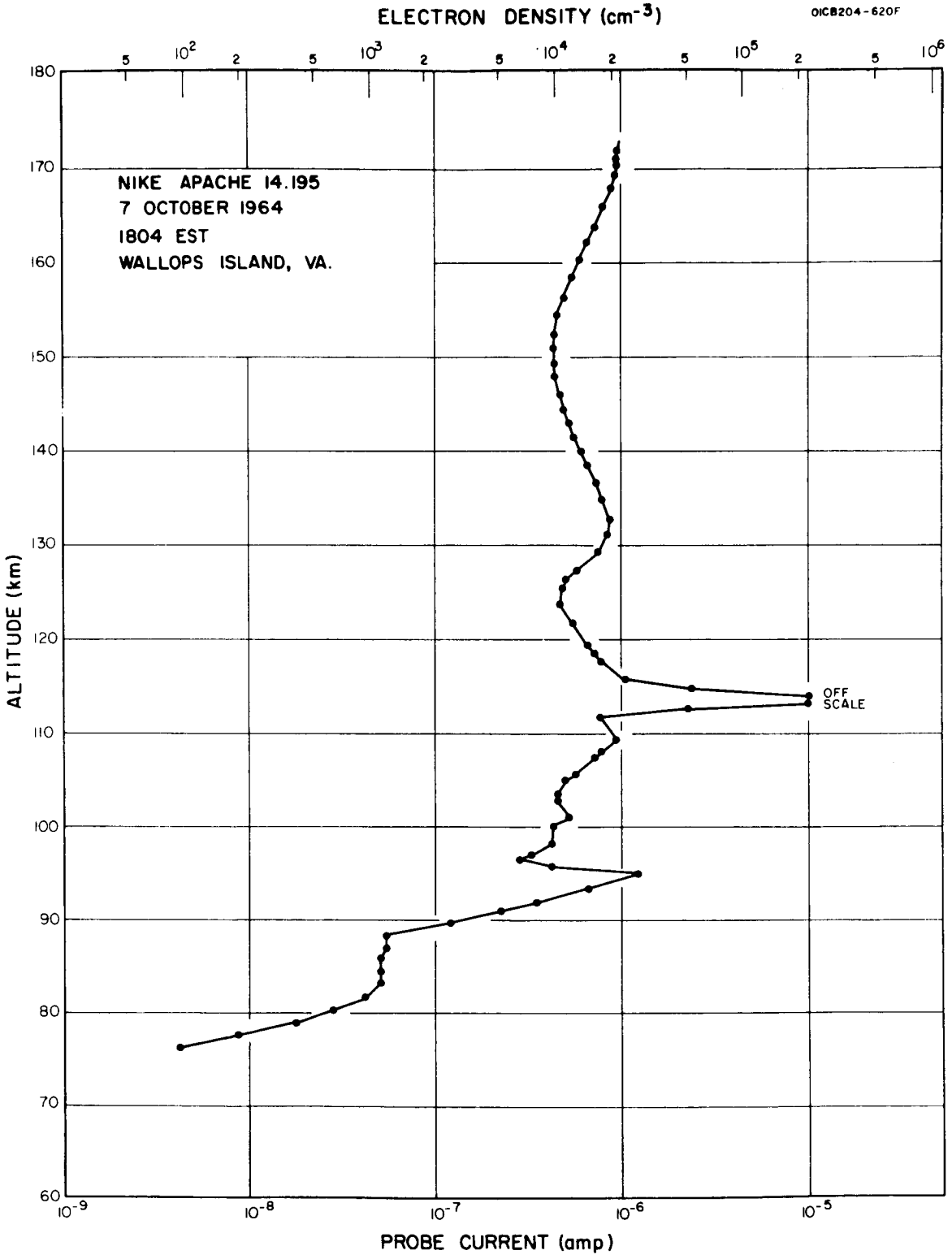

Figure 4. Electron density profile from Nike-Apache 14.195.

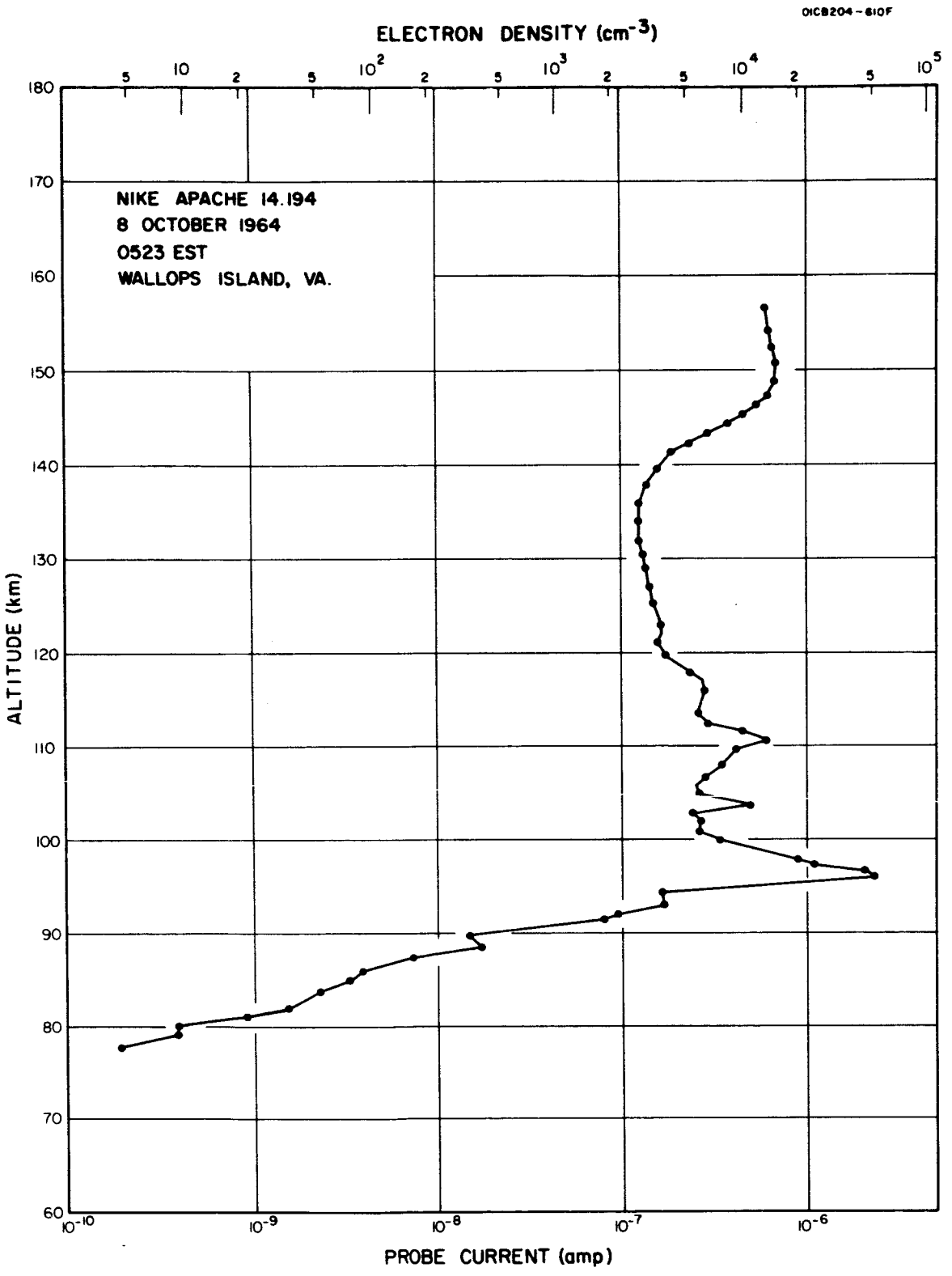

Figure 5. Electron density profile from Nike-Apache 14.194.

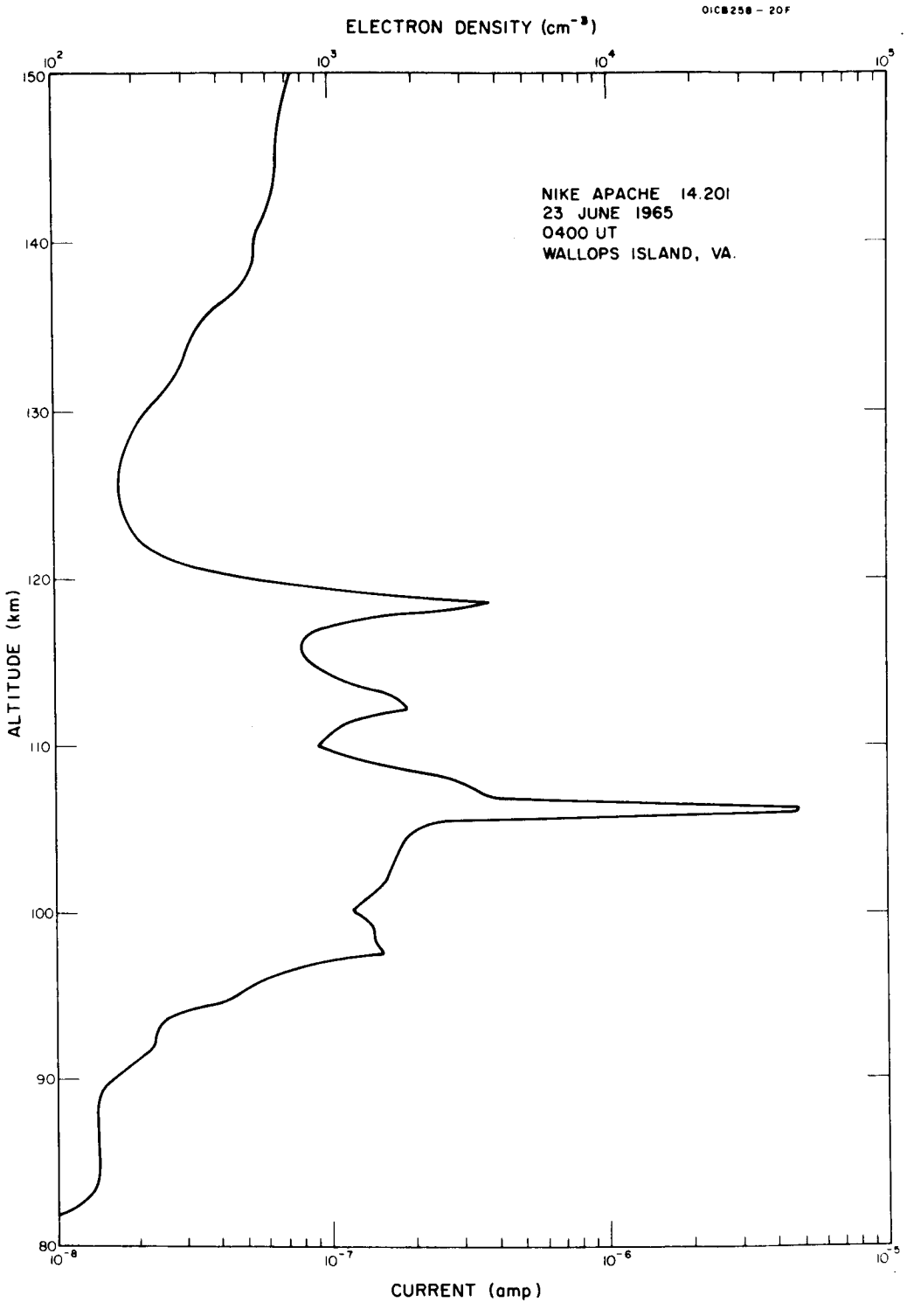

Figure 6. Electron density profile from Nike-Apache 14.201.

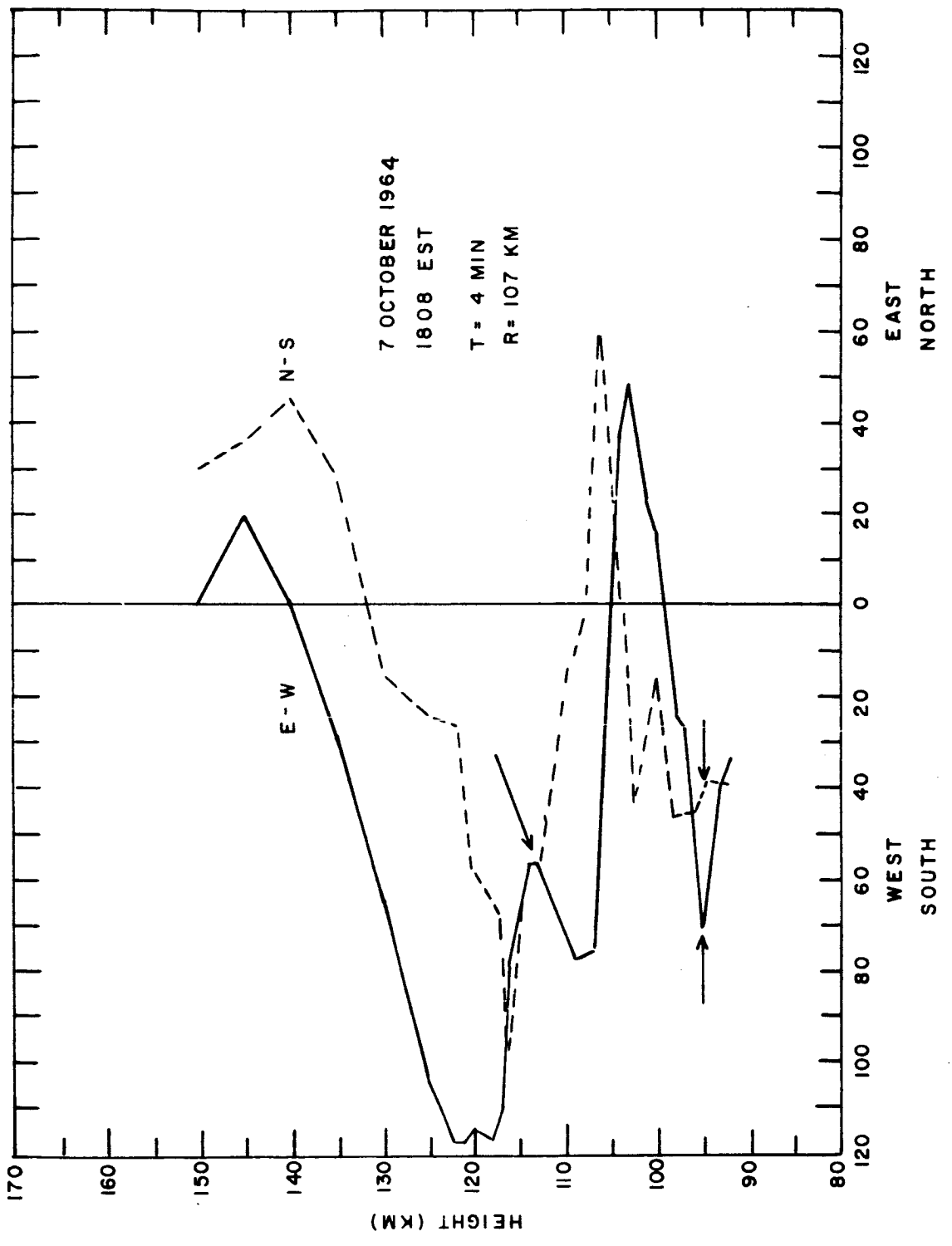

Figure 7. East-west and north-south components of wind profiles from Nike-Apache 14.195. Arrows show regions of increased electron density.

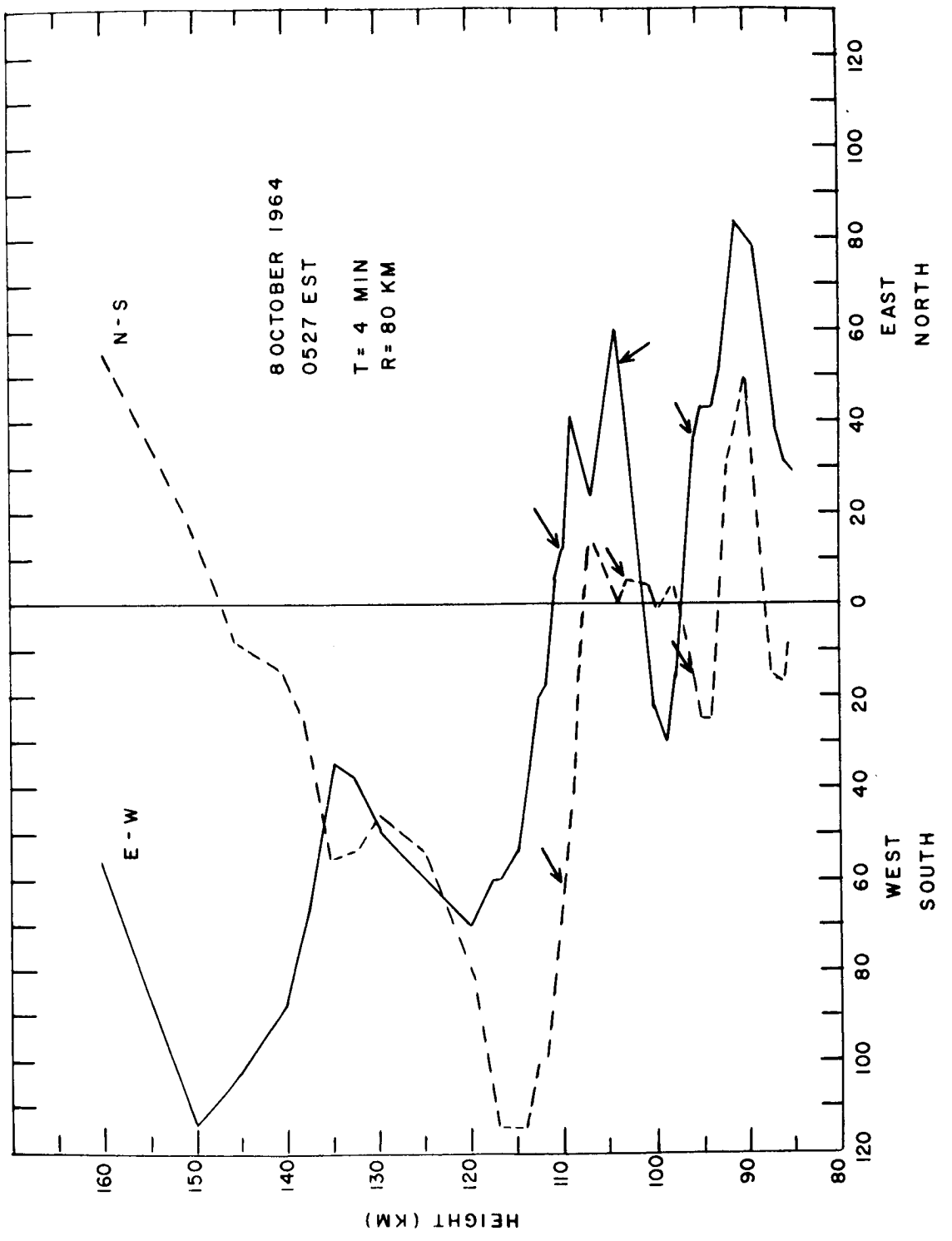

Figure 8. East-west and north-south components of wind profiles from Nike-Apache 14.194. Arrows show regions of increased electron density.

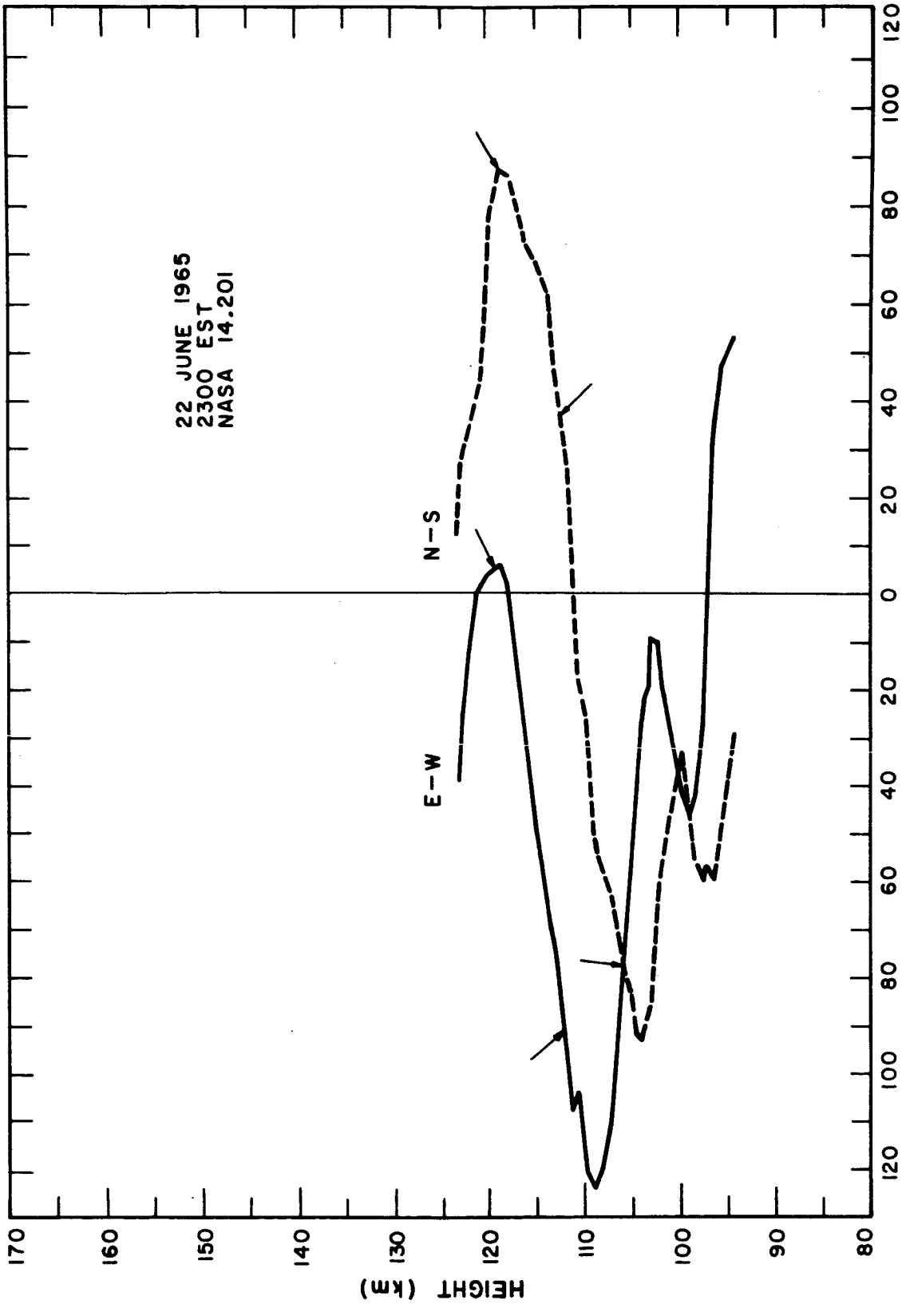

Figure 9. East-west and north-south components of wind profiles from Nike-Apache 14.201. Arrows show regions of increased electron density.

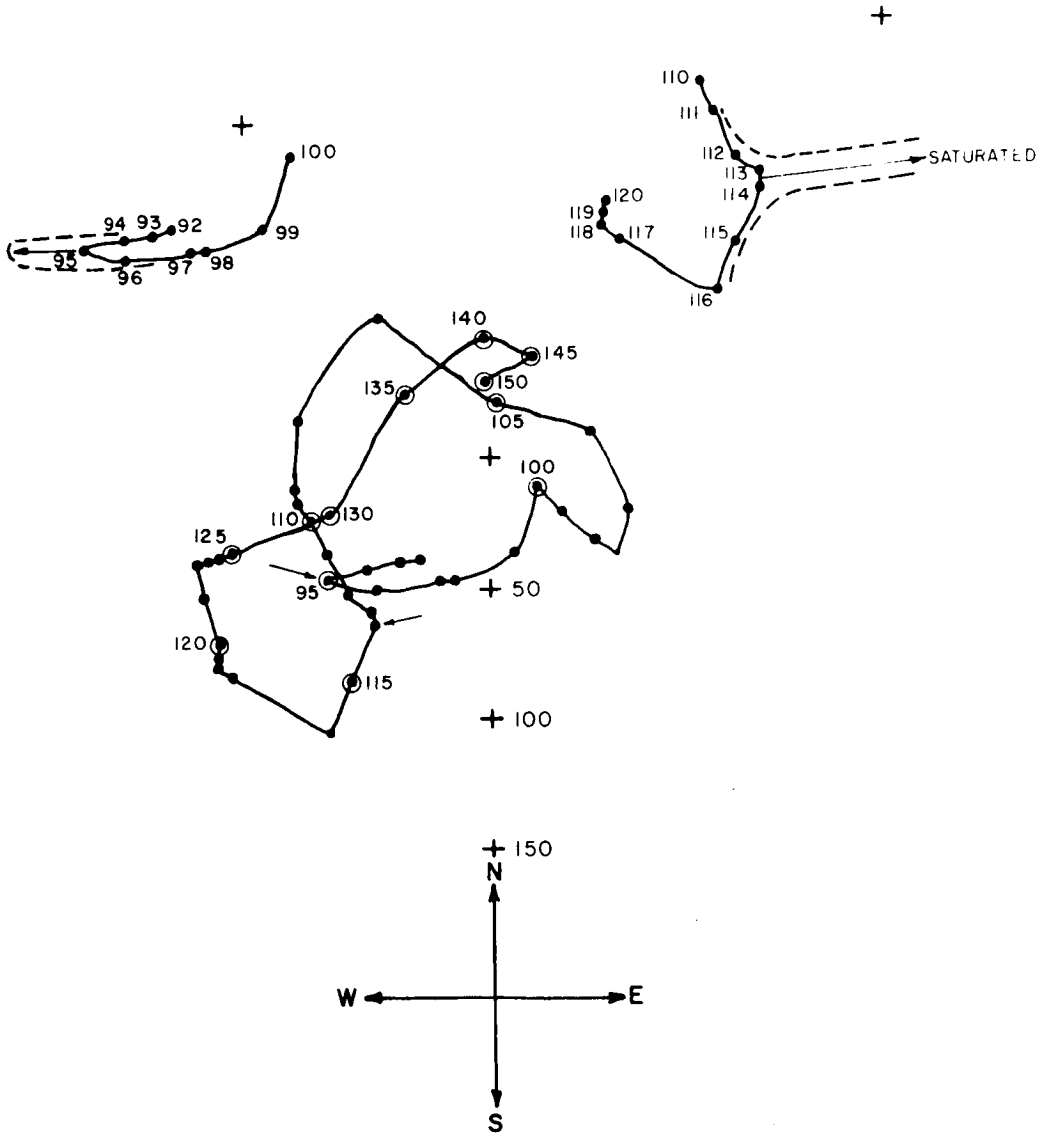

Figure 10. Hodograph of the wind profile from Nike-Apache 14.195. Regions of enhanced electron density are marked by arrows. These regions are shown separately on the same scale. The dashed lines represent the general region covered by the ionized layer.

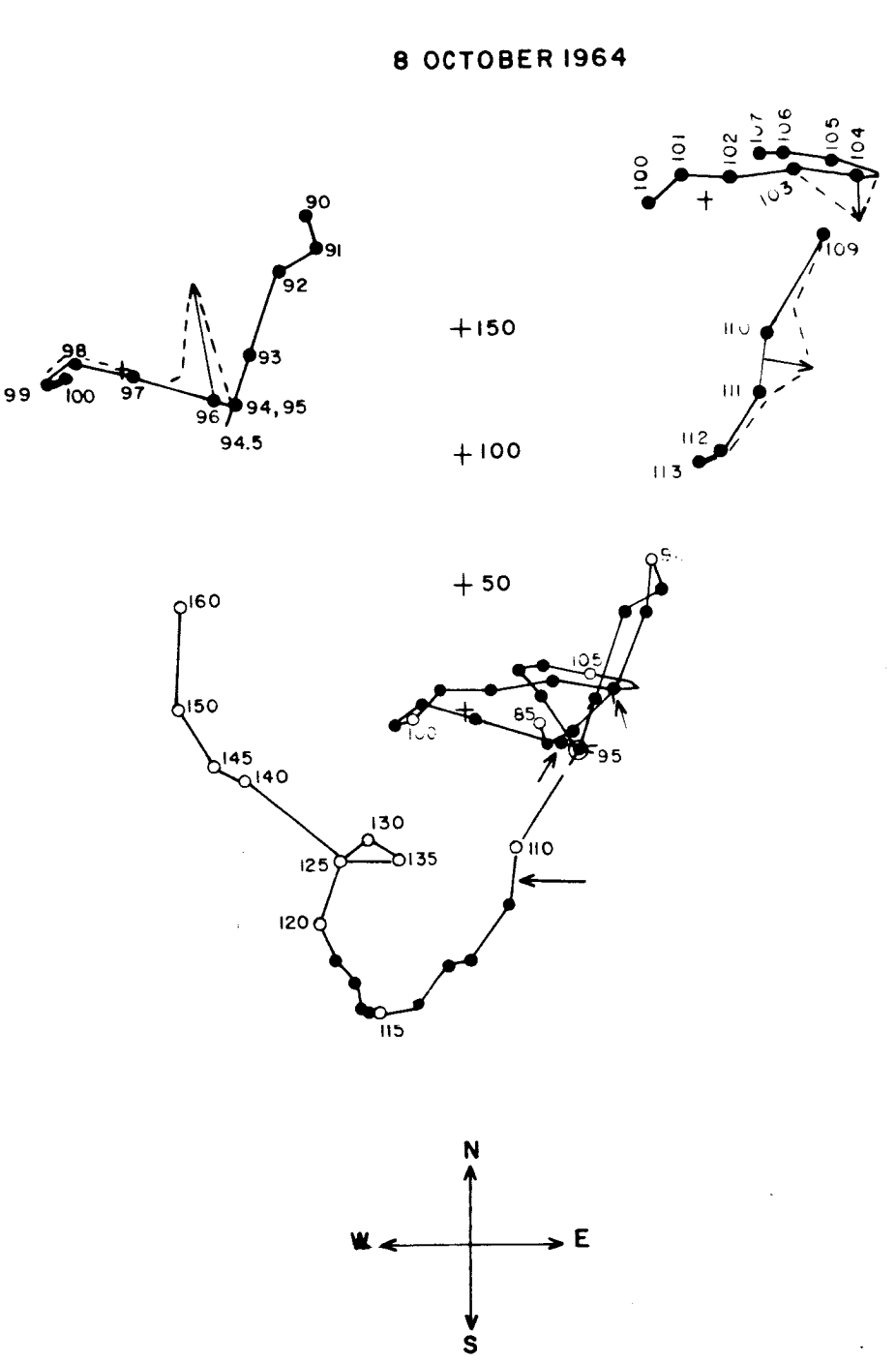

Figure 11. Hodograph of the wind profile from Nike-Apache 14.194. Regions of enhanced electron density are marked by arrows. These regions are shown separately on the same scale. The dashed lines represent the general region covered by the ionized layer.

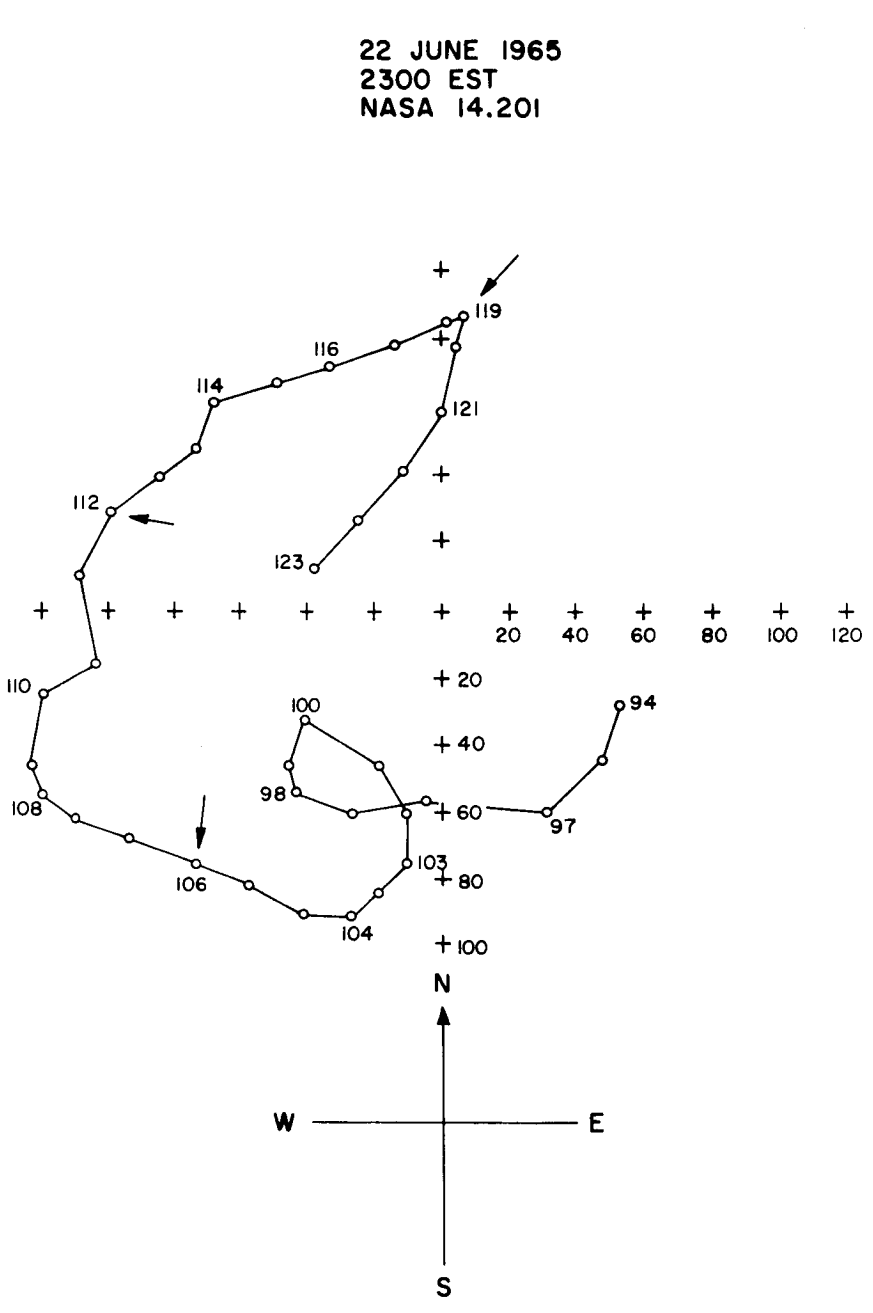

Figure 12. Hodograph of the wind profile from Nike-Apache 14.201. Regions of increased ionization are marked by arrows.

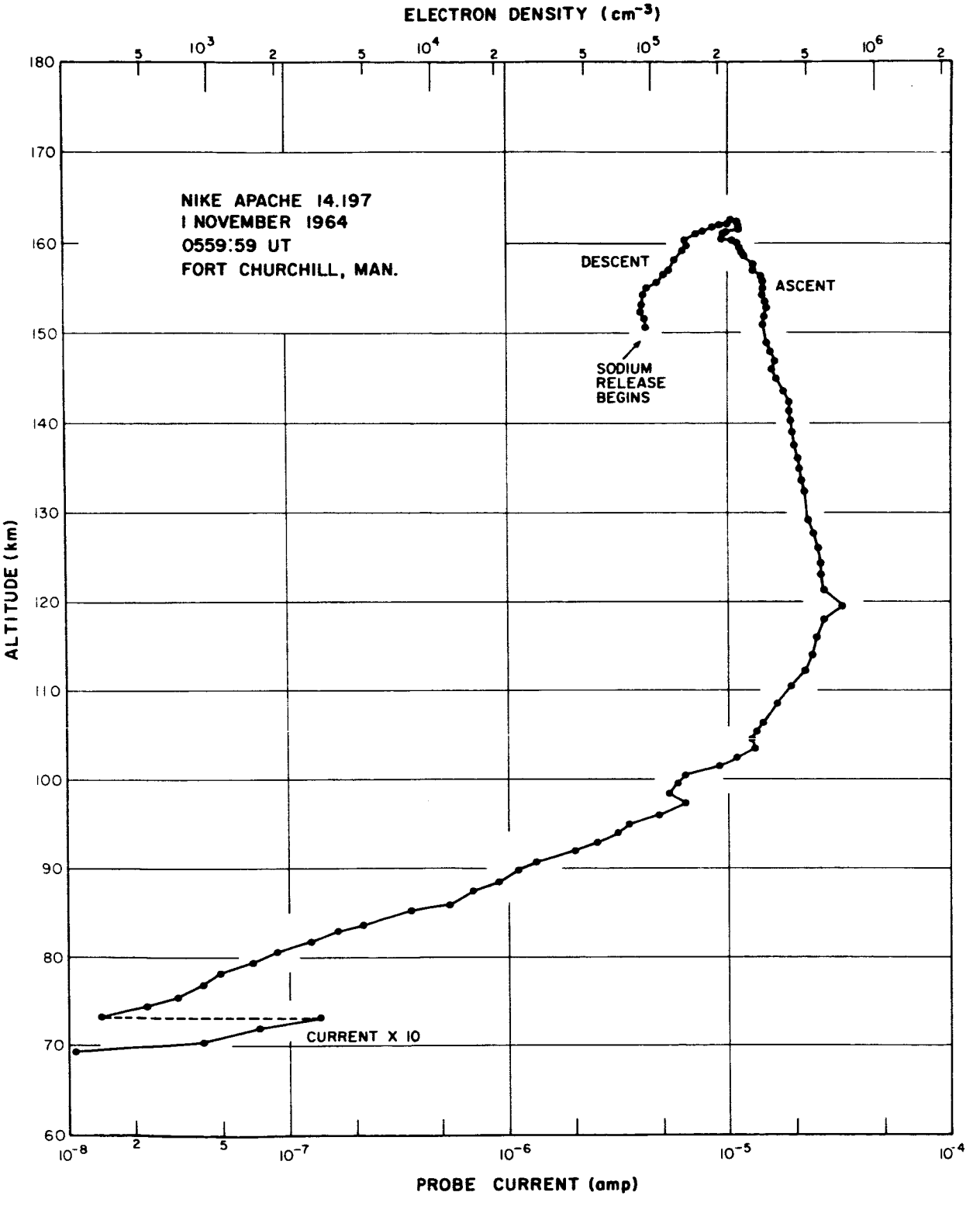

Figure 13. Electron density profile from Nike-Apache 14.197.

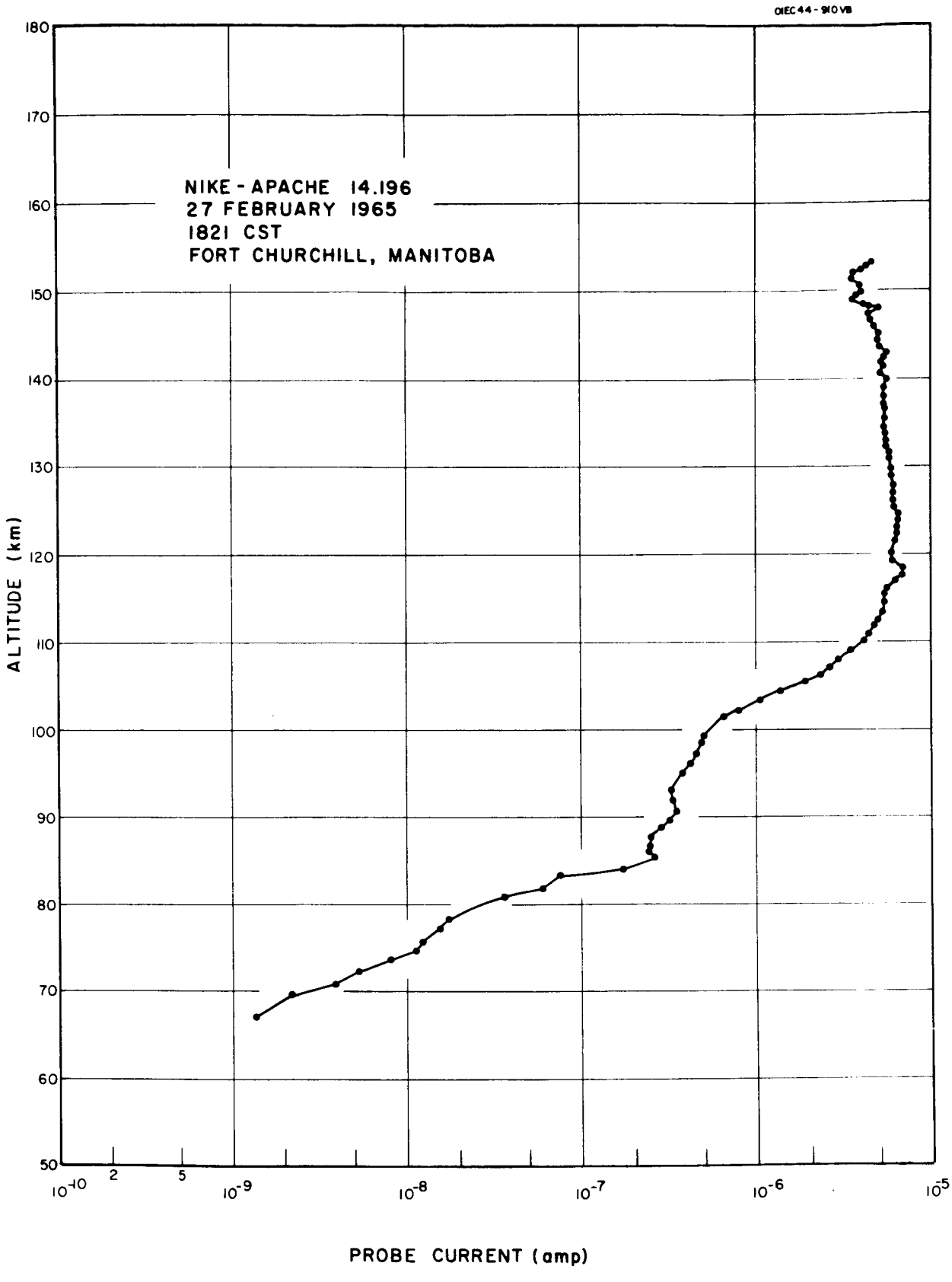

Figure 14. Electron density profile from Nike-Apache 14.196.

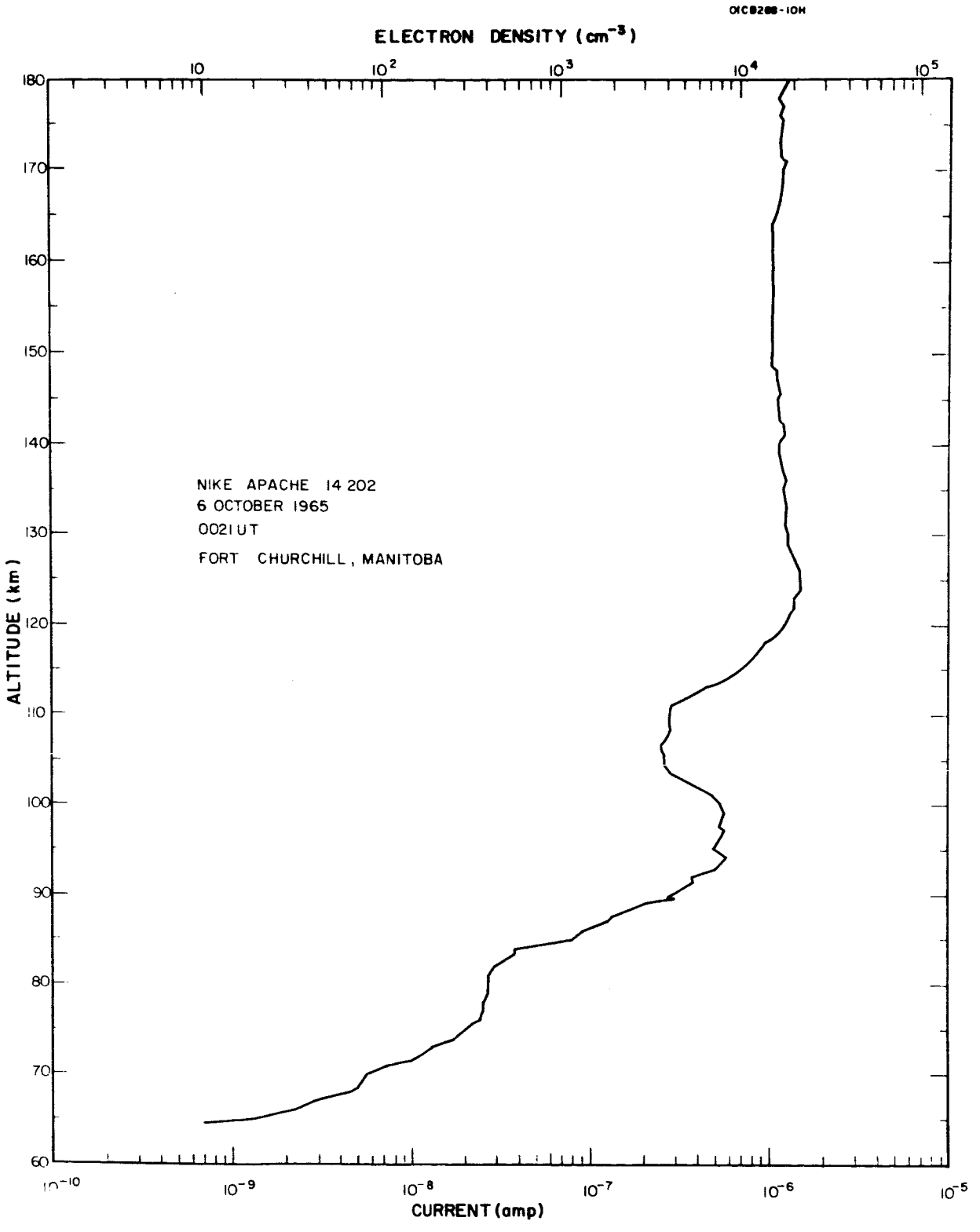

Figure 15. Electron density profile from Nike-Apache 14.202.

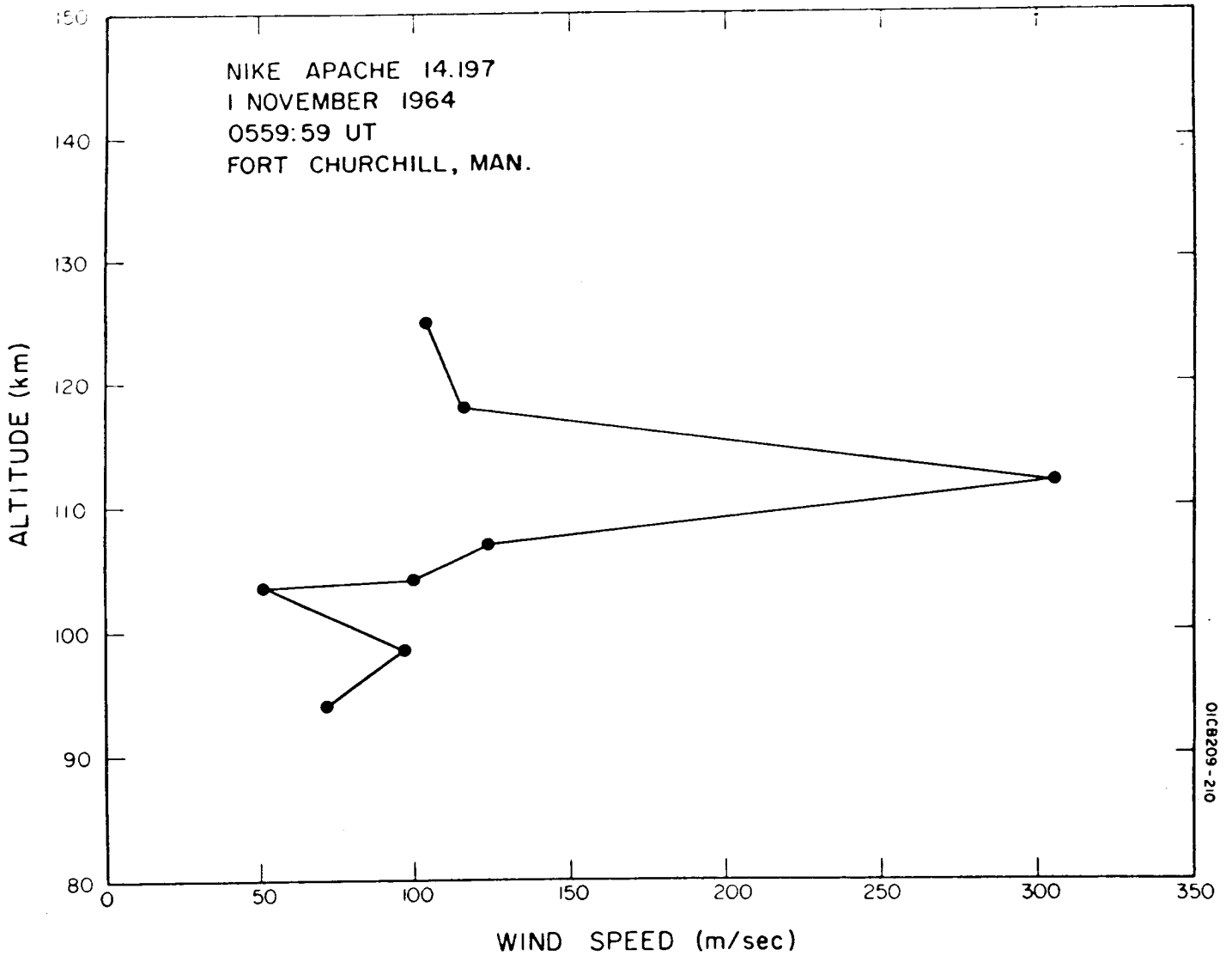

Figure 16. Wind velocity data from Nike Apache 14.197.

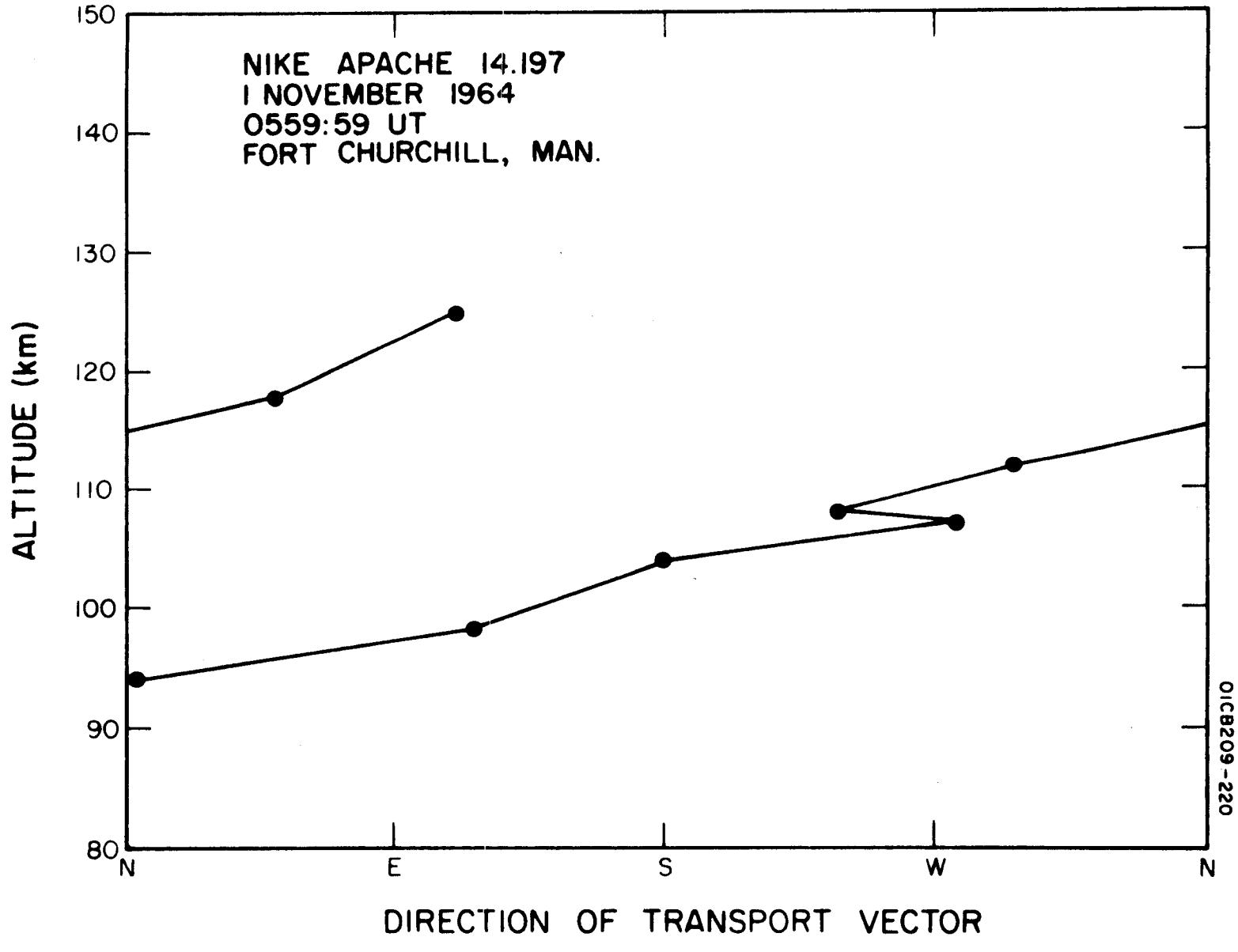

Figure 17. Wind direction from Nike Apache 14.197.

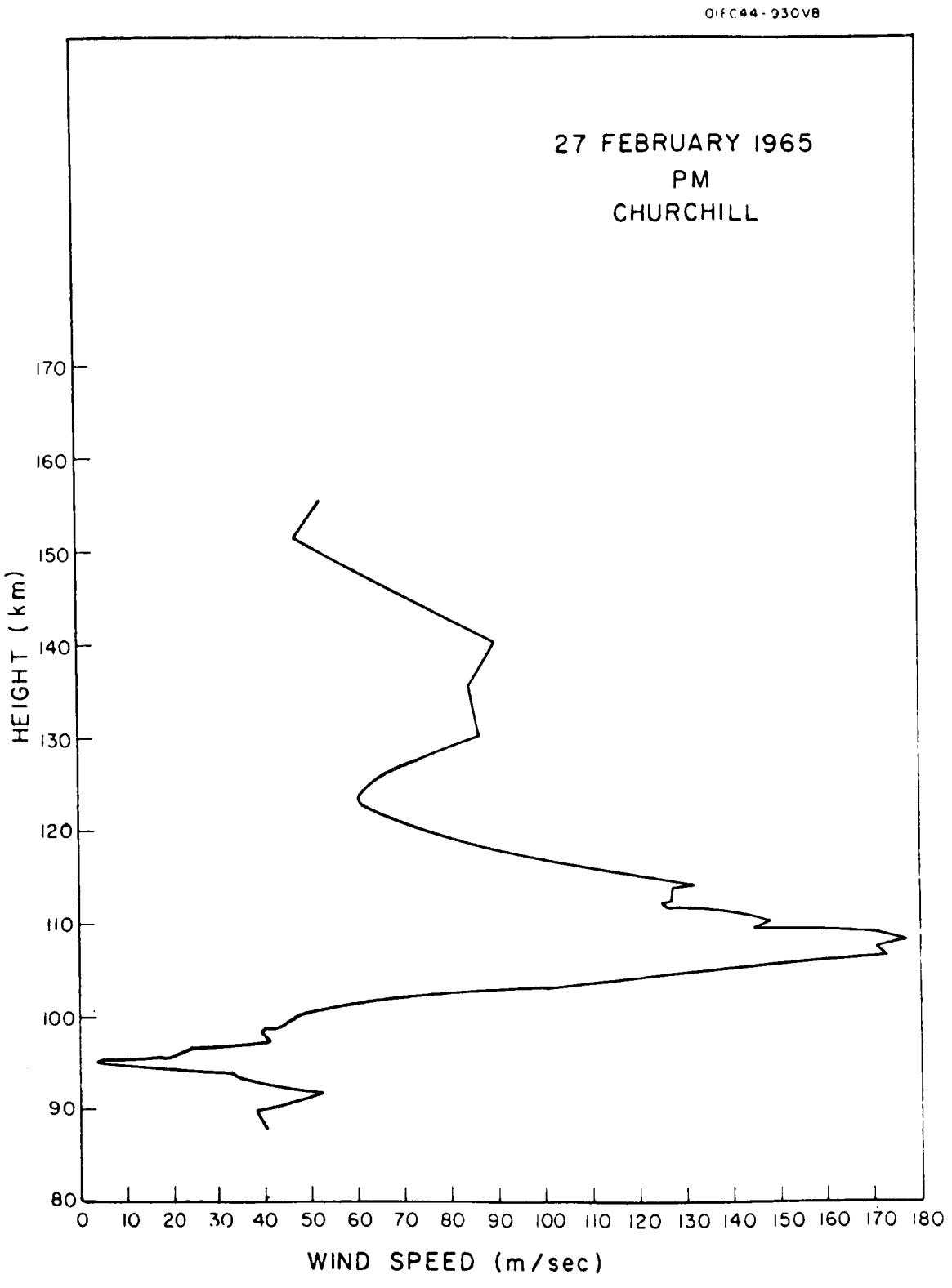

Figure 18. Wind speed from Nike Apache 14.196.

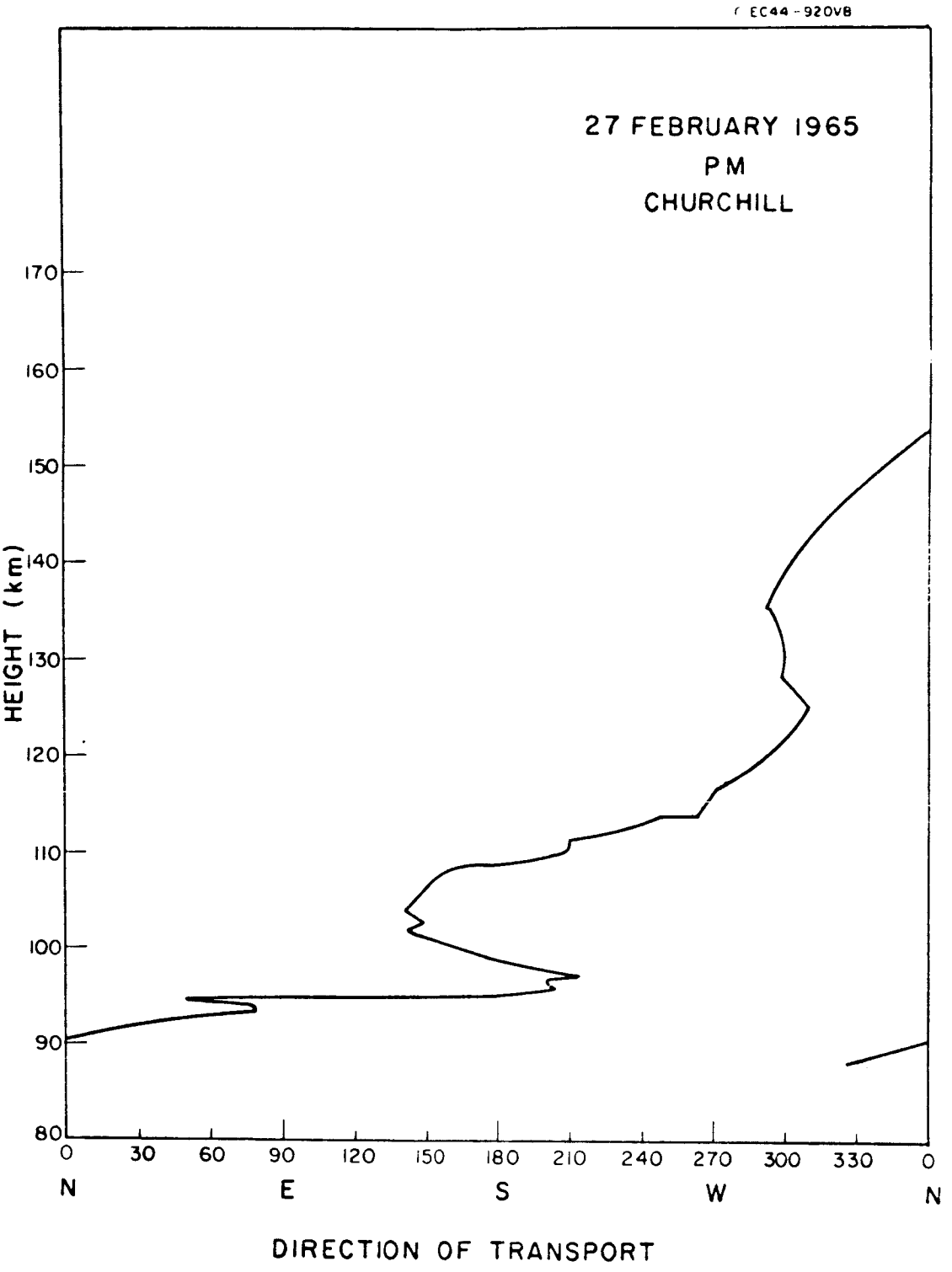

Figure 19. Wind direction from Nike Apache 14.196.

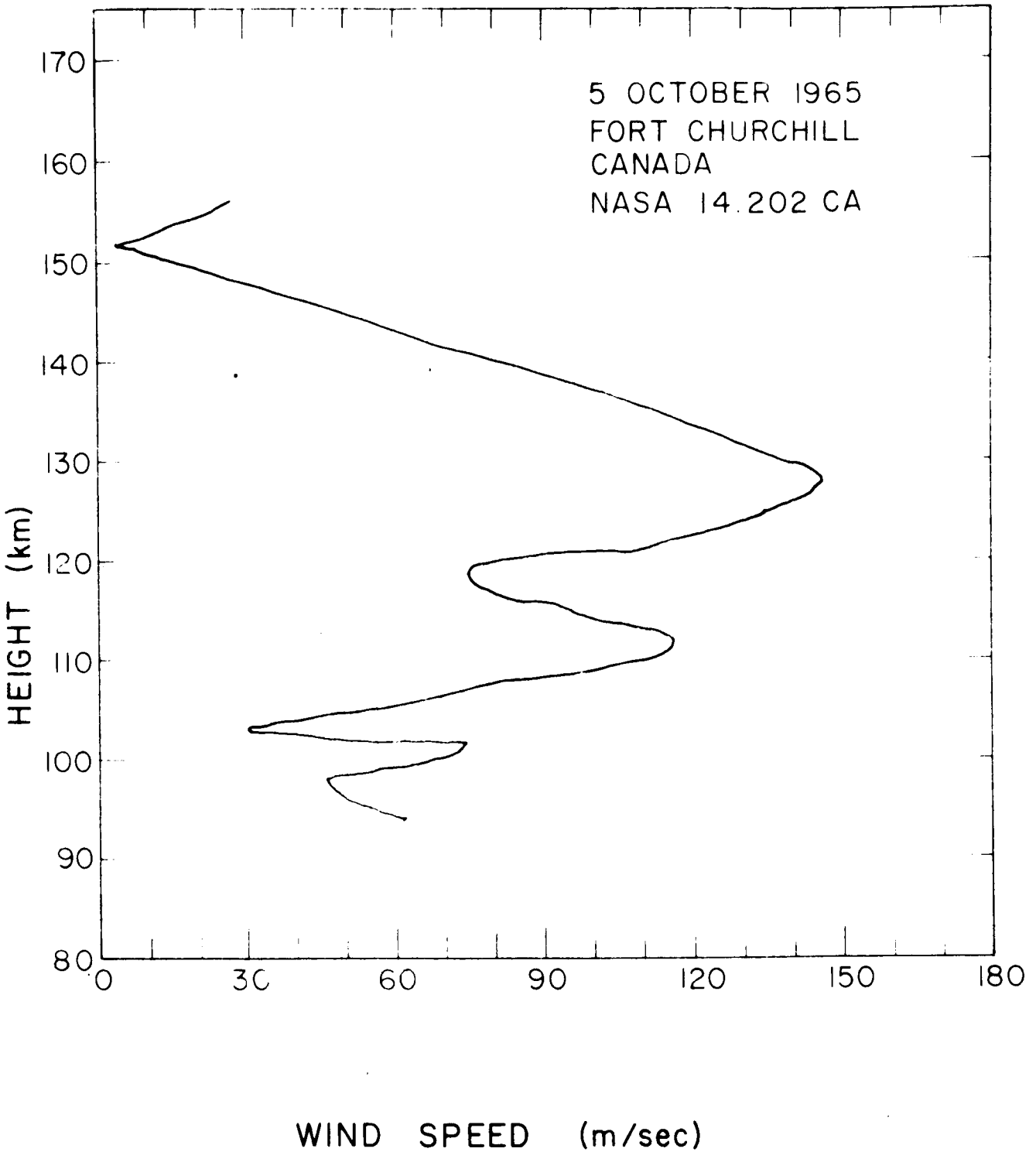

Figure 20. Wind speed data from Nike Apache 14.202.

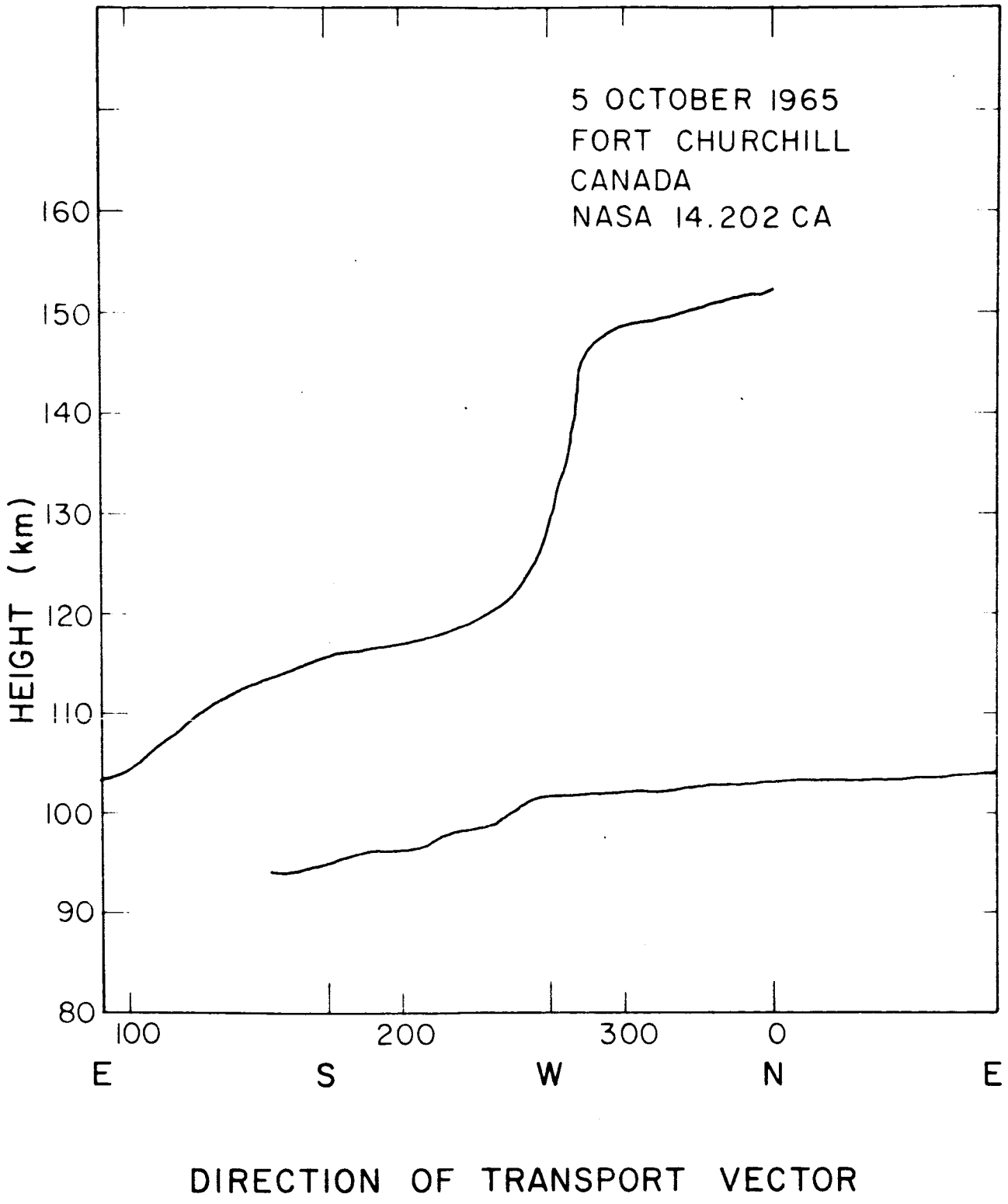

Figure 21. Wind direction from Nike Apache 14.202.

The wind profiles have structures similar to those obtained at mid-latitudes and show no direct relation to the ionization profile. The rocket difficulties prevented the observations of time variations, which were a major objective of the program and are considered important to the understanding of the dynamics of the ionosphere in the northern latitudes. For instance, local disturbances in the magnetic field are frequently observed during auroral displays, and it is usually assumed that these disturbances are caused by currents, called auroral electrojets, flowing in the auroral regions of increased ionization. Those currents may be produced by ionospheric winds driving local charged particles or by high altitude electric fields produced by incoming radiation and conducted downward along magnetic field lines. The measurement of winds and electron densities with the combined payload will help verify the wind hypothesis. Recently, Bostrom [9] calculated that winds of 440 m/sec and electron densities of 10^6 cm^{-3} are required to explain the larger magnetic disturbances which are observed. Since winds greater than 150 m/sec have seldom been observed at lower latitudes, he concluded that the currents probably result from electric fields high in the magnetosphere. However, during the rocket flight of 12 November 1964 at Fort Churchill, a wind speed in excess of 300 m/sec was observed with an electron density of 8×10^5 cm^{-3}. These conditions are very close to those computed to be necessary if the wind hypothesis is valid. Suggestions for future observations at Wallops Island, Virginia and from Fort Churchill are given in the concluding section of this report.

MEASUREMENTS OF UPPER ATMOSPHERE TEMPERATURES USING THE FLUORESCENCE SPECTRUM OF ALUMINUM OXIDE

The computer program for the calculation of synthetic molecular spectra requires detailed information on the solar spectrum. It is also necessary to describe accurately the fluorescence mechanism in order to write the program. Spectra of the sun were obtained on several days at Fort Churchill, with a resolution of 1.5Å, complete with polarization measurements. While there is now enough information available to describe the initial excitation-initial radiation process, there is some doubt as to the speed of vibrational and rotational relaxation. At low altitudes it is safe to assume that the aluminum oxide (AlO) molecules regain a Boltzmann distribution of vibration and rotation energy levels, but at higher altitudes possibly including the region of principal interest, it is no longer safe to make this assumption, due to the relative infrequency of collisions with the ambient atmosphere. It would appear that the rotational spectrum should be capable of giving accurate temperatures at higher altitudes. Discussion of this point follows the analysis of solar spectrum data given below. Using data already published for the relative intensity of vibrational bands in the three brightest sequences, temperatures have been tentatively estimated for the trails laid at Wallops Island in June 1965 and at Fort Churchill in October 1965. As would be expected, these are slightly higher than required for agreement with the 1962 Standard Atmosphere. These results are presented following the discussion of the fluorescence process.

Measurements of the Solar Spectrum

Detailed measurements of the solar spectrum have already been published, but the information given is not adequate for our purposes. High resolution (about 0.01-0.02Å) spectra are given by Minnaert, et al. [10]; however, these measurements were made on a small spot in the center of the solar disc. Consequently the Fraunhofer lines are deeper and narrower than when observed in the integrated light of the sun. Measurements on the integrated light of the sun have been made by Stair and Johnston [11] and by Dunkelman and Scolnik [12]. These were made primarily for the absolute determination of the solar constant, and the bandpass in both cases was greater than 10Å. Measurements were made of the sun from Fort Churchill at a variety of elevation angles. Ideally this type of measurement should be made from a site located at high altitude, low latitude, and renowned for its atmospheric clarity. Fort Churchill does not satisfy any of these requirements, but since only relative intensity was required, and since the atmospheric absorption spectrum contains no strong features in the region 4600-5200Å [13,14], the Fort Churchill location may not be too serious a disadvantage.

A 1/2-meter spectrometer made available by Mr. W. G. Fastie of the Johns Hopkins University was used. A telescope of diameter 12.382 cm and focal length 61.277 cm images the feature of interest on the entrance slit. As the primary solar image would be about 0.5 cm in diameter, and the required slit width was less than 0.1 mm, it was decided to place a diffusing screen over

the telescope lens. A sheet of paper was found to be nonpolarizing and to have uniform transmission in the range 4600-5200Å. The use of this also prevented damage to the entrance slit jaws by the intense image of the sun that would otherwise have been formed. Screening the diffuser from large sections of the sky showed that the signal contained a negligible contribution from the sky. The sighting telescope had already been lined up so that had a solar image been formed, it would have been accurately centered on the entrance slit. It was found that, thanks to the diffuser, pointing was not critical, and the problem of guiding accurately on the sun was also avoided. It was found that the resolution attainable was limited by the inability to control the slit width below the smallest setting (0.1 mm). Although the slits could be closed right down to zero width, the smallest setting that could be achieved proved to have a bandpass of 1.5Å. Although this could possibly have been improved by a complete check on the instrument, this was not tried, since the signal decreased much more rapidly close to zero slit width than it did at larger settings. Measurements were made at approximately 5° intervals of solar elevation with the diffuser only, and with the polaroid placed in front of the diffuser lined up both parallel to, and perpendicular to, the grating rulings. At 1.5Å resolution it was apparent that few Fraunhofer lines were large enough to cause a significant deviation from a continuous spectrum. A comparison spectrum was taken where the sun's disc was imaged on the slits, so that light from a narrow strip along a solar diameter was examined. This showed the Fraunhofer lines more strongly, as would be expected.

The Molecular Fluorescence Process

Excitation. - If the number of molecules in the ground state vibrational level v'' is $N(v'')$ and the number of photons in the energy range $\nu \rightarrow \nu + d\nu$ is $f_p(\nu)d\nu$, then the rate of excitation to the vibrational level v' (of the excited electronic state) is given by Bates [15] to be

$$\sum_{v''} \left\{ N(v'')\ p(v'v'') \int K_p(\nu)\ f(\nu)\ \nu\ d\nu \right\} \text{ per sec}$$

$K_p(\nu)$ is zero except when ν is very close to $\nu(v'v'')$. Bates used the "vibrational overlap integral squared" (now called the Franck-Condon factor) for $p(v'v'')$, on the assumption that the transition moment varied slowly with mean internuclear distance. Although this is certainly true in the case of parallel-type transitions ($\Delta\Lambda = 0$), it is now known that it is more accurate to write

$$p(v'v'') = R_e^2\ (\bar{r}_{v'v''})\ q_{v'v''}$$

where $q_{v'v''}$ is the Franck-Condon factor, $p(v'v'')$ is known, from laboratory measurements of the relative intensity of bands $q_{v'v''}$ may be calculated, and thus the function $R_e^2\ (\bar{r}_{v'v''})$ is determined. Here $R_e(r)$ represents the electronic transition moment and its variation with internuclear distance, and

$$\bar{r}_{v'v''} = \frac{\int \psi_{v'}\, \psi_{v''}\, r\,dr}{\int \psi_{v'}\, \psi_{v''}\, dr}$$

is termed the r-centroid of the transition.

Emission. - It is now possible to calculate the rate of excitation of each vibrational level of the excited electronic state. If $g(v')$ is the rate of population of the level v', and since the spontaneous transition probability associated with the band $(v'v'')$ is proportional to $p(v'v'')\ \nu(v'v'')^3$, the rate of photon emission in this band is given by

$$a(v'v'') = \frac{g(v')\ p(v'v'')\ \nu(v'v'')^3}{\sum p(v'v'')\ \nu(v'v'')^3} \text{ per sec.}$$

The intensity $I(v'v'') = h\ \nu(v'v'')\ a(v'v'')$. Here again we see that the Franck-Condon factors are involved, since

$$p(v'v'') = R_e^2\ (\bar{r}_{v'v''})\ q_{v'v''}$$

Franck-Condon Factors. - A simple method for the calculation of Franck-Condon factors in the case where the molecular vibrations have simple harmonic motion has been given by Mannenback [16,17]. Values of $(v'v'')$ for v' and v'' in the range 0-3 have been calculated, and have been found to be in agreement [18] with those used by Armstrong [19]. Bates has published a set of tables [20] allowing the evaluation of Franck-Condon factors in both the harmonic oscillator case and in the case where a nonlinear term is introduced. Franck-Condon factors have also been evaluated using these, and there is fair agreement with the results given by the Mannenback method. However, the most accurate model of molecular internuclear potential is given by the Morse curve, and calculations of Franck-Condon factors for AlO using this model have been made by Nicholls [21]. Excellent agreement with Nicholls' results is obtained by Tawde and Korwar [22] using the numerical integration method of Bates [15], also based on the Morse potential curve. Intensity measurements have been made on the spectrum of an aluminum arc in air by Hebert and Tyte [23] and by Tawde and Korwar [24] in order to determine the variation of R_e with r. Both allowed for the overlapping of adjacent bands, and both provided a least-mean squares fit to this data. In spite of this, Hebert and Tyte obtained a variation of the form

$$R_e(r) = \text{const.}\ (1\text{-}0.46\ r)$$

while Tawde and Korwar obtained

$$R_e(r) = \text{const.}\ (1\text{-}1.093\ r)$$

The results of Hebert and Tyte may be accepted in view of the fact that a later set of measurements by them [25] on widely differing sources of AlO bands gave substantial agreement with their earlier result.

A discrepancy in the published values of $p_{v'v''}$ has been noted, which had not been noticed by Hebert and Tyte. Regardless of the manner in which the upper vibrational levels are excited, the relative transition probabilities, and hence the relative intensities in any v' progression (horizontal row of a Deslandres table) should show a constant magnitude. Looking at the published data for the v' = 0 progression, we obtain Table 3.

TABLE 3

Experimenters	Source	Vibrational Temp. °K	0-0	0-1	0-2
Hebert & Tyte	AC arc	2900	100	9.4	0.5
Tawde & Korwar	DC arc	5000	100	13.7	-
Tyte & Hebert	Shock Tube	3600	100	23	1.2
Tyte & Hebert	Expl. Foil	5800	100	38	1.1

Considerable smoothing of the plot of $R_e(r)$ versus $\bar{r}$ was used by Hebert and Tyte in obtaining their expression

$$R_e(r) = \text{const.}\ (1\text{-}0.46\ r)$$

Thus it cannot be ascertained whether the scatter in relative intensities is due to variation of $R_e(r)$ with the conditions of excitation, or is due to optical thickness of the more intense bands. If the data of Tawde and Korwar is excluded, the variation of $I_{0\text{-}0}/I_{0\text{-}1}$ with temperature would favor the latter assumption.

It is felt that with the present values of relative transition probabilities, the computer program is not justified and accurate data on vibrational temperatures may not be obtained. The spectroscopic data is not of sufficient quality to yield rotational temperatures.

Relaxation. - The absorption and emission processes described above (a and b) will be repeated as long as the AlO molecules remain sunlit. After one cycle the ground state distribution of vibrational and rotational levels will not

be a Boltzmann distribution until the molecules have made a sufficient number of collisions with the ambient atmosphere. In the complete absence of such collisions (which would effectively be the case at extremely high altitudes) the vibrational and rotational temperatures would ultimately correspond to the temperature of the solar radiation. The vibrational levels may also be depopulated by radiative processes. In this case the equilibrium distribution will be determined by the infrared radiation from the sun and from the earth. The transfer of vibrational energy in heteromolecular collisions is slow, except where there is a similarity in the vibrational energy levels of the two molecules [26]. The vibrational energy quantum for the prevalent atmospheric molecule, N_2, is much greater than that of AlO. Vibrational relaxation is also relatively rapid when the nonrelaxing molecule is light (e.g., H_2 or He_2) [27], but this will not apply to the present AlO trails. The number of collisions necessary is certainly not less than 10^4 and may be as great as 10^8.

In the case of rotational relaxation, since the energy involved is small, relatively few - perhaps 10-20 - collisions are necessary [28]. It would thus appear that while the vibrational energy level distribution in the ground state may not be determined by the translational temperature, there is good reason to believe that the rotational energy level distribution does correspond to the ambient atmospheric temperature up to about 200 km. Above this limit, it may be necessary to measure the Doppler width of emission lines, whether of atmoic or molecular origin.

Estimated Vibrational Temperature

A trail of TMA was ejected at Fort Churchill at evening twilight on 5 October 1965 and the blue-green band system of AlO was observed for some 35 minutes. Spectra of the $\Delta v = 0$ and ± 1 sequences were obtained at the following times and resolutions.

Time (CST)	Slit Width (mm)	Resolution (Å)
1824:10 - 1827:51	0.2	3.5
1827:51 - 1829:00	0.1	3.0
1829:00 - 1845:37	0.2	3.5
1845:37 - 1900:00	0.5	6.0

The resolution was obtained by the measurement of the half-width of the profile of the 4916Å line of mercury before and after each set of scans at a particular slit setting. Because the local temperature and dew-point were both 32°F considerable trouble was caused by condensation on the spectrometer telescope and on the sighting telescope.

Measurements were made on the peak intensity of each band, having subtracted the continuum background (which varied smoothly with wavelength). The areas under each band were also measured. An error is introduced in the measurement of peak intensities since adjacent bands overlap. Measurement of the

areas would tend to reduce this error, but although the bands are sufficiently similar in form to justify measuring the total intensity of bands where the rotational lines are unresolved, it is necessary to decide the upper and lower wavelength limits of the integration so as to include identical ranges of rotational quantum number. Thus the area method is not free from error.

Temperatures were estimated (see Table 4) using the published data of Authier for the $\Delta v = \pm 1$ sequences [29], and of Armstrong [30] for the $\Delta v = 0$ sequence. Comparison of the intensity ratio, given by the use of the two different sets of Franck-Condon factors shows that the latter will yield temperatures which are too high.

TABLE 4

Time (CST)	Altitude (km)	Band Ratio	Method	Temperature (^{o}K)
1826:42	155	11/00	Armstrong (A) Peak	> 3000
			(A) Area	1790
1827:26	155	21/10	Authier (B) Peak	> 2375
			(B) Area	1950
1828:25	130	21/10	(B) Peak	900
1828:42	130	11/00	(A) Peak	1700
1829:25	155	21/10	(B) Peak	1130
		21/10	(B) Area	1125
		32/10	(B) Peak	1190
1830:00	155	12/01	(B) Peak	1450
		12/01	(B) Area	1190
		23/01	(B) Peak	1280
		21/10	(B) Area	1120
1830:25		21/10	(B) Peak	1050
		21/10	(B) Area	1025

A temperature of 900^{o}K was also obtained for a point at altitude 130 km. The average temperature obtained from the peak intensity ratio at 155 km is 1020^{o}K, and for the integrated band intensity ratio is 1115^{o}K. The 1962 Standard Atmosphere gives a temperature of 960^{o}K. It is expected that making allowance for the overlapping of adjacent bands would bring better agreement. The collision frequency here is about 17 sec^{-1}, but the intensity calibration made available with the spectrometer was not sufficient to enable the average rate of excitation of each molecule to be obtained. Both Authier and Armstrong showed that the interval between electronic excitations of the average molecule is 10-100 seconds. While this is insufficient for vibrational deactivation by collisions, it is long enough for the vibration-rotation bands to be emitted (about 10.22μ). It appears that Authier, in calculating vibrational band intensities, used Franck-Condon factors for the band strength, whereas it would be more accurate to use

$$p_{v'v''} = R_e^2 \, (\bar{r}_{v'v''}) \, q_{v'v''}$$

OBSERVATION OF THE SPECTRUM OF COMET IKEYA-SEKI USING A ONE-HALF METER FASTIE SPECTROMETER

Comet 1965f was discovered by K. Ikeya and T. Seki on 18 September 1965. Subsequent observations and computations showed that it would pass close to the sun, coming within about 290,000 miles of the photosphere, perihelion occurring at 0415 UT on 21 October 1965. Although eighth magnitude at discovery, it was anticipated that the close approach to the sun would cause an enormous increase in brightness, accompanied by a well-developed tail. Since the declination of the comet is always negative, the southern hemisphere and low northern latitudes would be the best locations for observations. Perihelion would occur at local noon over the Pacific, and the nearest suitable site being Hawaii, an instrumented Convair 990 made several flights from Oahu in order to provide experimenters with an observing platform above most of the clouds, and also above about 70 percent of the atmosphere.

The spectrometer that was in use at Fort Churchill for measurements of the A10 spectrum could not be transported back in time for installation in the aircraft. Fortunately, there were enough components available at the Johns Hopkins University to build another instrument. The telescope incorporated the only change -- two 2-inch diameter mirrors were used, as a suitable lens was not available. They were mounted facing each other and 100 cm apart, so that a real image was formed between them and in the plane of the slit circle. The second mirror transferred this image, with unity magnification, onto the entrance slit. The first mirror had a focal length of 50 cm and the second about 25 cm.

The first flight took place on 19 October, in an attempt to make use of the short period before dawn when the comet would perhaps have a tail rising before the sun, but lying close to the horizon. Since the comet was reported to be strong in sodium emission, the wavelength range was set to scan 5400 to 6000Å. Observations started at 0500 LST, scanning the sky to the south of the sunrise point. (Local standard time (LST) = UT - 14 hours.) The first sign of dawn occurred at 0557 LST, but no resonance lines or enhanced emission lines of the upper atmosphere were observed. A slit width of 0.015 in. chosen so that the amplifier could be saturated when pointed at the day sky with the lowest possible gain (high voltage setting). At 0602 LST the D lines appeared in absorption, well resolved, and showing an apparent bandpass of 2.5Å. The small slit width probably accounts for the lack of 5577Å signals on the night sky. The sun rose at 0617 LST and observations ceased at 0634 LST. The comet was not sighted visually, nor was it detected with the aid of any instruments or filters on board. It was noted that, when observations were being made with the dawn sky background,or the sky near the sun, the roll of the aircraft modulated the intensity of continuum seen by the instrument. The roll appeared to have a characteristic period of just over 5 seconds, and by comparison with the diameter of the solar image, the amplitude was estimated to be about 3°. Corresponding variations in yaw were present, with about 1° amplitude. There were calm periods when the solar image remained steady to about $1/4^{\circ}$ for about 1 minute, and also periods of turbulence when the roll reached 10°. The

intensity modulation of the signal at times could have masked the presence of emission or absorption lines or bands. It was hoped that since the duration of the signal from a line was not more than 1 second, lines could be identified.

An afternoon flight was made on 20 October so that perihelion could be observed (1415 LST on 20 October, local standard time ≡ 0415 UT on 21 October). During this flight, observations were made over a 4-hour period during which the comet was within 10 minutes of arc of the sun. Although the comet head could be seen from the ground by occulting the sun and looking through a sodium D-line filter, this was not possible in the aircraft. It is thought that the tiny scratches on the window were responsible for this, since they scattered sunlight even when the sun was occulted. These scratches also fed a considerable amount of solar radiation into the spectrometer, which for all but the last two observation flights was looking through a standard double plexiglass window. The slits were widened while the aircraft headed east to accelerate sunset. In the night sky, the 5577Å emission line was detected, but nothing else. Observations ceased at 2030 LST.

Observation was resumed at 0455 LST on 21 October, the slit now being 0.050 in. and the passband about 10Å. The oxygen green line was detected. The twilight enhancement of the sodium resonance lines was detected by 0530 LST and became strong at 0540 LST. By 0555 LST the sky background was increasing rapidly, with the solar depression 6°. Roll modulated continuum caused the loss of the 5577Å signal by 0557 LST and of the D lines by 0559 LST. At 0604 LST the D lines appeared in absorption, with the sun about 2° below the horizon. The sun rose at 0626 LST and observations ceased at 0629 LST.

The next flight took place early on 23 October. Since the twilight sodium was masking any possible presence of D-line emission from the comet, the wavelength range was changed to 3700 to 4300Å in order to detect the calcium lines, which were reported to be present, but nothing was seen. The ranges 4000 to 4600Å and 4600 to 5200Å were also covered, but only Fraunhofer lines were seen, when the background had increased sufficiently. At 0546 LST the comet head rose, but was only visible through binoculars. At 0603 LST the increasing sky brightness made it impossible to detect.

On 24 October the tail was visible to the unaided eye for the first time, appearing at 0506 LST. The observations commenced at 0444 LST, and the 5577Å line of oxygen was detected. The Zodiacal light became prominent by 0452 LST, and when the comet tail appeared about 14 minutes later, it had about the same visual intensity. Scanning the Zodiacal light, the comet tail, and the sky background produced similar results. Only the oxygen green line appeared with no measurable change in the continuum. The enhanced D lines became strong by 0524 LST and at 0525 LST the head rose; however, the dawn sky was producing a significant background. Observations ceased at 0551 LST.

An optical window (plate glass) became available for the last two flights. Observations commenced on 25 October at 0435 LST. The Zodiacal light became prominent by 0443 LST and the comet tail became visible at 0452 LST. The comet head rose at 0515 LST, 56 minutes before the sun. On this occasion the

oxygen green line could not be detected. The entire visible spectrum was scanned, but no signals were obtained until the continuum of morning twilight appeared. The comet head rose at 0523 LST, but gave no signal that could be differentiated from that due to the background.

On October 28, signals were obtained from the head of the comet over a period of 4 minutes before roll-modulated continuum swamped the signals. The spectral content of the head appeared to be that of scattered sunlight, simimar to the sky background. The range 4600 to 5200Å was being used, but no lines or bands could be found. The tail had a similar spectrum but the signal was barely above that due to the background.

Since the only spectra obtained were continua and no trace of any line emission attributable solely to the comet was found, it must be concluded that the tail formed by the comet following perihelion was composed chiefly of dust particles. The signals were not obtained over a long enough time to allow polarization measurements to be made, nor were the observations steady enough to permit the evaluation of a color excess.

CONCLUSIONS AND RECOMMENDATIONS

Temperate Zone Sporadic-E

The difficulty of evaluating simultaneous measurements of wind and electron density profiles was discussed previously. However, at present, most of the observational data have been obtained from single, isolated rocket launches. This information is valuable although incomplete. The theory should explain the rate of build up, magnitude, persistence, and decay of ionized layers. Such verification can only be obtained from a series of observations of both phenomena spaced at suitable intervals. These sequential measurements would also aid in the interpretation of the ground based ionograms. Other very useful observations concern the comparison of the electron density and wind profiles taken simultaneously at two or more sites. Both of these phenomena are known to have spatial variations. The relation of these variations must also be contained in a complete sporadic-E theory. Spatially separated observations would also allow detection of random ionization due to meteors. The need for continued observations is evidenced by the recent modification and development of the wind shear theory of sporadic-E which was directly initiated by the simultaneous measurements of wind and electron density profiles.

Measurements At Fort Churchill

It was previously observed that during periods of auroral activity, the electron density is high in the E-region and the height profile is smooth. However, the high wind speed and electron density observed at 120 km on 12 November 1964 at Fort Churchill indicates that dynamo action in the ionosphere may be more important than previously expected. Thus, measurements within an auroral arc might help determine the origin of the auroral electrojets and also give information on the relative motions of visible auroral arcs and the ambient atmosphere.

The observations of 5 October 1965 at Fort Churchill show that there is structure on the electron density profile at times when auroral activity is low or absent. More observations at such times are required to specify the characteristics of such profiles. This may require new theories. As in temperature latitudes, the greatest information will be obtained from a series of sequential measurements which show the time variations of both the wind and electron density profiles.

Observation Of Vapor Trails From An Aircraft

The difficulties associated with the field trips to Fort Churchill emphasized two major problems which can limit the usefulness of the vapor trail method of observing winds. These are the requirements for clear weather and for establishment of remote camera sites. If these problems could be eliminated in whole or even in part, the vapor trail method could be utilized more effectively at many locations including Fort Churchill. Both of these problems may be overcome if observations are made from a high flying aircraft. The use of an aircraft has other advantages. Usually additional optical sites are established so that some cloudiness may be tolerated. However, the availability of some equipment is limited and can be placed at only one site. The aircraft could insure that the site from which photometric, spectrometric, or other special observations are being made will always be clear. The aircraft would also allow viewing from any desirable direction without regard to suitable terrain.

The establishment and usage of an airborne camera site requires some development work. However, most of the system only requires the application established techniques. Basically, there are two processes involved. The first is to obtain photographs of the vapor trail which contain the information necessary to determine winds. The speed of the camera and stability of the mounting must be such that the images have a minimum of blurring and that a background of stars is obtained to establish pointing directions. Methods of accomplishing this are well known and have been used for many years for similar purposes, as, for example, for photographing reentry vehicles.

The other area of development is in the computation of the winds from the photograph of the trail. The efficiency of this procedure is of course a function of many factors including the quality of the photographs, available observation time, complexity of the wind profile, and parameters of the flight of the aircraft. The winds may be obtained by either of two general methods. In both cases it is assumed that the winds are constant over the period of observation and there is no vertical velocity component. These assumptions have been shown to be realistic from previous ground based observations. In one method, the exact location of the aircraft is known for each of the photographs. This method may be very accurate in areas where ground based radar can track the aircraft. In this case the exact position of the vapor trail is determined.

In places where radar tracking is not available another method may be more accurate. In this case only an approximate aircraft position (within a mile or so) is required, but the parameters of the flight, i.e. altitude, heading, ground speed, are known accurately and held constant. In this method the relative motion of the trail and aircraft is measured and that of the aircraft may then be eliminated.

Temperature Determination

The method of temperature determination from the fluorescent spectrum of a TMA trail was investigated in detail on this contract. There are some areas which require more investigation. The completion of a computer program requires detailed and accurate information on the solar spectrum. It is strongly recommended that the necessary measurements be made. It is also recommended that methods and analysis be continued so that errors due to overlapping regions of adjacent bands be eliminated and that the useful altitude range of the method be determined.

REFERENCES

1. Smith, L.G., "Langmuir Probes for Measurements in the Ionosphere," NASA Contract No. NASw-1141, GCA Tech. Report No. 65-25-N (Oct. 1965).

2. Bedinger, John F., "Study of Winds, Diffusion and Expansion of Gases in the Upper Atmosphere," Final Report NASA Contract No. NASW-396, GCA Tech. Report No. 63-16-N (May 1963).

3. Corman, A. and Guarino, N.J., "Canister for Producing TMA Trails in the Upper Atmosphere," NASA Contract No. NASw-1083, GCA Tech. Report No. 65-2-N (Feb. 1965).

4. Smith, L.G., "A Simple Method of Trajectory Determination for Sounding Rockets," NASA Contract No. NASw-489, GCA Tech. Report No. 63-9-N (Mar. 1963).

5. Whitehead, J.D., "The Formation of the Sporadic-E Layer in the Temperature Zones," J. Atmos. Terr. Phys. 20, No. 49 (1961).

6. Axford, W.I. and Cunnold, D.M., "The Wind Shear Theory of Temperate Zone Sporadic-E," Cornell-Sydney Univ. Astronomy Center-Report CSUACH (Sept. 1965).

7. Taieb, E., "Groupe Resch. Ionospherique," (C.N.E.T.-C.N.R.S.-I.P.G.) GRI/MT/18 (1964).

8. Bedinger, John F. and Knaflich, H.B., "Observed Characteristics of Ionospheric Winds," NASA Contract No. NASw-1083, GCA Tech. Report No. 65-26-N (Aug. 1965).

9. Bostrom, Rolf, "A Model of Auroral Electrojets," J. Geophys. Res. 69 No. 23, 4983-99 (Dec. 1964).

10. Minnaert, M., Mulders, G.F.W., and Houtgast, J., Photometric Atlas of Solar Spectrum, Amsterdam (1940).

11. Stair, R. and Johnston, R.G., "Preliminary Spectroradiometric Measurements of the Solar Constant," J. Res. Nat'l. Bur. Std. 54 No. 4, 205-11 (Oct. 1956).

12. Dunkelman, L. and Scolnik, R., "Solar Spectral Irradiance and Vertical Atmospheric Attenuation in the Visible and Ultraviolet," J. Opt. Soc. Am. 49 No. 4, 356-67 (April 1959).

REFERENCES (continued)

13. Anon., Handbook of Geophysics, Macmillan, New York, pp. 15-16 (1961).

14. Curcio, J.A., Drummeter, L.F., and Knestrick, G.L., "An Atlas of the Absorption Spectrum of the Lower Atmosphere from 5400Å to 8520Å," Applied Optics 3, 1401-09 (Dec. 1964).

15. Bates, D.R., "The Intensity Distribution in the Nitrogen Band Systems Emitted from the Earth's Upper Atmosphere," Proc. Roy. Soc. (London) 196A, 217-250 (March 1949).

16. Mannenback, C., "Computation of the Intensities of Vibrational Spectra of Electronic Bands in Diatomic Molecules," Physica 17 No. 11-12, 1001-10 (Nov.-Dec. 1951).

17. Mannenback, C. and Rahman A., "Computation of Intensities of Vibrational Spectra of Electronic Bands in Diatomic Molecules II," Physica 20, 497-500 (1954).

18. Armstrong, E.B., Private Communication.

19. Armstrong, E.B., "Observations of Luminous Clouds Produced in the Upper Atmosphere by Exploding Grenadas-II Emissions of AlO Bands from Sunlit Clouds," Planet. Space Sci. 11, 743-50 (1963).

20. Bates, D.R., "Relative Transition Probabilities in Band Systems of Diatomic Molecules, M.N.R.A.S.," 112 No. 6, 614-36 (1952).

21. Nicholls, R.W., "Franck-Condon Factors to High Vibrational Quantum Numbers II: SiO, MgO, SrO, AlO, VO, NO," J. Res. Nat'l Bur. Std. 66A No. 3, 227-231 (May-June 1962).

22. Tawde, N. R. and Korwar, V.M., "Franck-Condon Factors r-Centroids for the Aluminium Monoxide $A^2\,\Sigma^+ - X^2\,\Sigma^+$ Band System," Proc. Phys. Soc. 80, 794-95 (Sept. 1962).

23. Hebert, G.R. and Tyte, D.C., "Intensity Measurements on the $A^2\,\Sigma - X^2\,\Sigma$ System of Aluminium Oxide," Proc. Phys. Soc. 83 , 629-34 (1964).

24. Tawde, N.R. and Korwar, V.M., "Electronic Transition Moment Variation in Bands of AlO ($A^2\,\Sigma^+ - X^2\,\Sigma^+$) System," Proc. Nat. Inst. Sci. India, 29A No. 3, 325-331 (1963).

25. Tyte, D.C. and Hebert, G.R., "The Electronic Transition Moment of the $A^2\,\Sigma - X^2\,\Sigma$ System of AlO," Proc. Phys. Soc. 80, 830-32 (Nov. 1964).

REFERENCES (continued)

26. Lipscomb, F.J., Norrish, R.G.W., and Thrush, B.A. and F.R.S., "The Study of Energy Transfer by Kinetic Spectroscopy - I. The Production of Vibrationally Excited Oxygen," Proc. Roy. Soc. 233A No. 1195, 455-64 (Jan. 1956).

27. Holmes, R., Smith, F.A., and Tempest, W., "The Vibrational De-Excitation of Oxygen in Heteromolecular Collisions," Proc. Phys. Soc. 83, 769-75 (May 1964).

28. Lambert, J.D., Relaxation in Gases, Atomic and Molecular Process," D.R.Bates, ed. No. 20, Academic Press, New York pp 783-806, (1962).

29. Authier, B., "Mesures De Temperature De L'Ionosphere A Partir De La Fluorescence De Molecules Prodiutes Artificiellement Au Moyen De Fusees," Ann. De Geophys. 20, 353-82 (Oct-Dec 1964).

APPENDIX A

ROCKET PERFORMANCE DATA

The predicted performance data are given in Table A-1 for the two types of payload used in the program. The data are based on an effective launch elevation angle of 80°. The actual weight of the Probe/Na Vapor payload was somewhat greater than the value used in the prediction: the probe section weighed 32.5 lb and the vapor section 53.5 lb, for a total payload weight of 86 lb. The actual weight of the Probe/TMA payload was much greater than expected: the TMA section weighed 40.5 lb for a total weight of 73 lb. The large difference resulted from design changes during the development phase.

The rocket launch data including stage ignition and burnout is given in Table A-2. This data is obtained entirely from the telemetry record. Two vehicles (14.198 and 14.199) broke up at Nike burnout and two others (14.200 and 14.203) during second-stage burning. Two payloads using sodium vapor (14.196 and 14.197) broke up late in the flight, but with no loss of scientific data.

The altitude and time of apogee for the six successful flights is given in Table A-3(a) and (b). The altitudes obtained by the time-of-flight method, using baroswitches in the payload is compared, in the case of the Wallops Island launches with the radar skin-track data. The baroswitch leads to altitudes 2 to 3 km greater than the radar value. This is rather greater than has been found on other series of flights: previously the difference has generally been less than 1 km. The time of apogee obtained by the two methods agree within 1 sec, which is comparable with previous experience.

TABLE A-1

PREDICTED ROCKET PERFORMANCE, 80° LAUNCH ANGLE

Payload Type	Probe/Na Vapor	Probe/TMA
Payload Weight	80 lb.	55 lb.
Nike Burnout Time	3.5 sec.	3.5 sec.
Nike Burnout Altitude	5,339 ft.	5,429 ft.
Nike Burnout Velocity	3,194 ft./sec.	3,247 ft./sec.
Apache Ignition Time	20 sec.	20 sec.
Apache Ignition Altitude	42,071 ft.	42,050 ft.
Apache Ignition Velocity	1,729 ft./sec.	1,699 ft./sec.
Apache Burnout Time	26.4 sec.	26.4 sec.
Apache Burnout Altitude	65,513 ft.	66,844 ft.
Apache Burnout Velocity	6,001 ft./sec.	6,530 ft./sec.
Peak Time	207.6 sec.	224.5 sec.
Peak Altitude	566,055 ft. (173 km)	660,204 ft. (201 km)
Impact Time	403.9 sec.	437.5 ft.
Impact Range	590,589 ft.	687,654

TABLE A-2

ROCKET LAUNCH DATA

Nike Apache 14.195 (7 October 1964, Wallops Island, Virginia)

Nike Ignition:	2304:00.1	UT	(T)
Nike Burnout:	2304:03.6	UT	(T + 3.7)
Apache Ignition:	2304:22.7	UT	(T + 25.0)
Impact (Loss of Signal):	2310:47.3	UT	(T + 395.4)

Nike Apache 14.194 (8 October 1964, Wallops Island, Virginia)

Nike Ignition:	1023:00.1	UT	(T)
Nike Burnout:	1023:03.8	UT	(T + 3.7)
Apache Ignition:	1023:25.1	UT	(T + 25.0)
Impact (Loss of Signal):	1029:35.3	UT	(T + 395.4)

Nike Apache 14.197 (1 November 1964, Fort Churchill, Manitoba)

Nike Ignition:	0559:59.2	UT	(T)
Nike Burnout:	0600:03.0	UT	(T + 3.8)
Apache Ignition:	0600:20.5	UT	(T + 21.3)
Impact (Loss of Signal):			(T + 579) approx.

Nike Apache 14.196 (28 February 1965, Fort Churchill, Manitoba)

Nike Ignition:	0021:00.0	UT	(T)
Nike Burnout:	0021:03.6	UT	(T + 3.6)
Apache Ignition:	0021:21.5	UT	(T + 21.5)
Impact Loss of Signal):	0030:53	UT	(T + 593)

Nike Apache 14.198 (28 February 1965, Fort Churchill, Manitoba)

Nike Ignition	0329:59.3	UT	(T)
Loss of Instrumentation Signals	0330:02.9	UT	(T + 3.6)
Impact (Loss of Signal):	0331:05.1	UT	(T + 65.8)

TABLE A-2 (Continued)

Nike Apache 14.199 (28 February 1965, Fort Churchill, Manitoba)

Nike Ignition:	0559:58.6	UT	(T)
Loss of Instrumentation Signals	0600:02.2	UT	(T + 3.6)
Impact (Loss of Signal):	0601:00.1	UT	(T + 61.5)

Nike Apache 14.200 (28 February 1965, Fort Churchill, Manitoba)

Nike Ignition:	1211:00.7	UT	(T)
Nike Burnout:	1211:04.1	UT	(T + 3.4)
Apache Ignition:	1211:21.6	UT	(T + 20.9)
Impact (Loss of Signal):	1215:47	UT	(T + 286.3)

Nike Apache 14.201 (23 June 1965, Wallops Island, Virginia)

Nike Ignition:	0359:59.9	UT	(T)
Nike Burnout:	0400:03.6	UT	(T + 3.7)
Apache Ignition:	0400:21.4	UT	(T + 21.5)
Impact (Loss of Signal):	0406:42	UT	(T + 402)

Nike Apache 14.202 (6 October 1965, Fort Churchill, Manitoba)

Nike Ignition:	0020:59.4	UT	(T)
Nike Burnout:	0021:02.9	UT	(T + 3.5)
Apache Ignition:	0021:21.1	UT	(T + 21.7)
Impact (Loss of Signal):	0027:56.2	UT	(T + 416.8)

Nike Apache 14.203 (6 October 1965, Fort Churchill, Manitoba)

Nike Ignition:	0259:59.6	UT	(T)
Nike Burnout:	0300:03.0	UT	(T + 3.4)
Apache Ignition:	0300:21.6	UT	(T + 22.0)
Impact (Loss of Signal)	0305:26.3	UT	(T + 326.7)

TABLE A-3(a)

APOGEE ALTITUDE

Nike Apache*	Radar	Baroswitch†
14.195	172.2 km	175.2 km
14.194	159.9 km	162.3 km
14.197	No Data	164.5 km
14.196	154.5 km**	No Data††
14.201	167.3 km	169.5 km
14.202	No Data	180.7 km

*Successful flights, in chronological order.

†Reference altitude used is 23.0 km.

††Sodium vapor release obscured baroswitch opening.

**No radar data; obtained from photography of vapor trail

TABLE A-3(b)

APOGEE, TIME FROM LAUNCH:

Nike Apache*	Radar	Baroswitch†
14.195	211.0 sec	210.1 sec
14.194	205.0 sec	204.7 sec
14.197	No Data	202.6 sec
14.196	199.0 sec**	No Data††
14.201	205.8 sec	206.5 sec
14.202	No Data	213.6 sec

*Successful flights in chronological order.

†Reference altitude used is 23.0 km.

††Sodium vapor release obscured baroswitch opening.

**No radar data; obtained from photograph of trail.

The precessional motion and the spin rate both measured near apogee are given in Table A-4 for the successful flights. The data are obtained from the magnetic aspect sensor. These figures show the range of values that can be expected in typical flights of Nike Apache rockets.

The spin rates for the vehicles in the early part of the flight are given in Figure A-1 for Nike Apaches 14.194/5/6/7 and 14.200 and in Figure A-2 for Nike Apaches 14.201/2/3. The former group consists of payloads using the quadraloop type of telemetry antenna while the latter group used the dipole type.

The spin rate of 14.196 is anomalous from T + 6 seconds to T + 21 seconds, but otherwise the variation within each group is attributable to unavoidable differences in fin alignments and in second-stage ignition times.

One interesting difference between the two groups is attributable to the type of antenna. Comparison of the data shown on Figures A-1 and A-2 with the data from Table A-4 show that for the payloads equipped with quadrapole antennas, the maximum spin rate occurs at second-stage ignition. In the group with dipole antennas, the maximum spin rate occurs about one second after second-stage burnout.

TABLE A-4

PRECESSIONAL MOTION AND SPIN RATE (AT APOGEE)*

Nike Apache	Precession Period (sec.)	Cone Angle (degrees)	Spin Rate (rps)
14.195	42.0	7.0	5.6
14.194	36.0	1.2	5.6
14.197	46.0	6.2	5.0
14.196	36.0	14.1	5.6
14.201	40.0	2.0	6.3
14.202	34.0	10.0	7.4

*Data obtained from magnetic aspect sensor.
Vehicles listed in chronological order.

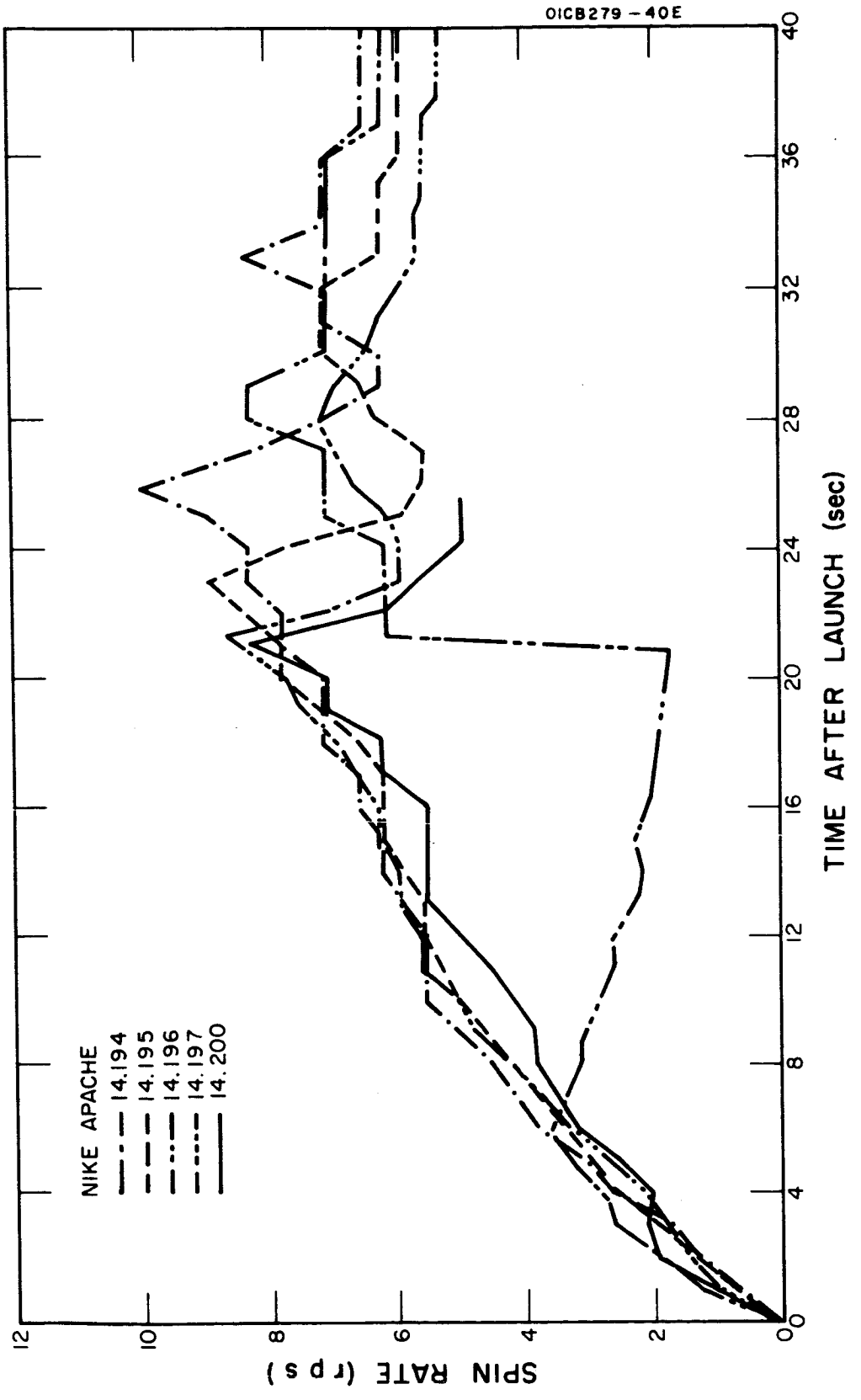

Figure A-1. Spin rates for payloads using quadraloop antennas.

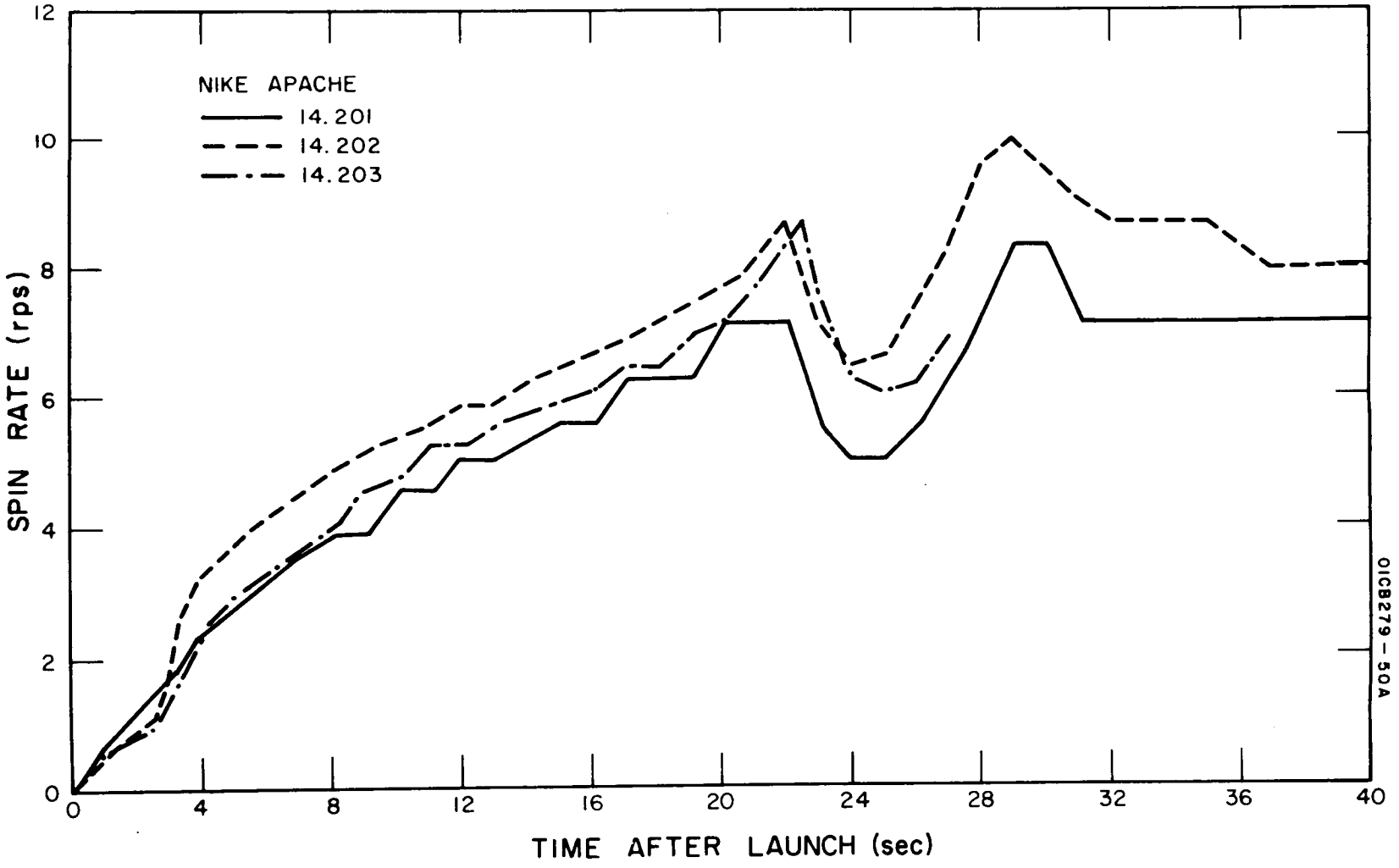

Figure A-2. Spin rates for payloads using dipole antennas.

APPENDIX B

REPORT ON THE LAUNCH OF NIKE APACHES 14.196, 14.198, 14.199 AND 14.200 AT FORT CHURCHILL, 27-28 FEBRUARY 1965.*

SEQUENCE OF EVENTS

Nike Apache 14.196 was launched at 1821 CST after a 90-minute countdown. No "holds" were called. This rocket carried a payload consisting of a sodium canister (for the wind measurement) attached to the Apache and an instrumentation section containing the probe, the magnetometer, and the telemetry system mounted on the forward end of the canister. The same type of payload had previously been flown on 14.194 and 14.197.

Excellent probe data was obtained on ascent. The sodium canister ignited at T+180 sec, as programmed. The sodium trail was of normal appearance and all camera stations reported excellent visibility.

Nike Apache 14.198 was subsequently launched at 2130 CST after an uneventful countdown. This rocket and the remaining two of the series carried a payload consisting of a TMA canister with the same type of instrumentation section used on the preceding flight. An identical payload had earlier been tested on 14.195. No ignition of the second stage was reported and this was confirmed by radar. The telemetry signal ceased abruptly 66 seconds after launch.

In view of the complete failure of this flight the launch time of the following rocket (14.199) was moved back from 0230 CST to 2400 CST so that a series of three measurements could be made at evening twilight, midnight, and morning twilight respectively. This change involved the rescheduling of an Aerobee and a Nike Tomahawk which were waiting on launchers.

The countdown again proceeded smoothly and the rocket was launched at the desired time. Again no second stage ignition was observed and the telemetry signal ceased abruptly at 61.5 seconds after launch. In this case, it was observed visually that the Nike disintegrated at or about its normal burnout time (3.5 seconds after launch).

Following this second failure there was considerable discussion as to the prospects for success of the last flight, scheduled for morning twilight. There was a precedence for two successive apparently random failures at Fort Churchill: Nike Apaches 14.89 and 14.90 had failed under similar circumstances during the eclipse of 20 July 1963 and had been immediately followed by four successful flights within a two hour period. Since there was still value in

*Reproduced without change from the Third Quarterly Report, Contract NASw-1083. Prepared by N.J. Guarino.

an evening twilight--morning twilight series, it was felt to be worthwhile to launch the last vehicle of the series. A telephone call to the NASA Vehicle Manager established that he had no reason to believe the failures were other than random.

Nike Apache 14.200 was launched at 0611 CST, again with an uninterrupted countdown. This vehicle appeared normal: the second stage motor was observed to burn although observers report an unusual uneveness in the burning. Radar reported low apogee and this was confirmed by visual observation of the TMA release which started at 250 seconds after launch (as programmed) when the vehicle was near the horizon. The data from the magnetometer shows that, in fact, the second stage had broken up about 4.5 seconds after ignition. No data of scientific value was obtained from this flight.

Telemetry Signals

Except for the period when sodium was being ejected from the payload of 14.196 the telemetry signals were continuous and strong from launch to impact. The two instrumentation signals (the aspect magnetometer and the probe) on 14.198 and 14.199 were lost at 3.5 seconds after launch. At this time the telemetry record shows the signals at the input to the two SCO's on each flight simultaneously fell to zero volts as though the connections between the telemetry package and the instrumentation package had been broken. Simultaneous shorts to ground on the two circuits would also have produced the observed effect but the adjacent circuits carrying power were not shorted to ground even momentarily.

Probe Signals

Only on 14.196 did the vehicle attain sufficient altitude to allow ionospheric measurements. The internal calibration and presence of the displacement current show that the probe operated properly on all flights. The tube in the probe electrometer is sensitive to vibration (microphonic) and gives a useful indication of the vibration level in the payload. The usual pattern of microphonics in a Nike Apache flight is found to consist of a continuous period from launch to about T+3.5 seconds while the Nike is burning, dying away in the next few seconds; a short burst is seen at Apache ignition (nominally at T+20 sec) and another, longer burst at Apache burnout (nominally T+27 sec).

The probe signal on 14.196 shows this usual series of microphonic signals. Nike Apaches 14.198 and 14.199 also appear normal up to T+3.5 seconds when the instrumentation signals are lost. The record from 14.200 is rather unusual however in three respects: first, following the Nike burnout the microphonics immediately drop to a low level; second, an extended period of microphonics is observed between T+9 sec and T+ 14 sec while the Apache is coasting; and third, more microphonics following break-up of the second stage at about 25.5 seconds.

Magnetometer Signals

The magnetic aspect sensor is included in the payload to sense the attitude of the vehicle. The electron density probe is largely independent of vehicle attitude, but it is important in the present series of experiments to establish that any irregular features of the electron density profile which may be observed are not associated with unusual vehicle motion. The aspect sensor is oriented transversely to the longitudinal axis of the payload and hence also gives spin rate which is another good index of vehicle performance.

The vehicle is caused to spin by canting the Nike fins and adding wedges to the Apache fins. These are carefully set so that the Apache spin rate increases more-or-less uniformly from zero at launch to 10 rps at Apache ignition. A decrease in spin rate normally occurs during Apache burning. This pattern has been observed on many previous flights. The separation of the two stages at about T+3.5 sec is not normally detectable by any feature of the spin rate.

Nike Apache 14.196, although a successful flight from the point of view of the experiments, has a spin rate history, Figure B-1, that deviates significantly from the normal pattern. Between T+6 seconds and T+20.5 seconds the spin rate is actually decreasing from about 3.5 rps to less than 2 rps. Then in the one-second interval before the Apache ignites at T+21.5 sec spin rate increases very suddenly to about 6 rps. This is associated with a severe yawing also indicated by the magnetometer. During Apache burning the spin rate increases to 8 rps, again contrary to usual behavior.

The spin data on 14.198 and 14.199 ends at T+3.5 sec. Up to that time the spin rate increases at exactly the same rate as was observed for the preceding rocket.

The spin rate history for 14.200, Figure B-2, shows only slight deviation from the usual case up to the point of break-up. There are two periods (T+2 to T+4 and T+13 to T+16 sec) in which the spin rate remains constant for an appreciable length of time. The significance of these "pauses" is not yet known.

Other Information

Open-shutter photographs are available showing the Nike burnout for the first three of the four launches. The third supports the visual observation of the explosion of the Nike of 14.199 at burnout, which occurred a short time (probably a few tenths of a second) after the end of continuous thrust and therefore probably after separation of the stages.

Parts of some of the rocket motors and payloads were recovered on the following days. Fragments of the Nike of 14.199 were found apparently confirming that it exploded and the payload of 14.198 was found with the head cap of the Apache still attached. Photographs of the instrumentation section of this recovered payload are shown in Figures B-3 and B-4. The rocket

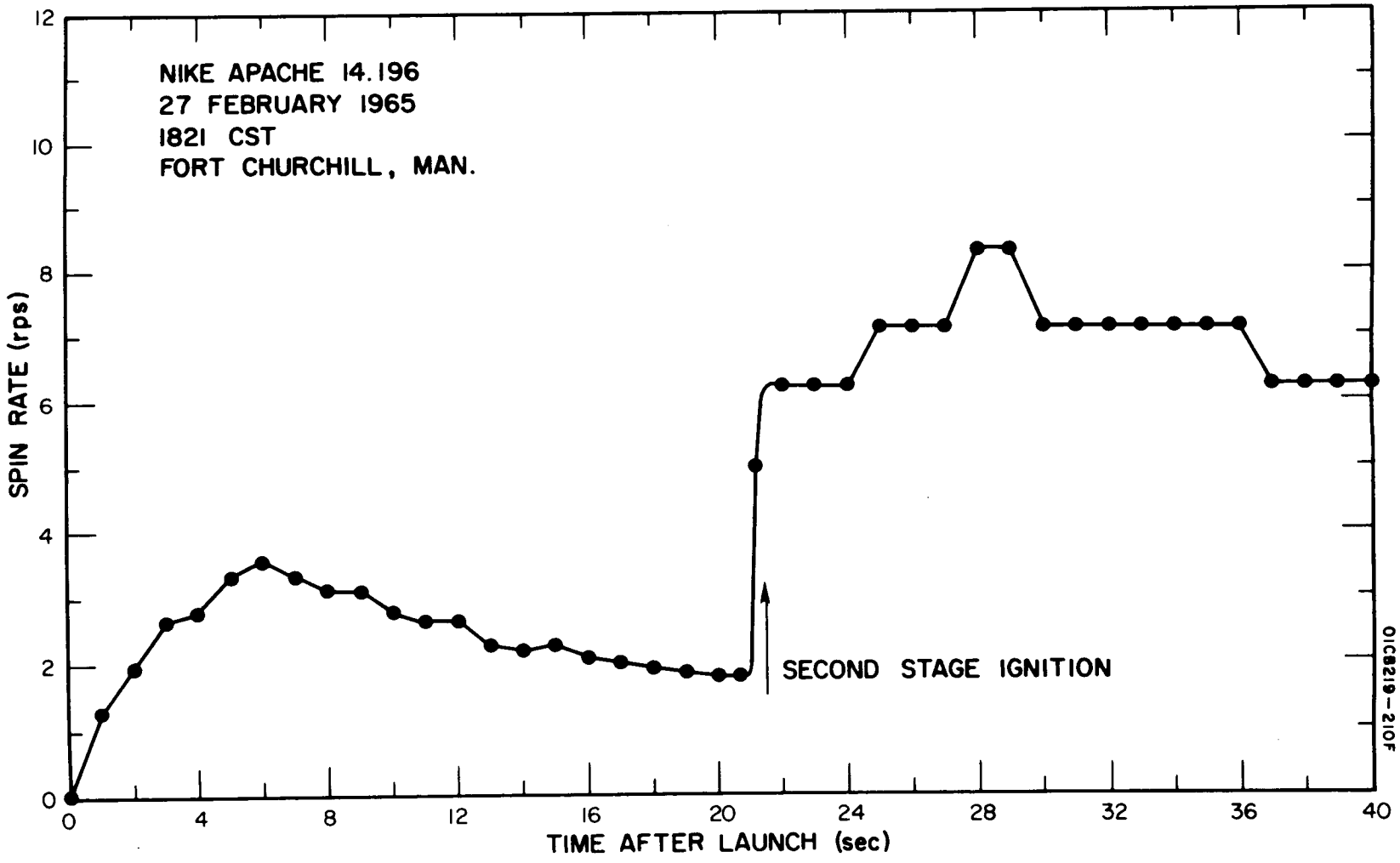

Figure B-1. Spin rate showing anomalous period from T + 6 to T + 20.5 seconds.

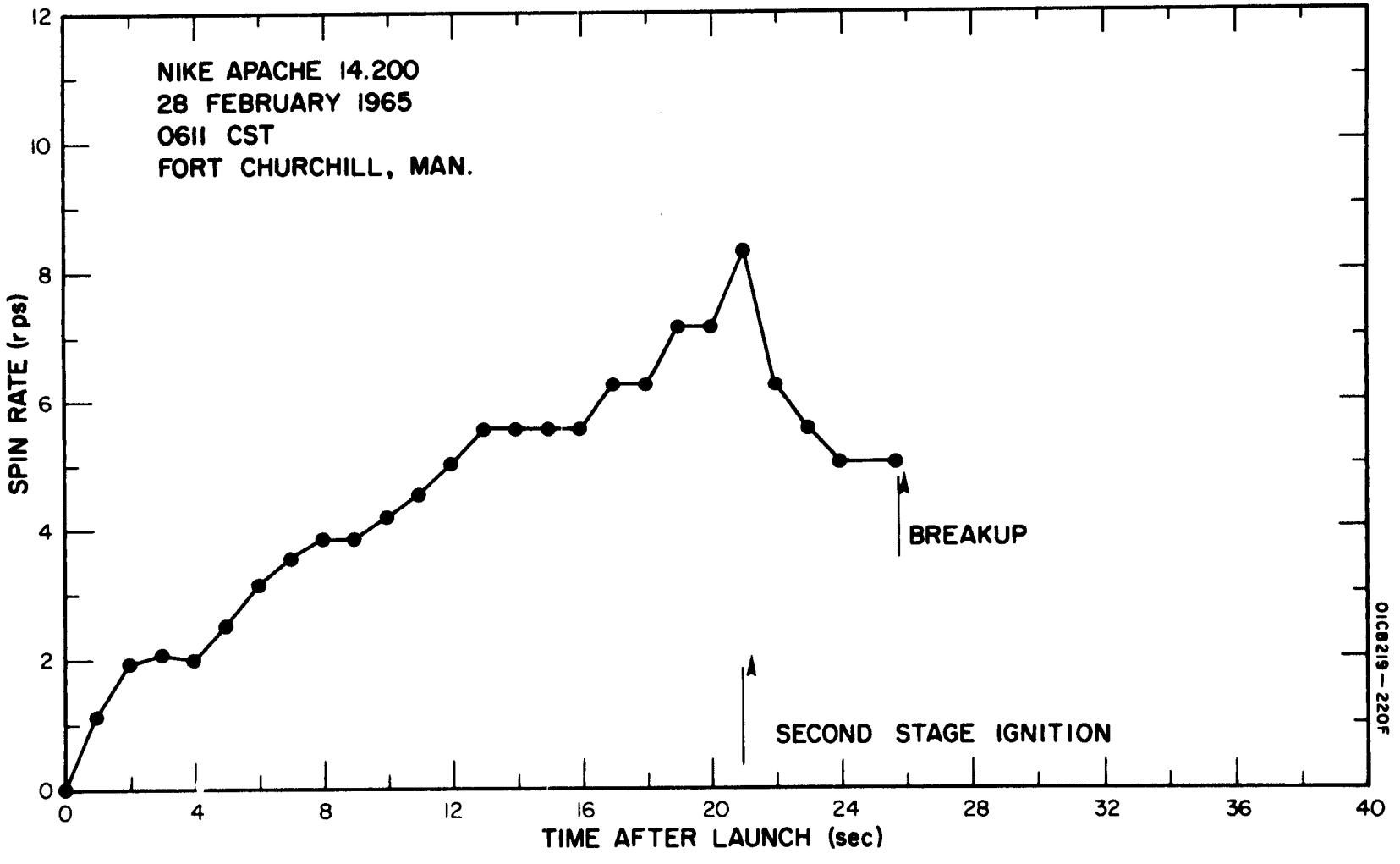

Figure B-2. Spin rate showing anomalous periods from T + 2 to T + 4 and from T + 13 to T + 16 seconds.

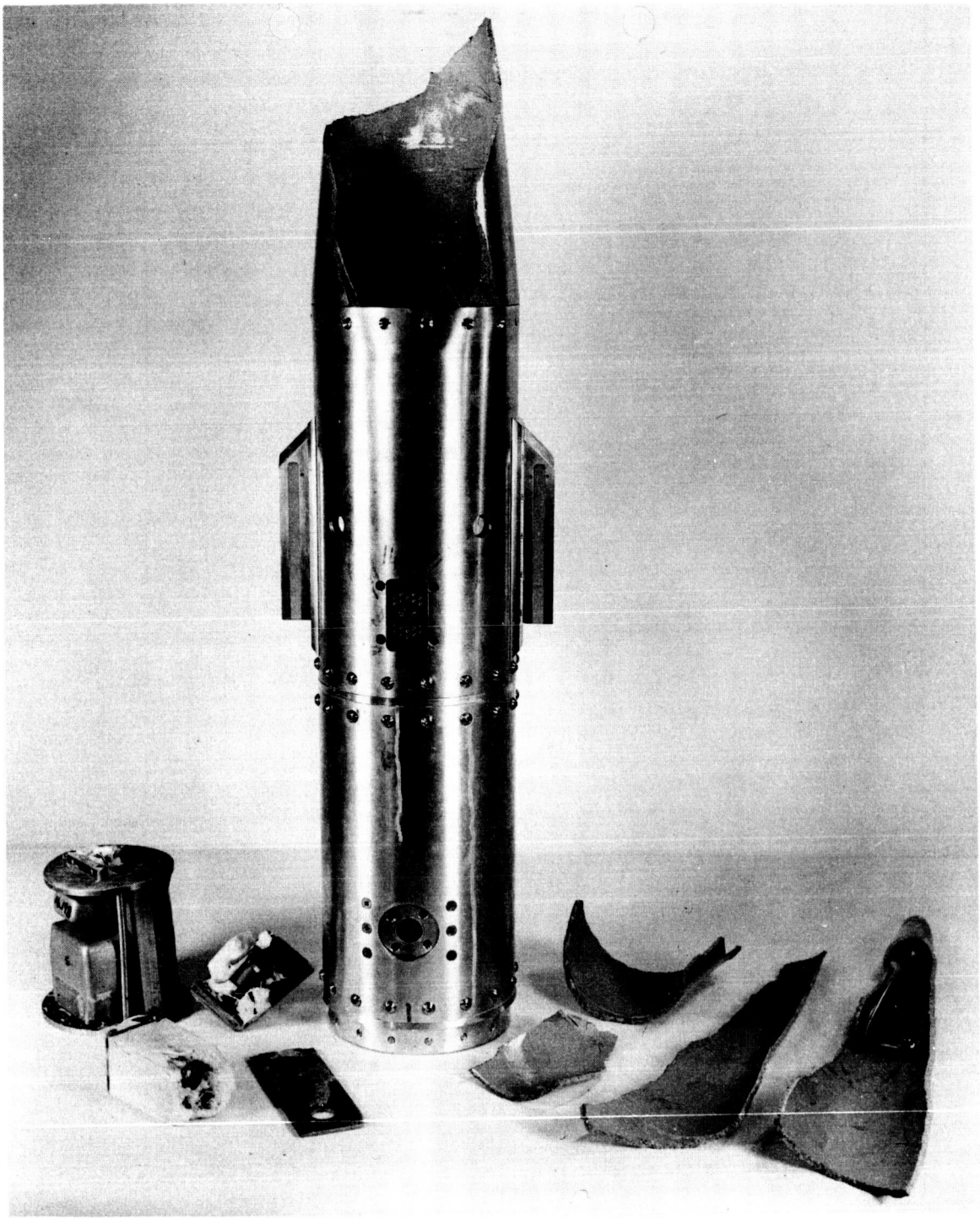

Figure B-3. Recovered 14.198 payload.

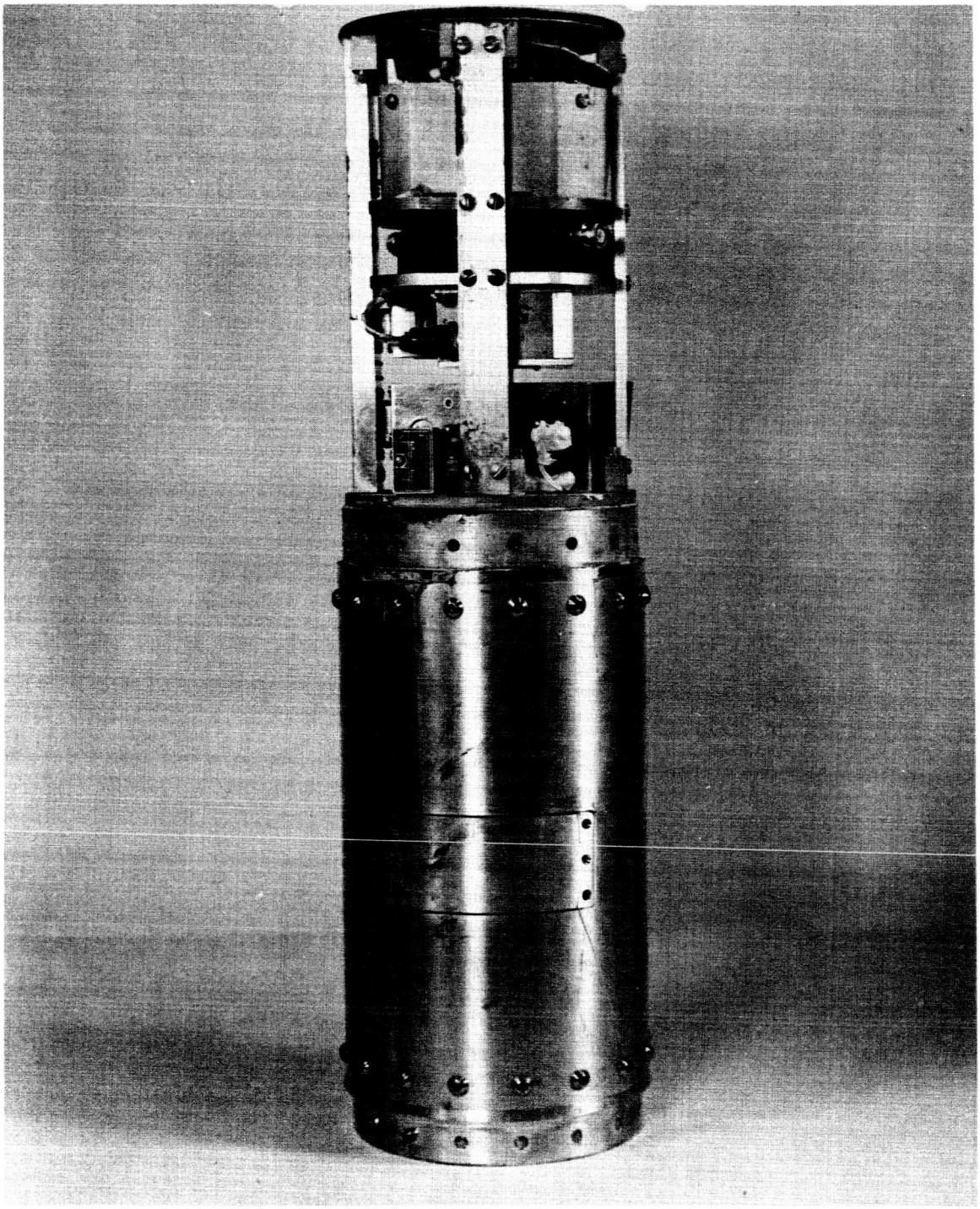

Figure B-4. Recovered 14.198 payload.

impacted before TMA ejection and thus the canister which separated from the rack at impact still contained a full load of TMA. Range safety officials at Fort Churchill are responsible for its removal and disposal. The Apache could not be found in the vicinity of the payload.

Discussion

The loss of the instrumentation signals (but not telemetry) at 3.5 seconds after launch on the second and third rockets (14.198 and 14.199) is difficult to explain in terms of the shock and vibration expected in the usual flight. The loss of instrumentation signal is instantaneous on both channels indicating a sudden, castastrophic failure rather than the cumulative effect of vibration. It must be presumed that something unusual happened at 3.5 seconds after launch which resulted in damage to the payloads. It is not unreasonable therefore that the Apache motor and/or igniter was damaged at the same time producing the observed result of no second stage ignition. The Nike of 14.199 exploded and could have inflicted such damage. There is no evidence however that the Nike of 14.198 exploded. The close parallel in the mode of failure of these two vehicles leads to the conclusion that the Nike explosion of 14.199 was a secondary or unrelated effect.

The failure of Nike Apache 14.200 occurred when the second stage broke up. It is not at all clear what caused this; the only evidence of unusual behavior is the visual observation of the Apache burning unevenly and the indication of severe vibration occurring between about T+9 and T+14 seconds. This seems to indicate that the cause of the failure was present early in the flight. The anomalous behavior of the spin rate between T+2 and T+4 seconds supports this view.

VEHICLE FAILURE ANALYSIS

Description of Failures

Four Nike Apache vehicles were launched from Fort Churchill on 28-29 February 1965. All four vehicles exhibited abnormal flight characteristics as follows:

1. Nike Apache 14.196: (DC probe and sodium) - The spin history of this vehicle was unusual because it did not spin up after booster separation. Spin decayed until 1/2 second before second-stage ignition at which time the vehicle spun up to 6 RPS.

2. Nike Apache 14.198: (DC probe and TMA) - Telemetry signal inputs were lost at 3.6 seconds and the payload was found in the vicinity of the launch complex. The Apache headcap was attached to the payload.

3. Nike Apache 14.199: (DC probe and TMA) - Telemetry signal inputs were lost at 3.6 seconds and observers reported that the Nike motor blew up.

4. Nike Apache 14.200: (DC probe and TMA) - Malfunction occurred 4.2 seconds after second-stage ignition. Telemetry carriers were received until impact, and expulsion of the TMA (trimethylaluminum) was observed to occur at an abnormally low altitude at the pre-set expulsion time.

Discussion of Failures

In September and October of 1964, prototype flights of the combined payload design, (both DC probe plus sodium and DC probe plus TMA) were flown from Wallops Island. Both of these certification rounds were completely successful with respect to vehicle and payload performance. Characteristics of these flights were reported in the Second Quarterly Report for this contract. The payloads flown at Fort Churchill in February 1965 were identical in design and construction to the certification payloads flown previously.

The performance of the February flights, in comparison with the certification flights, strongly suggest that one or more adverse factors biased their behavior. Payload design and construction are ruled out as possible causes of failure since these factors were common to both sets of flights. Further, structural analysis of the payload indicates adequate safety margins with respect to payload integrity. Possible factors which may have influenced the performance are (a) Bad Nike motors, (b) Bad Apache motors, (c) Adverse vehicle spin, (d) Aerodynamic divergence, and (e) Winds. Although it is impossible to deduce explicitly the cause (or causes) of failure, it is possible to arrive at the most probable cause of failure. Unfortunately, the payload did not contain diagnostic instrumentation such as vibration levels, motor pressure, time of booster separation, etc. to record vehicle performance. The spin-rate magnetometer is the only instrumentation in the payload which provides some indication of vehicle behavior; microphonic pick-up on the DC probe electrometer channel also gives some knowledge as to motor ignition and thrust. Each flight telemetry record has been perused so that the probable cause of failure might be determined.

Nike Apache 14.196

The unusual spin history for this vehicle is shown by the telemetry record reproduced in Figure B-5. Note there is only a slight change in spin following booster separation and a gradual decay in spin mid-way during the coast phase. This behavior appears characteristic of the interaction between vehicle roll and pitch rates. When the vehicle roll rate coincides or approaches the nutational (pitch) frequency of the vehicle, it is possible for the roll frequency to follow the nutational frequency for some period of time. This phenomenon is known as roll-pitch "lock-in". Reference B-1 deals with this phenomenon for the Aerobee vehicle and Figure B-6 (reproduced from Reference B-1) shows theoretical lock-in caused when a certain body-fixed misalignment is altered (the direction of the thrust misalignment vector). Little or no analysis of the Nike Apache has been performed regarding this problem. Figure B-7 shows spin histories for several Nike Apache flights flown under another program (Solar Eclipse). Two vehicles, 14.87 and 14.88,

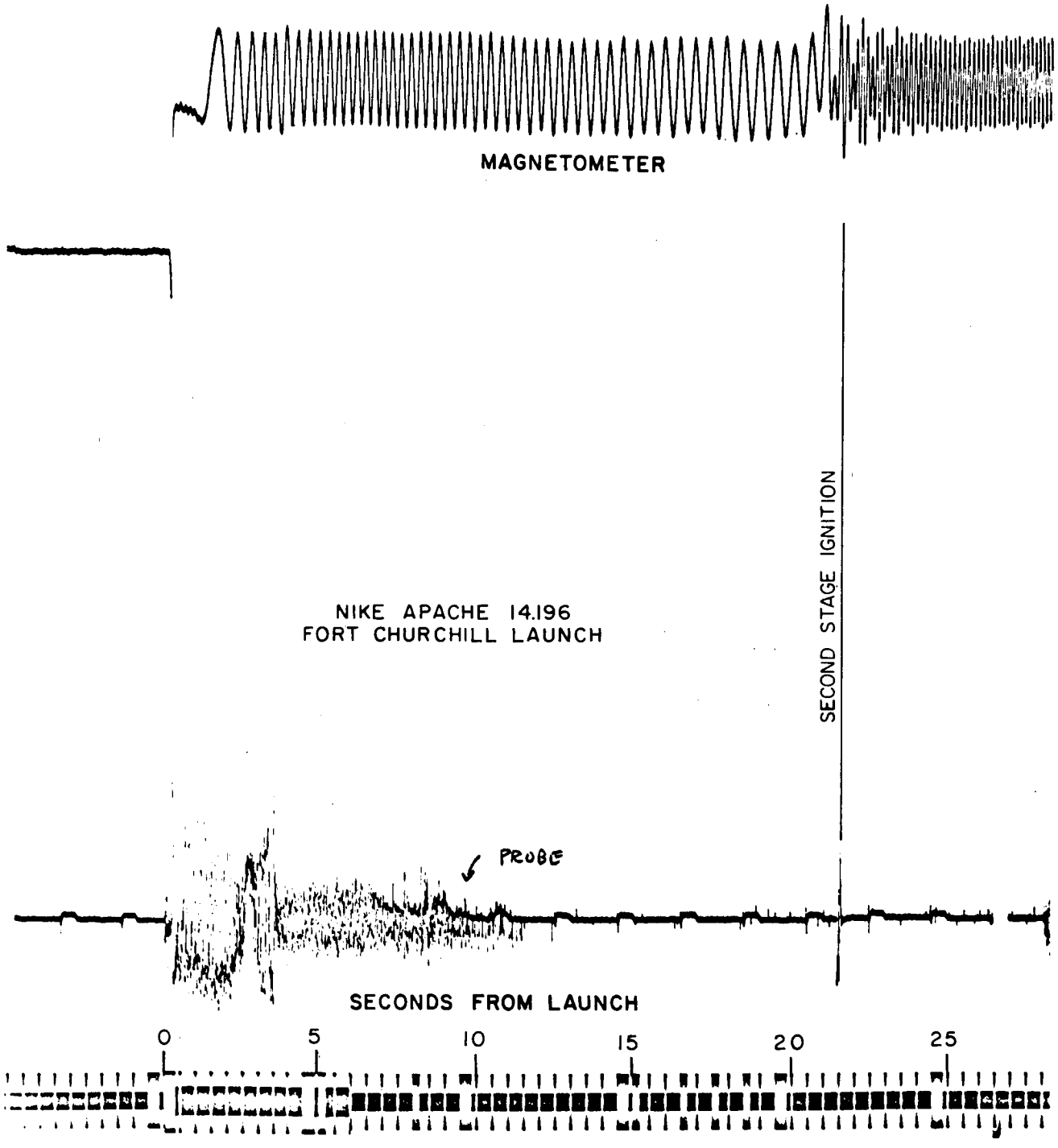

Figure B-5. 14.196 telemetry record.

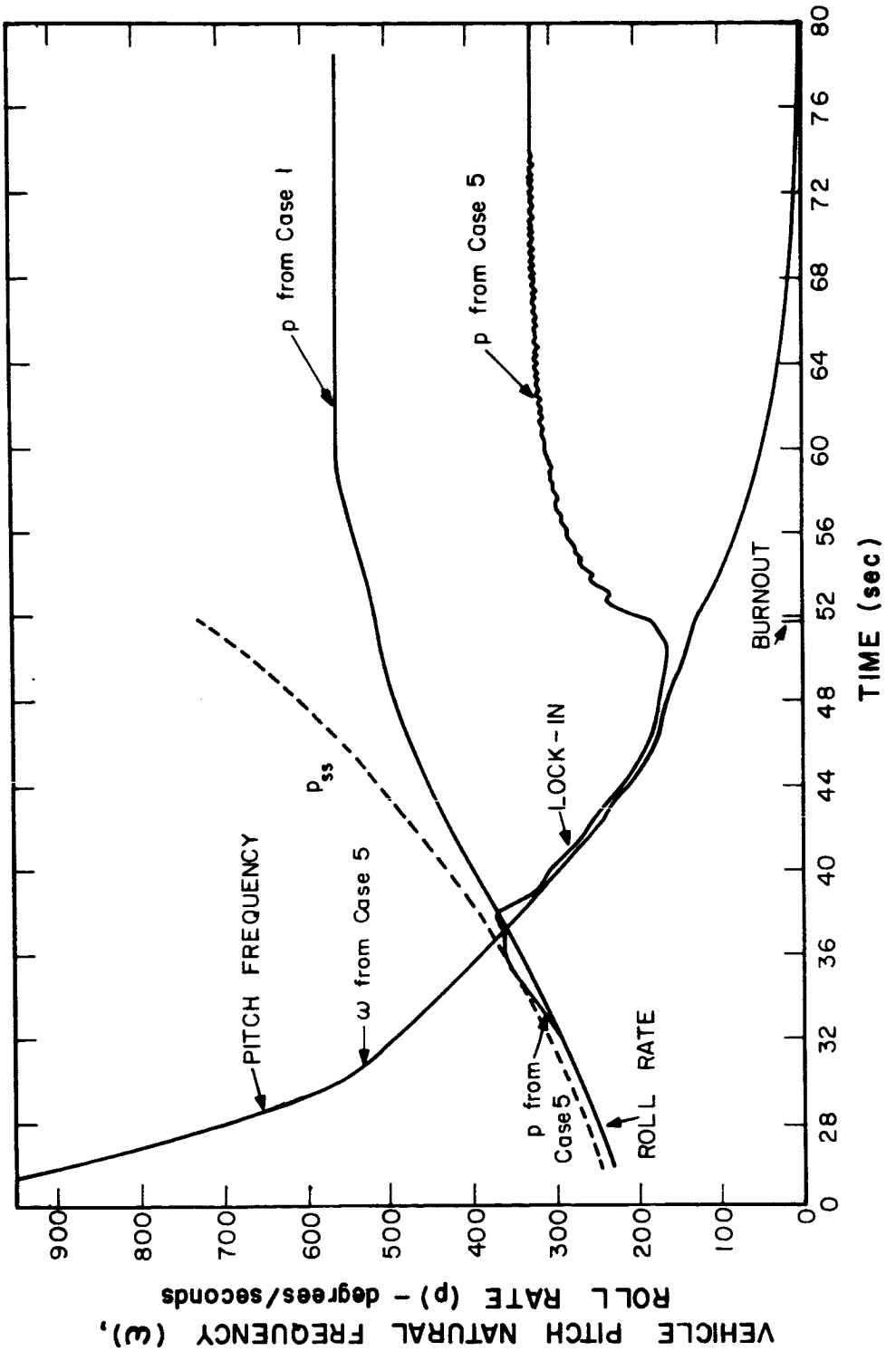

Figure B-6. Theoretical roll-pitch lock-in for Aerobee 150 vehicle.

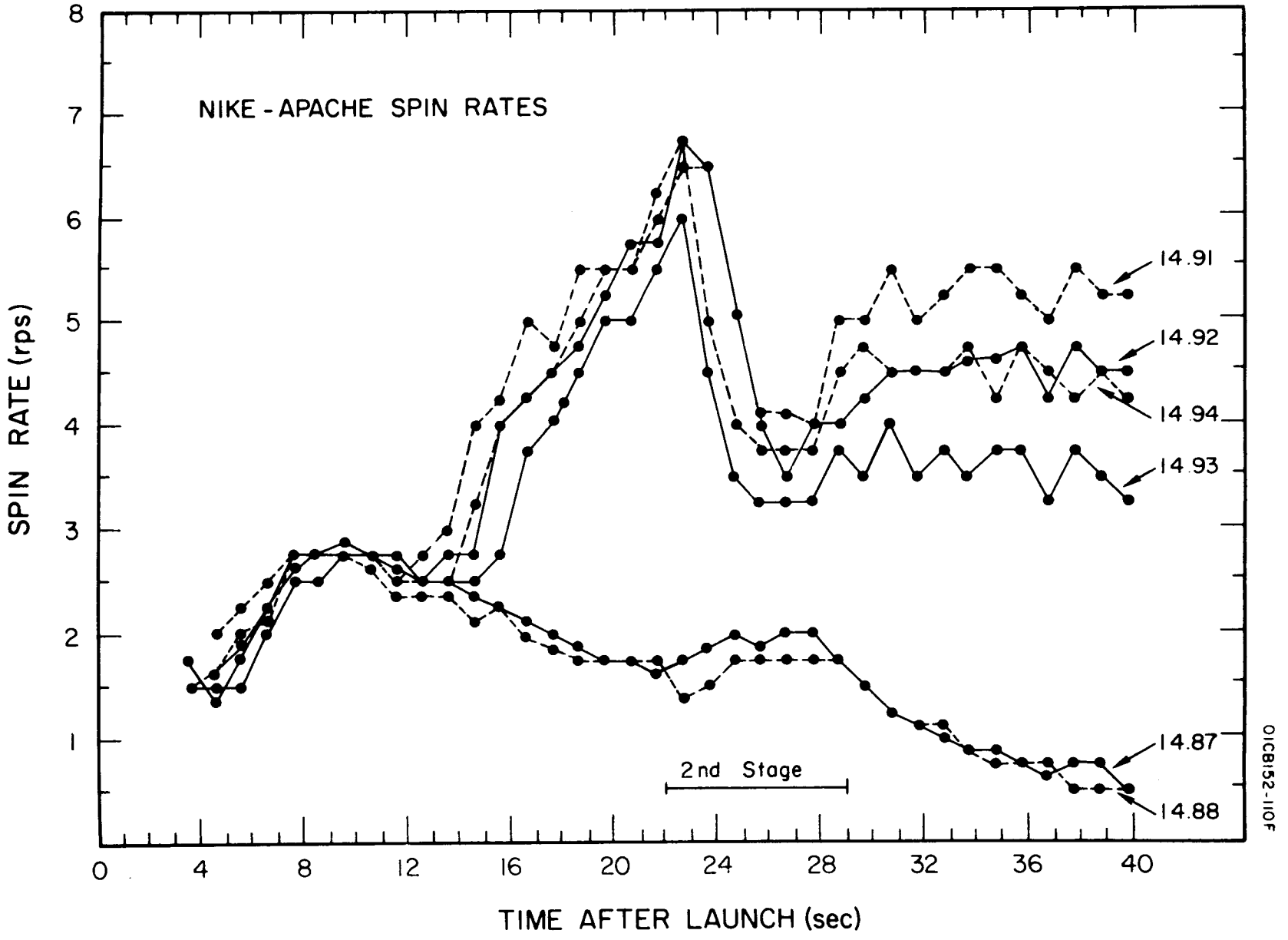

Figure B-7. Spin rate histories for Nike Apaches 14.87/8 and 14.91/4.

exhibited roll-pitch lock-in from about 8 seconds through second stage burning. The "unlocking" of 14.196 one-half second before second ignition is inexplicable. Note, however, that a relatively large excursion in cone angle occurs immediately prior to the rapid spin-up, and during burning the cone angle varies an unusually large amount in comparison with normal flights. The increase in cone angle as the vehicle leaves the sensible atmosphere is typical of a spinning vehicle with some body-fixed misalignment. It is noted that the only difference between this flight and the successful flights of 14.194 and 14.197, both of which were the combined sodium and DC probe, is the higher roll rate during Nike boost.

Nike Apaches 14.198 and 14.199

Telemetry records for these two vehicles are shown in Figures B-8 and B-9. The similarity of the records is striking and certainly suggests a common cause of failure. It is particularly important to observe that telemetry was not lost but only the signal modulation on the subcarriers. One Nike motor case was found in several pieces and recovered for analysis by NASA personnel. It is thought that this case belonged to 14.199, which observers saw "blow-up". The Nike motor case from 14.198 was not found. The abrupt loss of signal modulation indicates a catastrophic impulsive loading of the payload.

Payload 14.198 was recovered intact with the Apache headcap attached to the TMA section of the payload. Screws that fastened the probe section to the TMA section were sheared at ground impact. The probe portion of the payload was returned to GCA; however, because of the hazardous nature of the TMA that portion of the payload was left at Fort Churchill for disposal. Figure B-3 shows the recovered probe payload section. Examination of the parts indicated that the magnetometer and DC probe instrumentation contained in the cone had separated from the top deck plate of the payload rack structure. The probe signal rod (1/4-inch stainless steel rod 18 inches long) had buckled, and indentation marks inside the nose cone were observed and attributed to longitudinal motion of the instrumentation package. It was concluded that a violent longitudinal impulse must have occurred in flight and caused internal separation of the instrumentation in the cone which caused the abrupt signal loss at 3.6 seconds.

Again it is noted that the booster roll rate for these two flights was higher than normal.

Nike Apache 14.200

Booster spin appeared slightly higher than usual; however, normal spin-up occurred following booster separation. A sudden aberration of the magnetometer record occurred 4.6 seconds after second stage ignition which indicates the payload experienced a rapid yaw motion. Figure B-10 shows the telemetry record for this portion of the flight. At about T + 280 the effect of TMA release is noted on the transmitting antennas. Observers at the launch site reported sighting the TMA trail at an unusually low elevation angle. On the

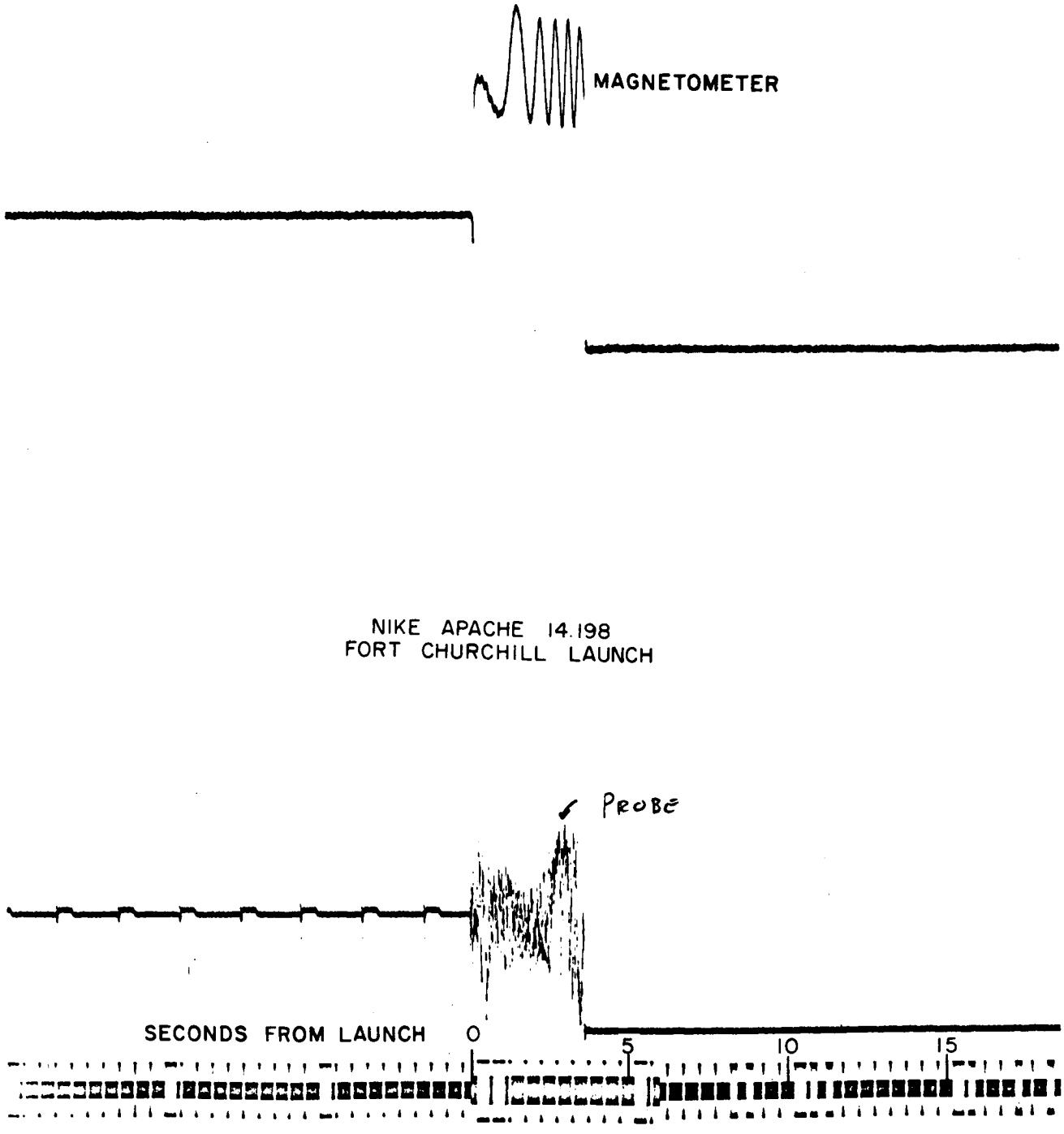

Figure B-8. 14.198 telemetry record.

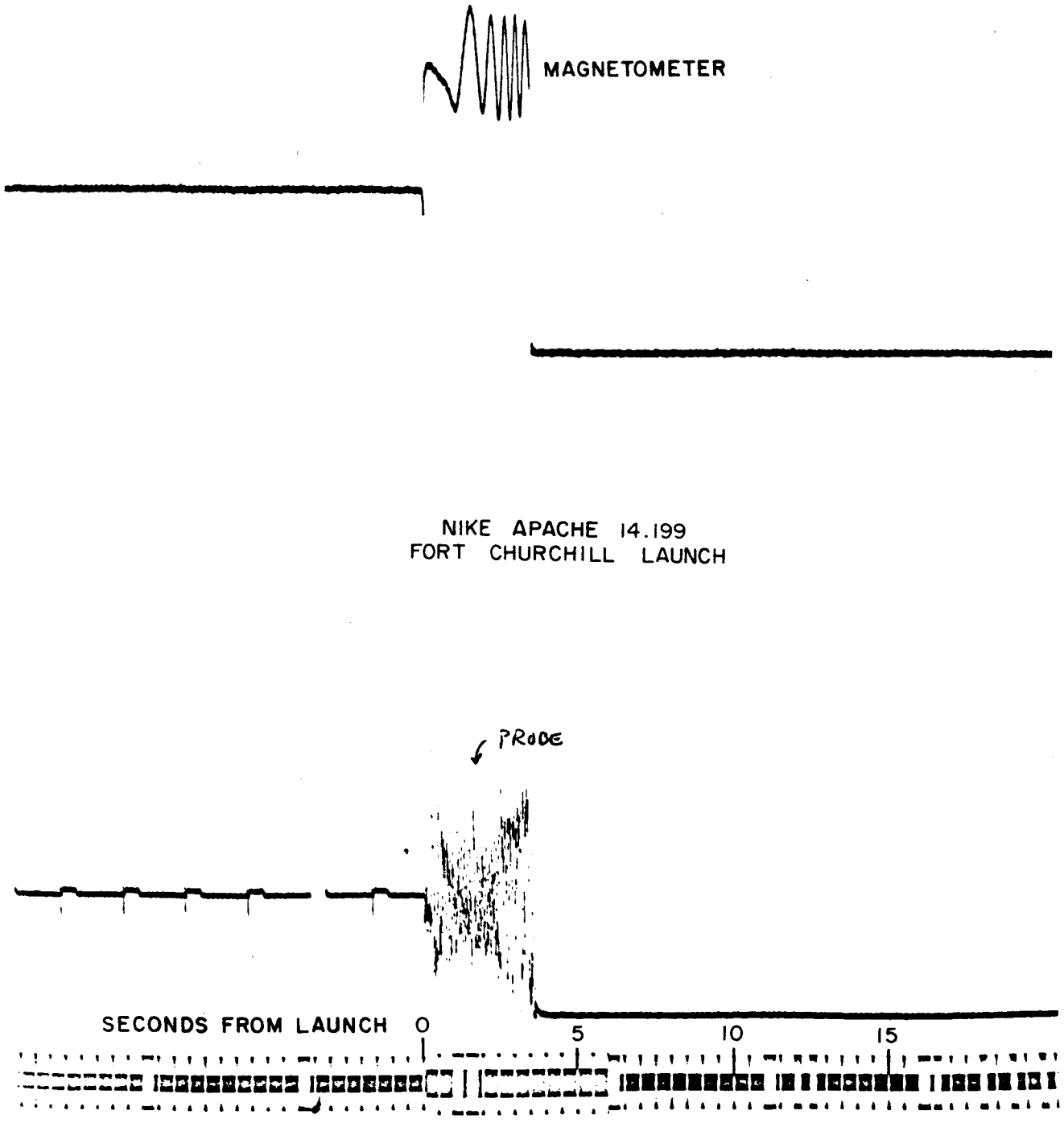

Figure B-9. 14.199 telemetry record.

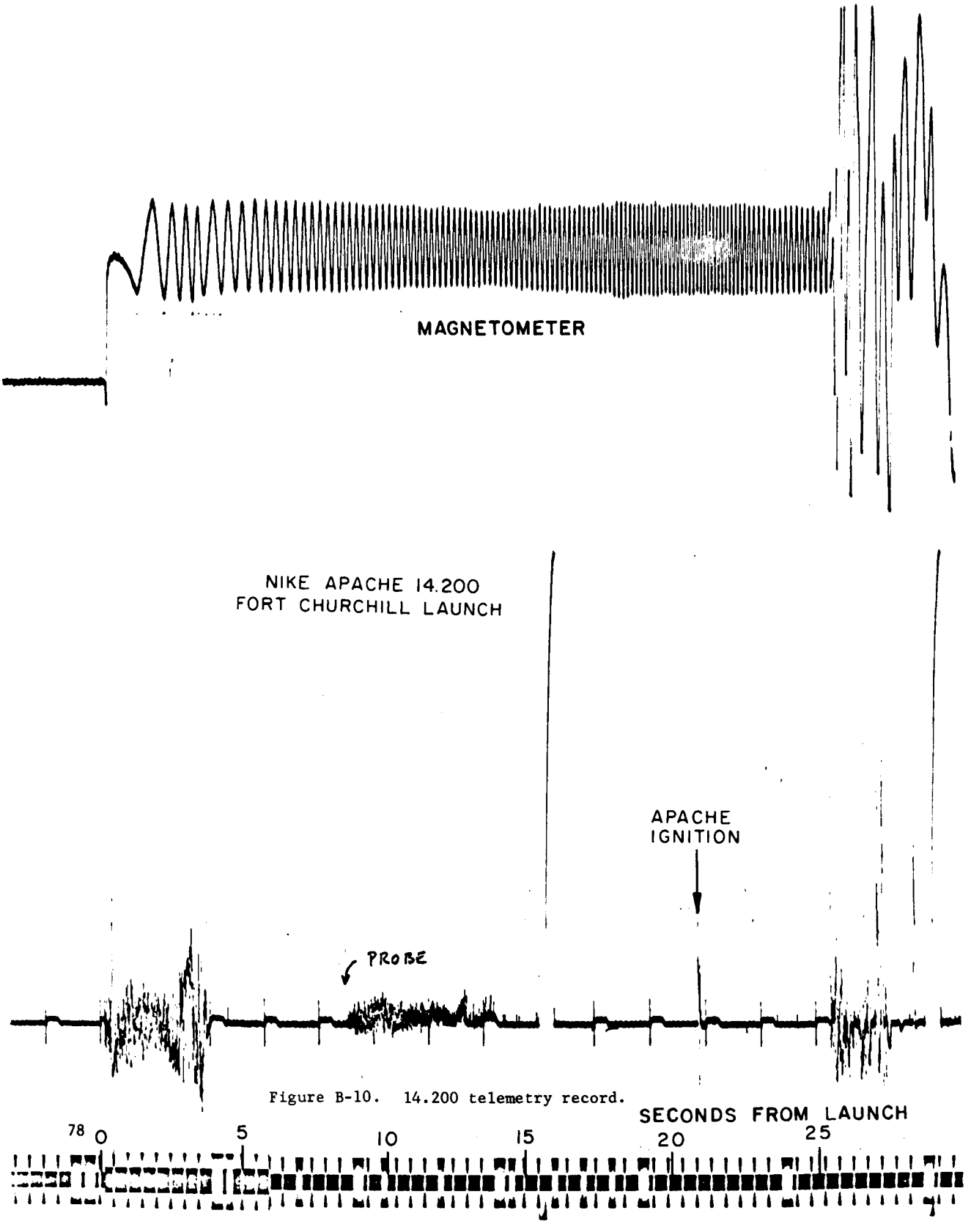

Figure B-10. 14.200 telemetry record.

Figure B-10. 14.200 telemetry record.

basis of telemetry records and visual observations, it is surmised that the Apache headcap snapped off the rocket motor and the payload remained intact during its subsequent trajectory. This mode of failure has been reported recently at the Eglin and White Sands Missile Ranges. One payload which detached from the Apache motor 4.5 seconds after Apache ignition was recovered intact at the Eglin Test Range; the Apache headcap still attached to the payload showed signs of overheating and shearing of a portion of the threads. The cause of this failure mode is unknown; however, a submarginal headcap joint is implied. Strength data of this joint under combined internal pressure and bending is not known.

Conclusions

It is concluded that the probable causes of failure are as follows:

(a) Nike Apache 14.196 experienced roll-pitch lock-in during boost and coast phase. The Nike spin rate was too high and approached the natural pitch frequency of the vehicle. Increased aeroelastic loads resulting from roll-resonance angle of attack magnification probably caused structural yielding of some portion of the Apache/payload configuration and thereby introduced a body-fixed misalignment which maintained the lock-in motion during coast. No explanation is advanced for the rapid spin up one-half second before Apache ignition.

(b) Nike Apaches 14.198 and 14.199 experienced roll-resonance during Nike-boost and attendant angle of attack magnification. A violent longitudinal impulse at 3.6 seconds broke loose the magnetometer and DC probe instrumentation, and thereby caused the loss of signal modulation to telemetry. It cannot be positively determined whether the severe impulse is related to the roll-resonance condition. One possible mechanism relating the two occurrences postulates break-up of the thin propellant webs near the end of burning, caused by excessive spin. This break-up, thus, creates a large number of slivers and increased burning surface. Such an occurrence could cause nozzle blockage which would temporarily reduce thrust and separate the Nike from the Apache. Clearing the nozzle blockage would result in a very high thrust and impact of the Nike with the Apache. Nozzle blockage, should it not clear in a short time, could also cause the internal pressure to rise and rupture the motor case, and in this instance, impact of the forward end of the Nike with the Apache would occur.

(c) Nike Apache 14.200 suffered separation of the Apache headcap during Apache burning. No probable cause has been determined; however, one strong possibility may be that the headcap joint became overstressed during Nike boost as a result of the higher than normal booster spin.

Table B-1 shows the unusually high spins which the four vehicles experienced. A comparison with other Nike Apaches is shown in the table. It is suggested that the high booster spin rate is the primary factor which compromised the performance of these vehicles. Figures B-11, B-12, and B-13 show telemetry records of the successful flights obtained with the combined DC probe and chemical payloads. The lower spin rate during boost may be noted.

Table B-1: Nike Apache Revolutions up to 3.5 Seconds From Launch

Vehicle Number	Revolutions	Percentage of Nominal	Payload Type	Launch Site	Launch Date
14.143	2.9	83	IQSY "A"	W.I.	April 1964
14.144	3.1	89	IQSY "B"	W.I.	July 1964
14.145	3.0	86	IQSY "A"		
14.146	3.0	86	IQSY "A"		
14.147	2.3	66	IQSY "A"	W.I.	Nov. 1964
14.149	2.4	69	IQSY "B"		
14.148	3.2	91	IQSY "A"	Ship	Nov. 1964
14.228	2.9	83	IQSY "A"	Ship	March 1965
14.229(1)	2.7	77	IQSY "B"		
14.194	3.0	86	Sodium/Probe	W.I.	Oct. 1964
14.195	3.2	91	TMA/Probe		
14.197	2.2	63	Sodium/Probe	F.C.	Nov. 1964
14.196(2)	5.1	146	Sodium/Probe	F.C.	Feb. 1965
14.198(3)	4.9	140	TMA/Probe		
14.199(3)	5.0	143	TMA/Probe		
14.200(4)	4.2	120	TMA/Probe		

Notes: (1) Vehicle successful but telemetry failed at T+57 seconds.
(2) Vehicle and payload successful but anomalous spin history.
(3) Vehicle broke up at Nike burnout.
(4) Vehicle broke up during Apache burning.

All other vehicles and payloads successful.

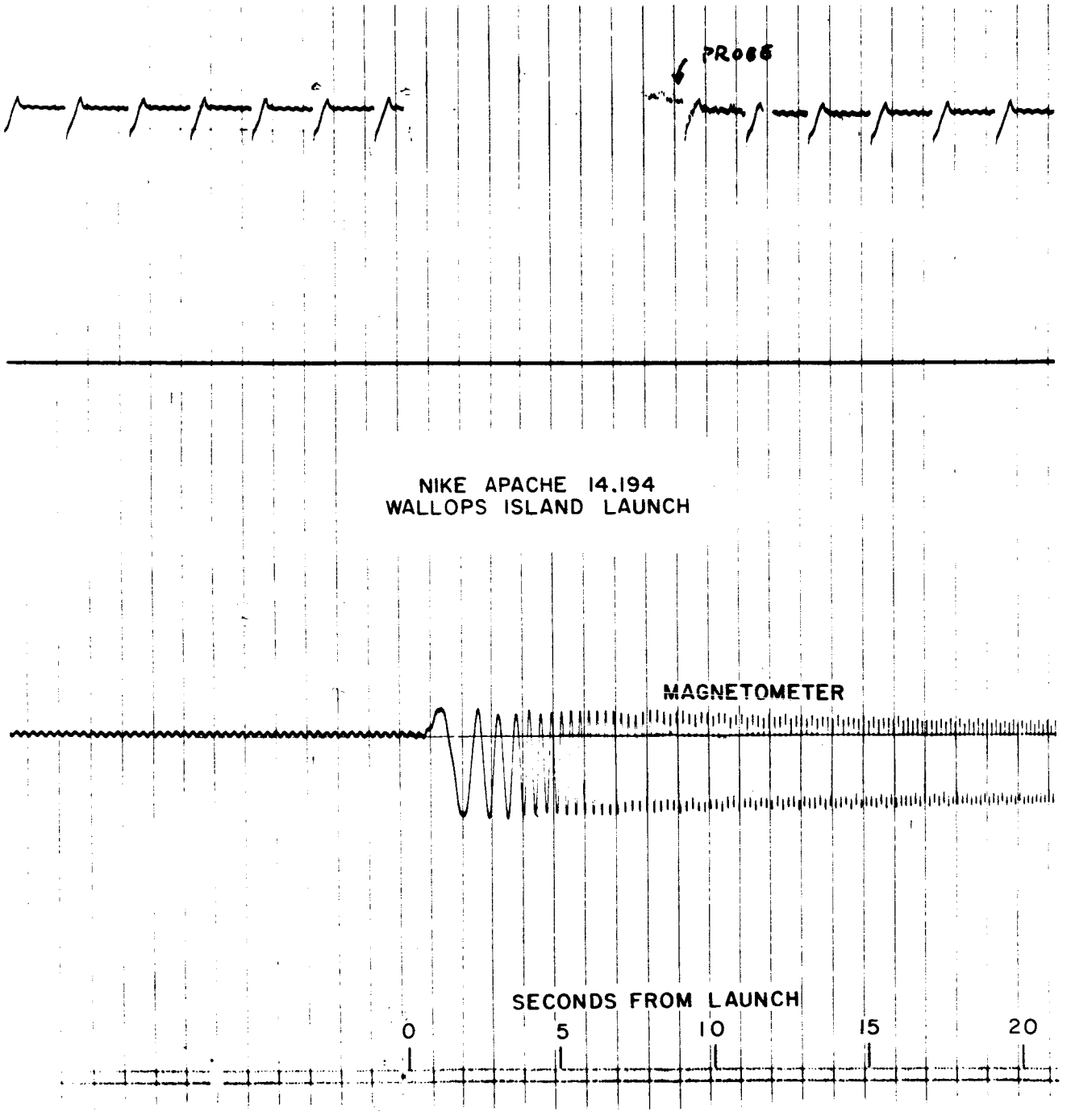

Figure B-11. 14.194 telemetry record.

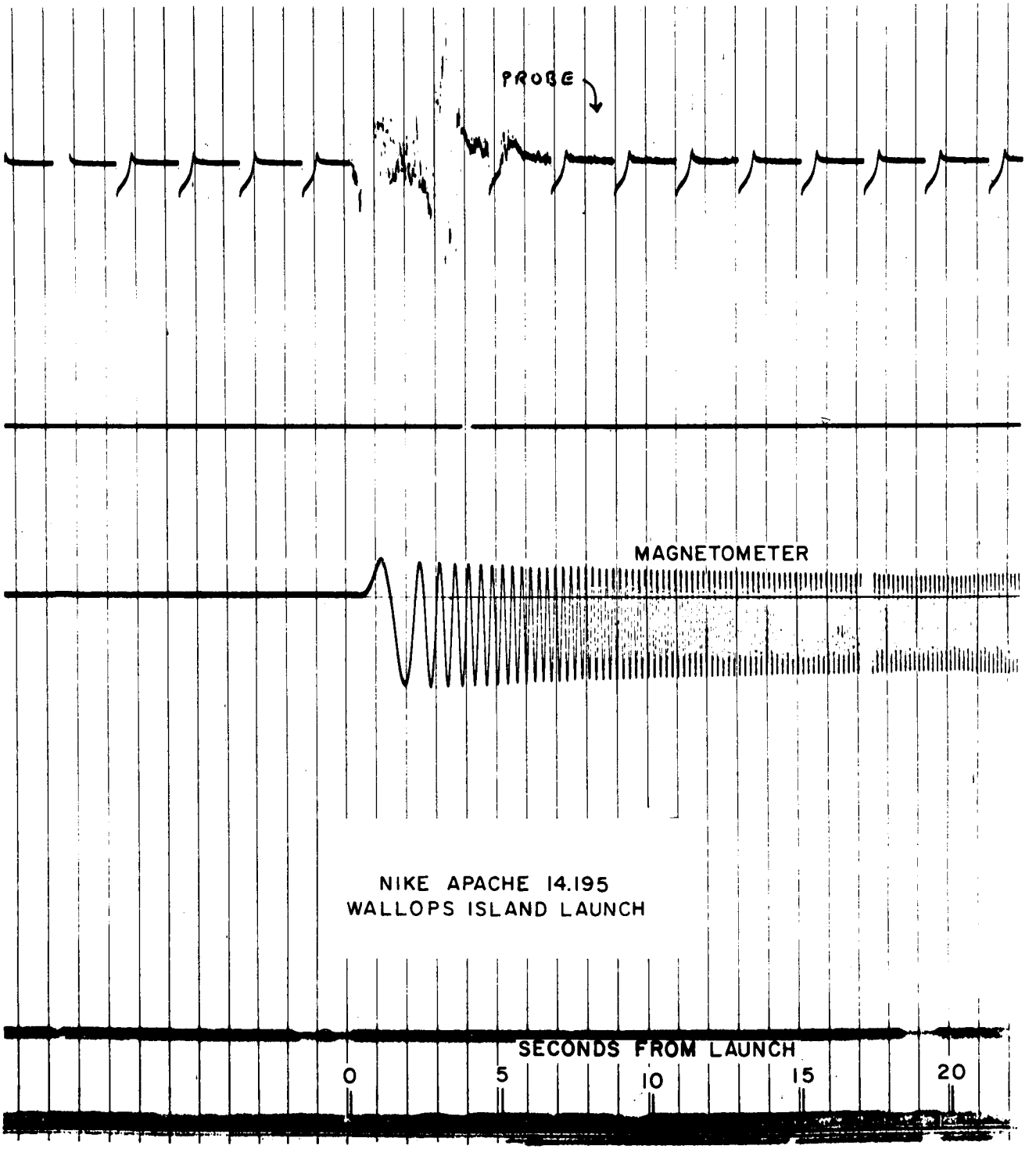

Figure B-12. 14.195 telemetry record.

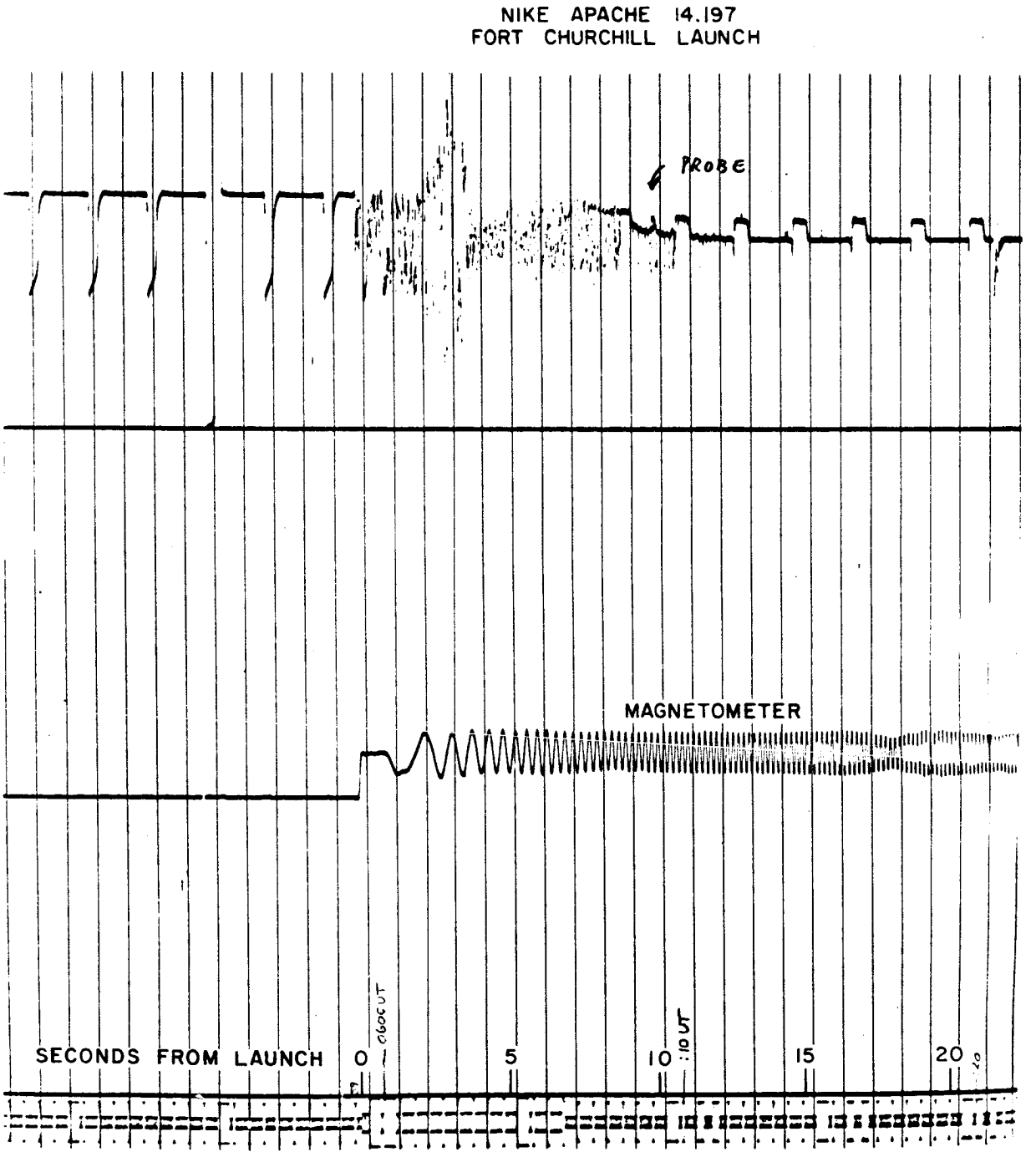

Figure B-13. 14.197 telemetry record.

Payload Structural Analysis

A rigid body analysis of the payload and Apache motor is given in Figure B-14. Final angle-of-attack is computed to be 1.75 and 1.6 degrees per initial degree angle of attach for a thin and heavy wall motor case respectively. For an initial rigid body angle-of-attack of 3 degrees, the bending moment at the headcap joint is computed to be:

(a) thin wall: (3) (1.75) (6100) = 32,000 lb-in.
(b) heavy wall: (3) (1.6) (6100) = 29,300 lb-in.

These bending moment values are well within the strength capacity of the payload joints.

Payload Joint Stresses

Radial screw joints are used throughout the payload except for the attachment to the motor headcap which is a 6-3/8 NC-8 thread. An analysis of the radial joint with respect to screw shear, shear tearout, bearing, and tension reveals the weakest structural member to be the screws; that is, the mode of failure is expected to be screw shear.* It can be shown that the maximum shear load in the screw is given by:

$$P_{max} = \frac{M}{NR/2}$$

where
M = bending moment
N = number of screws
R = radius to shear area

For the NASA IQSY and combined electron density and chemical payloads the maximum shear load per in-lb moment is:

$$P_{max} = \frac{1}{\frac{(16)(3.18)}{2}} = 0.0393$$

The screws used in the payload are rated at 3928 pounds shear ultimate across the body.** Hence, the joint ultimate moment capacity is obtained from:

$$\frac{3928}{0.0393} = 100{,}000 \text{ in-lb}$$

---

* Note that this has been borne out by structural failure of payloads when they impacted the ground.
** This value based on tests performed by NASA.

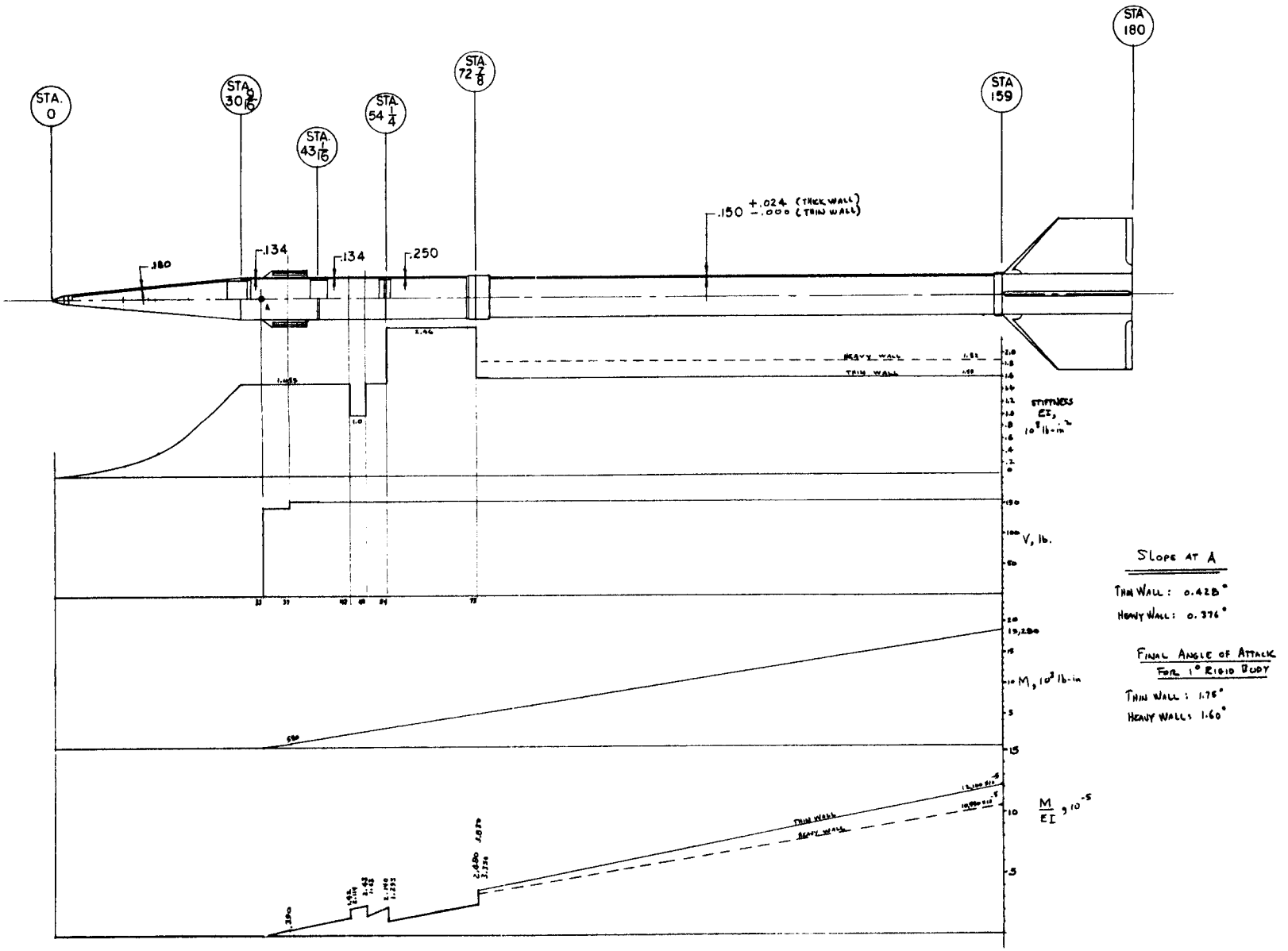

Figure B-14. Rigid body analysis. Combined payload dc probe and TMA.

Joint stiffness cannot be theoretically derived since the elastic deformation of the screws and shell depends on the fit tolerances. A stiffness value may be obtained by tests. It should be noted that the use of buttonhead shear screws results in a stiffer joint than one using flathead screws. Bending tests of payload housings and joints, performed by GCA Corporation showed that the flathead screws bend considerably. Although similar tests have not been performed with the buttonhead screws, it is known that the shear deformation of the screws is negligible compared with bending. Hence, the stiffness of the radial joint having a large number of shear screws should be high and approach that of a uniform structure. The payload joints manufactured by GCA Corporation are held to close tolerances; hole locations are held to 0.001-inch of true position and hole diameters to within 0.002-inch for the radial screws. These tolerances are achieved through the use of special manufacturing tools and drill templates.

Flight experience has shown that the payload joints are stronger than the motor headcap joint. This joint consists of a 6-3/8 - NC-8 thread. All payloads that have been recovered after premature impact had the Apache headcap attached. This indicates that the headcap had been pulled off the motor case. The strength of the headcap to motor case joint is not known. Bending strength tests of this joint should be performed. Knowledge of the failure moment may be used in conjunction with an aeroelastic analysis of the payload plus vehicle system so the flight angle-of-attack at failure can be determined. It is apparent that the theoretical joint strength is less than the payload radial joint discussed. Hence, the strength of the headcap joint is probably less than 100,000 in-lb ultimate. Note that recent information obtained from Thiokol-Elkton, (the motor manufacturer), indicated the failure moment to be 94,000 lb-in. based on one bend test specimen.

Stresses in the radial screw joint at the base of the payload are determined (for the thin Apache wall condition) as follows:

(a) Screw Shear

$$P_{max} = \frac{32,000}{(16)(3.18)/2} = 1250 \text{ lb}$$

$$\text{Margin of safety (MS)} = \frac{3928}{1250} - 1 = +2.14$$

(b) Shell Bearing Stress (7075 - T6 extruded)

$$f_{br} = \frac{1250}{(0.25)(0.124)} = 40,300 \text{ psi}$$

$$e/d > 2$$

$$f_{bru} = 125,000 \text{ psi (MIL-HBK 5)}$$

$$MS = \frac{125,000}{40,300} - 1 = +2.1$$

(c) Shear Tearout Stress

$$f_s = \frac{1250}{2[(0.750 - 0.125 \cos 40^\circ)0.124]} = 7720$$

$$f_{su} = 43,000$$

$$MS = \frac{43,000}{7720} - 1 = +4.57$$

(d) Shell Bending Stress

$$f_b = \frac{32,000\ (3.32)}{14.4} = 7380 \text{ psi}$$

$$\text{for } d/t = 49.5\ f_{bu} = 0.9\ f_{tu} = 67,500$$

$$MS = \frac{67,500}{14,150} - 1 = +3.76$$

(e) Bending at Sta. 49 (access cutout)

$$f_b = \frac{12,800\ (3.31)}{(10)\ \ (K)} = 14,150 \text{ psi}$$

where K = 3 (stress concentration factor for square cutout)

$$MS = \frac{67,500}{14,150} - 1 = +8.15$$

The rigid-body stresses are well within the structural capacity of the payload for a 3-degree initial angle-of-attack.

Roll-Resonance Condition

Dynamic coupling between vehicle roll rate and pitch frequency results in a magnification of the no-roll trim angle-of-attack. Analysis of this phenomenon is presented by Nelson in NACA TN 3737. Figure B-15 shows the magnification factor with respect to the ratio of roll rate to pitch frequency. For vehicle 14.199 the roll rate at 3 seconds was 2.6 RPS; referring to Figure B-16, which is a computed pitch natural frequency curve for the Nike Apache, the pitch natural frequency at 3 seconds is 3.4 cps which gives a ratio of 0.77. At a ratio of 0.77, the angle-of-attack magnification is approximately 2.6. Hence, the rigid body bending moment at the Apache headcap would be 83,400 lb-in. The headcap may fail under this condition. Knowledge of the statistical structural characteristics of the Apache headcap joint would be most useful in determining the maximum allowable roll rate during Nike boost. In general practice the Nike is never spun higher than 2.0 RPS at burnout.

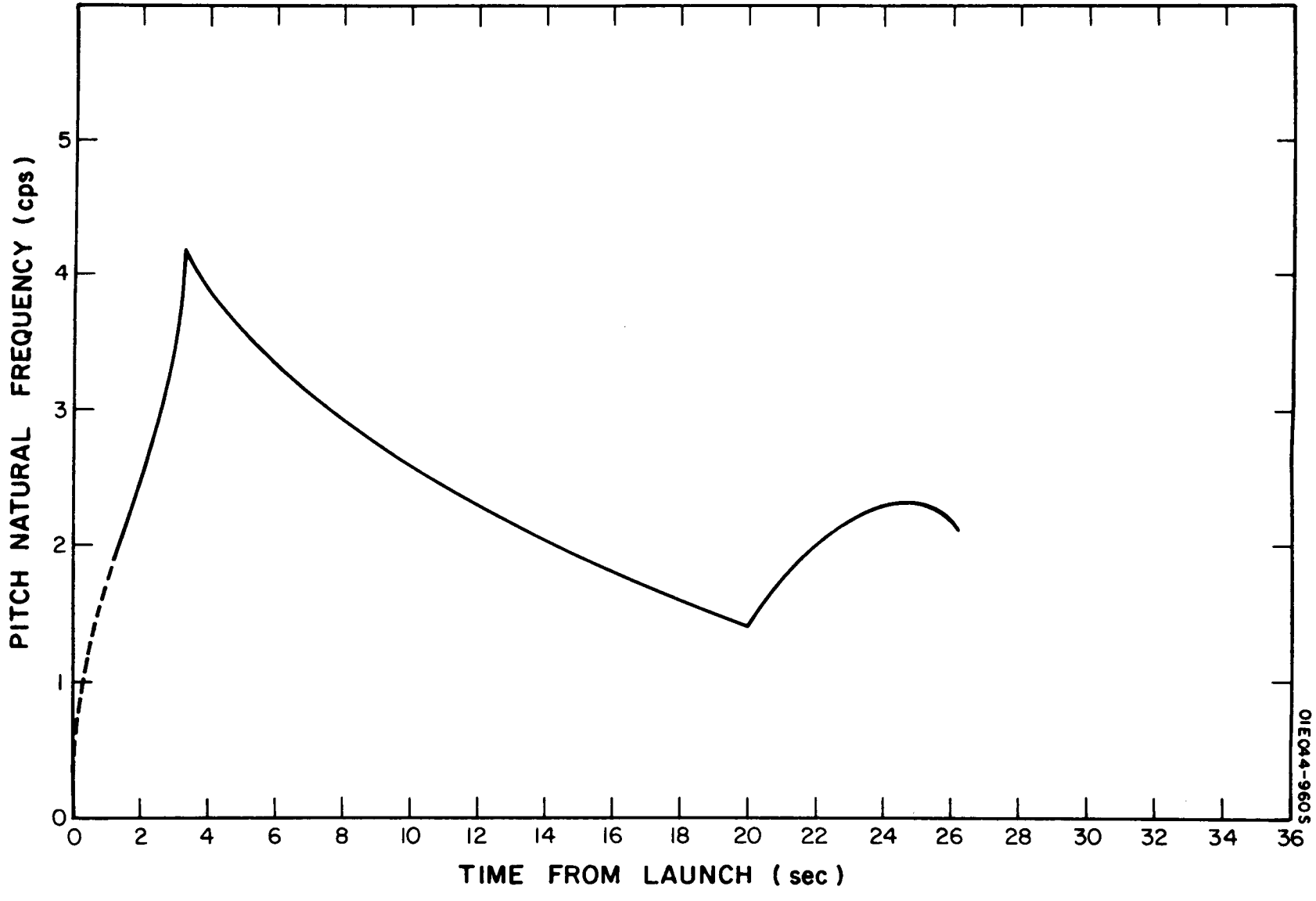

Figure B-15. Magnification of angle of attack due to roll-pitch coupling.

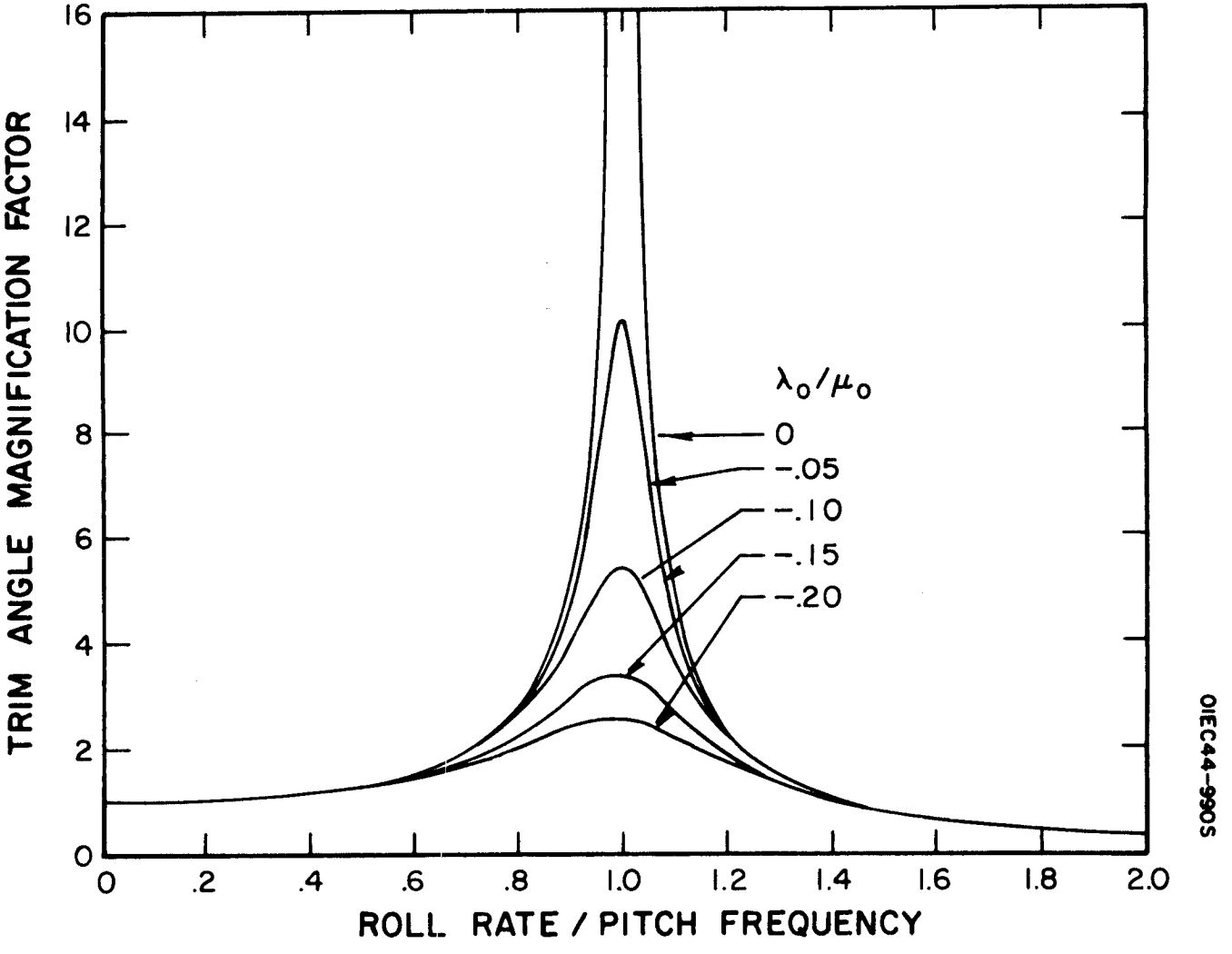

Figure B-16. Pitch natural frequency versus time for Nike-Apache.

LIFT FORCES ON QUADRALOOP ANTENNAS

The lift and drag forces on the quadraloop antennas may be estimated from supersonic theory using the assumption that they consist of flat plate airfoils. It is important to determine the increase in bending moment at the Apache headcap owing to the presence of the quadraloop antennas.

Lift

$$L = C_1 \, (0.7 \, PM^2) \, A - \text{Tip Loss}$$

$$= \frac{4}{\sqrt{M^2 - 1 \; (57.3)}} \, (0.7 \, PM^2) \, A - \text{Tip Loss}$$

$P_{5000 \text{ ft}} = 1760$ psf

$M = 3$

$$A = \frac{7.5}{144} = 0.052 \text{ ft}^2$$

$$L = \frac{4}{\sqrt{8}} \, (0.7) \, \frac{(1760)9(0.052)}{(57.3)} - \text{Tip Loss}$$

$$= (14.2 - \text{Tip Loss}) \text{ lb/degree}$$

Theory indicates that the pressure within the Mach cone region is approximately one-half the value if the wing were 2-dimensional. Hence, the pressure of the tip region causes a decrease in both lift and drag. Since about one-half the area lies within the Mach cone, the approximate loss in lift is 25 percent.

Lift Load = 10.6 lb/degree per antenna.

This value is conservative since the antenna is not a good airfoil (streamline) shape, and body interference effects were neglected.

Using the conservatively estimated antenna load, the bending moment at the Apache headcap is increased by 13.2 percent over a clean configuration (no antennas). The quadraloops do not add sufficient bending moment to cause failure for normal flight angles-of-attack. It should be noted that quadraloop antennas of much larger size (and hence greater theoretical load), have been flown on many payloads in the past. Smaller quadraloops were developed primarily to reduce vehicle drag. If however, the vehicle is spun at its pitch resonance roll rate, the aeroelastic loading is greatly increased and the probability of break-up is high.

Drag

The drag load on the antenna may be estimated from:

$$D = C_d\ (0.7\ PM^2)\ A = 76.7\ \text{lb/degree angle-of-attack.}$$

The drag coefficient is computed to be 0.0114; this value is conservative. The induced drag (due to lift) contributes a very small amount to the total drag, and may be neglected. The increase in bending moment at the headcap is 48 in-lb per degree, which is negligibly small.

Vehicle performance would be improved if the present quadraloop antennas were replaced with either the new "spike" quadraloop antennas currently available from New Mexico State University or 60 degree swept turnstile antennas. The "spike" antennas consist of two thin rods about 12 inches long, swept at a 60 degree angle. Wind tunnel tests, conducted by AFCRL, show these antennas to have less drag than the "wedge" type quadraloops.

Recently, the decision was made to use two 60 degree swept turnstile antennas in place of the quadraloops for future combined payloads. The flight performance of the vehicles should be improved owing to less drag.

ANTENNA LOADS FROM WIND TUNNEL DATA

Figures B-17 and B-18 show lift and drag coefficient data for the quadraloop antennas.

(a) Quadraloop Lift Load

M = 2.5

$SC_{n\alpha} = 0.055\ ft^2/RAD$

tunnel q = 184 psf

Normal force $Z = (SC_{n\alpha})\ q\alpha \simeq$ Lift Load

$= (0.055)(184)\ (\frac{1}{57.3}) = 0.176$ lb/degree

M = 4.0

$SC_{n\alpha} = 0.0372\ ft^2/RAD$

tunnel q = 294 psf

$Z = (0.0372)(294)\ \frac{1}{57.3} = 0.191$ lb/degree

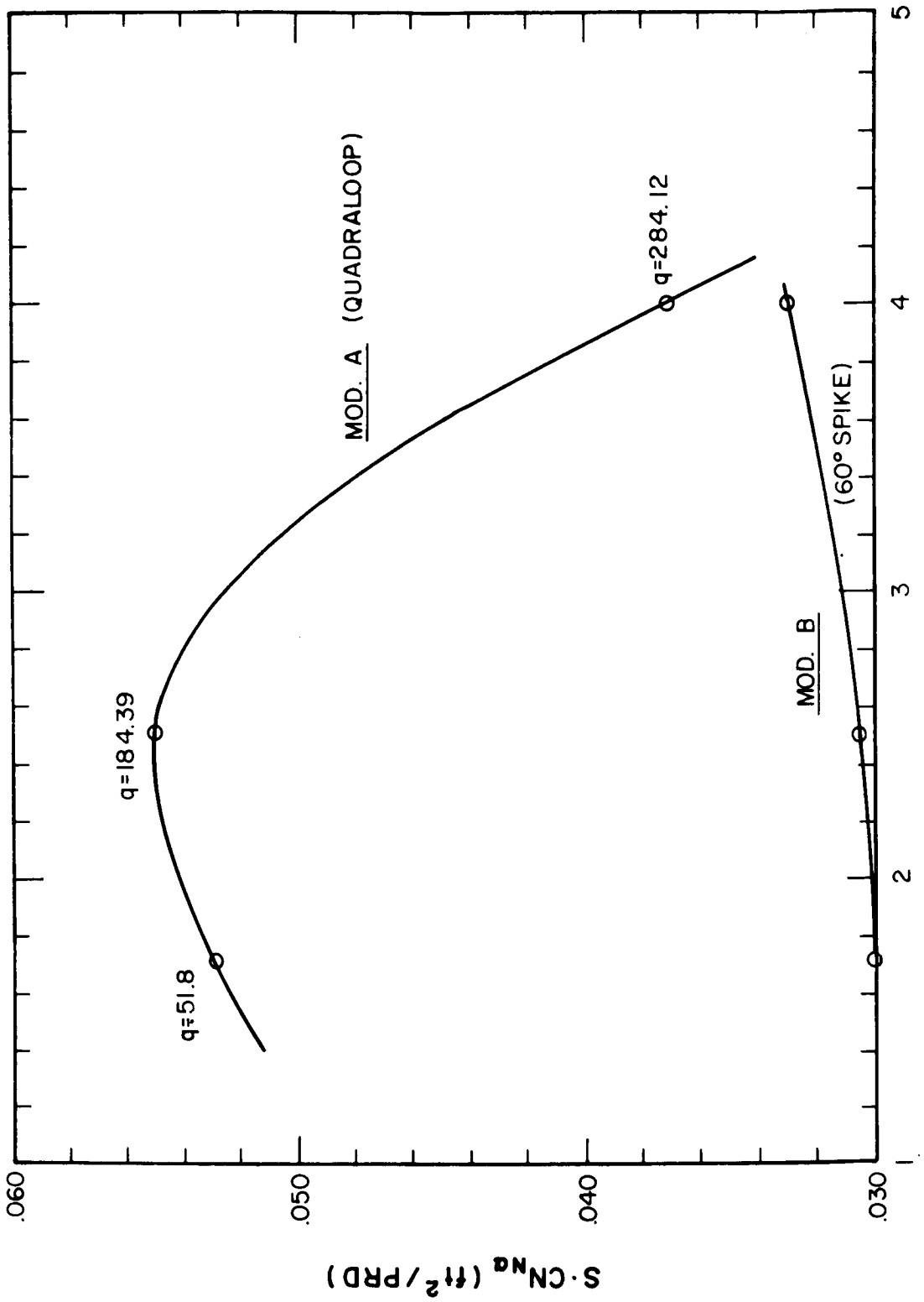

Figure B-17. Lift coefficient curve slope versus mach number for antenna.

M = 1.71

$SC_{n\alpha}$ = 0.053

tunnel q = 51.8 psf

$$Z = (0.053)(51.8)\frac{1}{57.3} = 0.048 \text{ lb/degree}$$

Flight Loads (lift)

M = 1.71: 3.44 lb/degree
M = 2.5: 7.37 lb/degree
M = 4.0: 12.8 lb/degree

For booster burnout of M = 3 at 5000 feet, the antenna load is approximately 9.4 lb/degree. The value of 9.4 lb/degree is less than the computed value of 10.6 lb/degree as expected since the theoretical supersonic lift coefficient is always higher than the actual. Note that both the tunnel test and computation are similar with respect to boundary condition at the root. Wind tunnel tests of scale models, with antennas, would be most useful. Such data would complement the tests reported in NACA Tech. Rpt. 1328 (Reference B-3).

(b) Quadraloop Drag Load

For M = 3, $SC_{D\alpha} = 4.8 \times 10^{-3}$ ft^2 which results in a computed drag of 52.8 lb/degree at booster burnout. This value is lower than the theoretically computed drag of 76.7 lb/degree as expected.

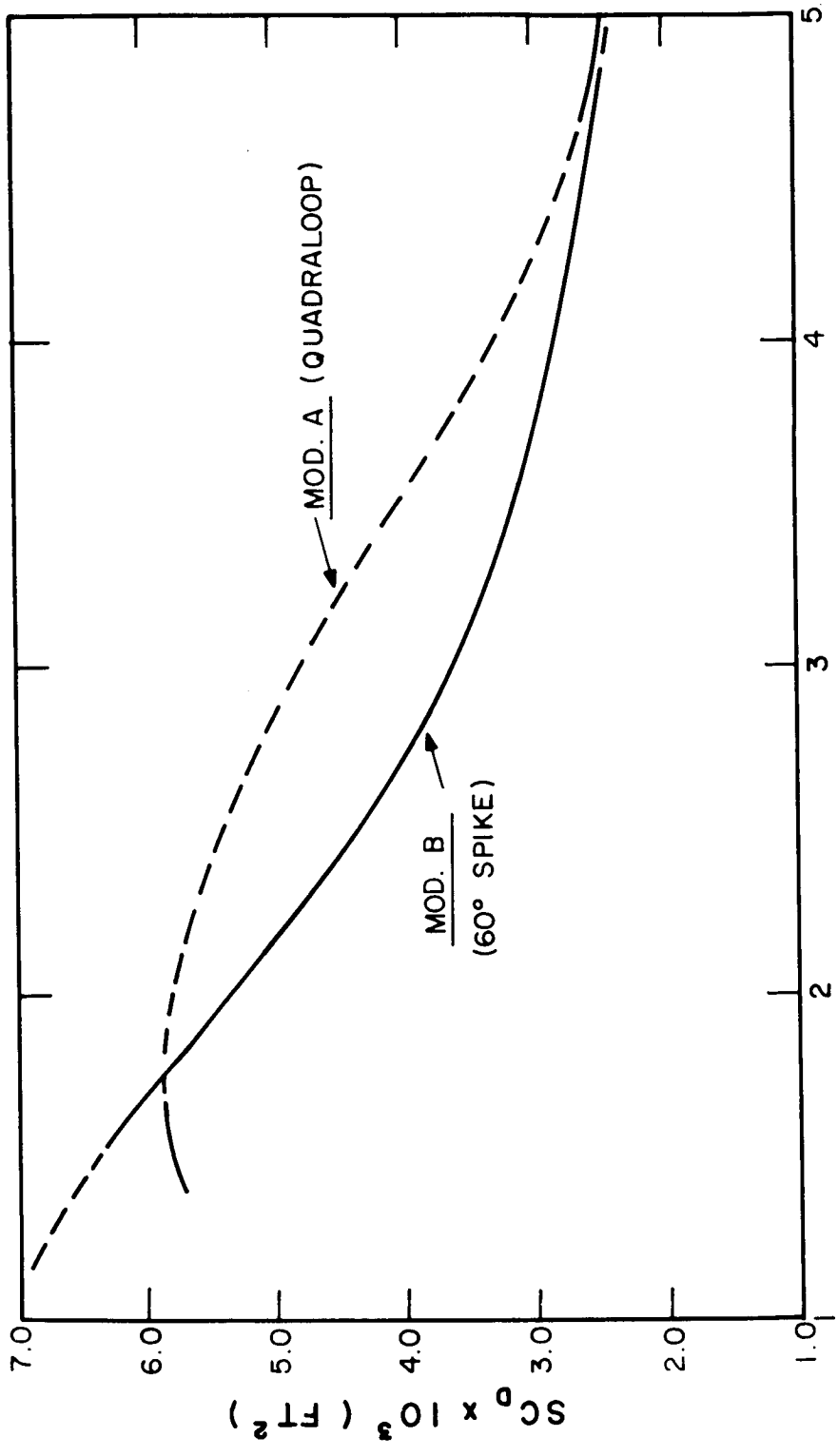

Figure B-18. Drag coefficient curve slope versus mach number for antenna.

REFERENCES

B-1 Aerobee 150 Flight Dynamics Study; Report No. 358FR1-11, Contract No. AF 19(628)-2800.

B-2 The Motions of Rolling Symmetrical Missiles Referred to a Body-Axis System; Robert A. Nelson; NACA TN 3737.

B-3 A Second-Order Shock Expansion Method Applicable to Bodies of Revolution Near Zero Lift; C. A. Syvertson and D. H. Dennis; NACA TN 1328.